INVESTIGATION OF PRIMARY AND RELAPSE ISOLATES OF BURKHOLDERIA PSEUDOMALLEI THROUGH BIOFILM ASSOCIATED ADAPTATION AND PROTEOMIC ANALYSES

UNIVERSITI KEBANGSAAN MALAYSIA

GALVIN STEVEN SEBASTIAN

UNIVERSITI KEBANGSAAN MALAYSIA

INVESTIGATION OF PRIMARY AND RELAPSE ISOLATES OF BURKHOLDERIA PSEUDOMALLEI THROUGH BIOFILM ASSOCIATED ADAPTATION AND PROTEOMIC ANALYSES

GALVIN STEVEN SEBASTIAN

UNIVERSITI KEBANGSAAN MALAYSIA

THESIS SUBMITTED IN FULFILMENT FOR THE DEGREE OF MASTER OF HEALTH SCIENCES

FACULTY OF HEALTH SCIENCES
UNIVERSITI KEBANGSAAN MALAYSIA
KUALA LUMPUR

2026

PENYELIDIKAN ISOLAT PRIMER DAN RELAPS *BURKHOLDERIA PSEUDOMALLEI* MELALUI ADAPTASI BERKAITAN BIOFILM DAN ANALISIS PROTEOMIK

GALVIN STEVEN SEBASTIAN

UNIVERSITI KEBANGSAAN MALAYSIA

TESIS YANG DIKEMUKAKAN UNTUK MEMPEROLEH
IJAZAH SARJANA SAINS KESIHATAN

FAKULTI SAINS KESIHATAN
UNIVERSITI KEBANGSAAN MALAYSIA
KUALA LUMPUR

2026

DECLARATION

I hereby declare that the work in this thesis is my own except for quotations and summaries, which have been duly acknowledged.

18 February 2025

GALVIN STEVEN SEBASTIAN
P119252

UNIVERSITI KEBANGSAAN MALAYSIA

UNIVERSITI KEBANGSAAN MALAYSIA *The National University of Malaysia*	UKM-SPKPPP-PT(PdP)-05-AK04-BO07	No. Semakan: 02	Tarikh Kuat Kuasa: 27/01/2026
	BORANG DAN SENARAI SEMAK PENYERAHAN TESIS / DISERTASI SELEPAS PEMBETULAN ***Form and Check List of Amended Thesis / Dissertation Submission***		

G. PERAKUAN TESIS/ DISERTASI SARJANA / DOKTOR FALSAFAH (*CERTIFICATION OF MASTERS / DOCTORAL THESIS / DISSERTATION*)			
Nama penuh pengarang (*Author's Full Name*)	GALVIN STEVEN SEBASTIAN		
No. Pendaftaran Pelajar (Student's Registration No.)	P119252	Sesi Akademik (*Academic Session*)	2025/2026
Tajuk Tesis / Disertasi (*Thesis / Dissertation Title*)	INVESTIGATION OF PRIMARY AND RELAPSE ISOLATES OF BURKHOLDERIA PSEUDOMALLEI THROUGH BIOFILM ASSOCIATED ADAPTATION AND PROTEOMIC ANALYSES.		

Semua tesis/disertasi dan penerbitan mengenai hasil penyelidikan pelajar adalah tertakluk kepada Dasar Harta Intelek Universiti Kebangsaan Malaysia.
All theses/ dissertations and publications relating to the research work of a student are subject to the Intellectual Property Policy of Universiti Kebangsaan Malaysia.

Saya mengaku bahawa tahap akses tesis/disertasi ini sebagai (*Tandakan ✓ dalam kotak bagi maklumat yang berkaitan; tandakan satu (1) kotak di bawah sahaja):
I hereby declare the level of access for this thesis/dissertation as follows (tick ✓ the relevant box below; tick only one option).

Pilihan Tahap Akses ***Access Level Selection***		**Tafsiran Tahap Akses Tesis/Disertasi** ***Definition of Thesis/Dissertation Access Level***
☐	**RAHSIA** ***(CONFIDENTIAL)***	Mengandungi maklumat rahsia sepertimana yang diperuntukan bawah Akta Rahsia Rasmi 1972. *Contains classified information as stipulated under the Official Secrets Act 1972.*
☐	**TERHAD** ***(RESTRICTED)***	Mengandungi maklumat yang hanya boleh diakses oleh pihak yang mempunyai kebenaran atau keperluan tertentu untuk mengetahuinya yang ditentukan oleh organisasi/ badan di mana penyelidikan dijalankan. *Contains information that may only be accessed by parties with specific authorization or a defined need to know, as determined by the organization or body where the research is conducted.*
/	**AKSES TERBUKA** ***(OPEN ACCESS)***	Tesis/disertasi versi akhir dalam format PDF yang boleh diakses secara percuma secara dalam talian dan bebas dari isu hak cipta dan pelesenan *The final version of the thesis/dissertation in PDF format that is freely accessible online and free from copyright and licensing issues.* Kementerian Pendidikan Tinggi melalui surat bertarikh 27 Mac 2025 memutuskan bahawa kebenaran akses tesis / disertasi dalam borang serahan akses terbuka ditentukan oleh penyelia (bukan pelajar).

UNIVERSITI KEBANGSAAN MALAYSIA

Universiti Kebangsaan Malaysia *The National University of Malaysia*	**UKM-SPKPPP-PT(PdP)-05-AK04-BO07**	**No. Semakan: 02**	**Tarikh Kuat Kuasa: 27/01/2026**
	BORANG DAN SENARAI SEMAK PENYERAHAN TESIS / DISERTASI SELEPAS PEMBETULAN ***Form and Check List of Amended Thesis / Dissertation Submission***		

		The Ministry of Higher Education, through a letter dated 27 March 2025, has decided that permission for thesis / dissertation access in the open access submission form shall be determined by the supervisor (not the student).
☐	**EMBARGO**	Tempoh masa di mana akses kepada tesis/disertasi disekat (ditutup) selama dua (2) tahun atas sebab-sebab tertentu sebagai contoh kerahsiaan atau hak cipta. Tesis/disertasi akan berstatus akses terbuka selepas tamat tempoh *embargo.* *The period during which access to the thesis/dissertation is restricted for two (2) years due to specific reasons, such as confidentiality or copyright. The thesis/dissertation will be granted open-access status upon the expiry of the embargo period.*

PENGESAHAN PELAJAR *(STUDENT VERIFICATION)*	**PENGESAHAN PENYELIA *(SUPERVISOR VERIFICATION)***
TANDATANGAN PELAJAR **(*STUDENT'S SIGNATURE*)**	**TANDATANGAN PENYELIA / PENGERUSI JK SISWAZAH** ***(SUPERVISOR'S / CHAIRPERSON SUPERVISION COMMITTEE SIGNATURE)***
Nama Pelajar *(Student name):* GALVIN STEVEN SEBASTIAN No. Pendaftaran Pelajar *(Student's Registration No.)* P119252 Tarikh: 24/01/2026 *(Date)*	Nama Penyelia / Pengerusi JK Siswazah : Dr Vanitha Mariappan *(Supervisor's / Chairperson Supervision Committee Name)* Tarikh: 24 Januari 2026 *(Date)*

UNIVERSITI KEBANGSAAN MALAYSIA

ACKNOWLEDGEMENT

Without Jesus, none of this would have been possible. He is my way-maker and the light in my darkness throughout this journey. Whenever I felt lost or overwhelmed, I turned to Him, and by His grace, I had reached the end of this path. Thank you, Jesus.

I acknowledge my supervisor, Dr Vanitha Mariappan, and my co-supervisors Prof Noraziah Mohamad Zin, Prof Sheila Nathan and Dr Kumutha Malar Vellasamy for their endless help in this project. I also extend my heartfelt thanks to UKM, which has blessed my family and me over the past ten years. From PERMATA Pintar UKM to the Faculty of Health Sciences, UKM KL, thank you for the opportunities that have shaped who I am today. I acknowledge the grant FRGS/1/2021/SKK0/UKM/02/8 for the funding of this project

I owe everything to my mother (Pn. Caroline), brother (Oliver), grandma (Madam Lourdemary), grandaunt (Madam Joema) and my granduncle (Mr. Eddie) who passed away recently. For all their prayers, love and understanding and their financial assistance. They pushed me when I wanted to quit. They believed in me and pushed me to continue the course although there were times where I could not take it anymore and may have differed or stopped my masters a long time ago. Thank you, my loving family.

To my best friends, Ariff, Acap, Aaron, Abang and Belle. Words cannot describe how much you mean to me. This victory is as much yours as it is mine. You guys were my coping mechanism throughout this entire journey. No matter how hard it was, the love and laughter always reminded me of the light at the end of the tunnel.

I would also like to thank Dr Eng Wee Chua as well as all my friends from UKM KL pharmacy faculty for tirelessly teaching me qPCR theories and techniques. Mock noona, Kim, Ben, Mila and Anushri. You guys taught me more than I could ever learn on my own and we had fun while doing it too.

To my friends from the UKM KL dental faculty, Malathi and the gang, thank you for your kindness in sharing the knowledge and reagents for the SDS page analysis. It was a tiring number of weeks, but we managed to get through it in the end. Malathi especially, thank you for helping me gain perspective in this life and this course. I will never forget the conversations we had while doing our work.

KC (University Malaya), you are an angel sent by God. I don't think I'll be graduating without you. I thank you from the bottom of my heart and I pray you achieve everything you sought to do. You are literally the best.

To my friends from CORE, Raveena and the gang. Again, words cannot describe how much you guys mean to me. From the knowledge, the time, to the gossip sessions, you guys could relate. I wish all of you the best in this journey and I pray you graduate on time with all the accolades you strive for.

UNIVERSITI KEBANGSAAN MALAYSIA

ABSTRAK

Melioidosis, penyakit berjangkit yang ditemui di negara-negara tropika, disebabkan oleh *Burkholderia pseudomallei*. *B. pseudomallei* ditemui dalam tanah dan air yang tercemar serta diketahui menghasilkan beberapa faktor virulens, termasuk biofilem, yang meningkatkan keupayaannya untuk bertahan terhadap antibiotik. Walaupun rawatan melioidosis bergantung kepada terapi antibiotik, keupayaan patogen untuk bertahan dalam tubuh boleh menyumbang kepada jangkitan kronik serta berpotensi menyebabkan relaps. Maka, kajian ini mempersoalkan bagaimana perbezaan dalam pembentukan biofilem, ekspresi gen berkaitan biofilem, dan profil proteomik antara isolat primer (PS_UMC083; ST51), jangkitan baru (NI_UMC082; ST1644) dan relaps (RS_UMC114; ST51) *B. pseudomallei* menyumbang kepada mekanisme adaptasi dan jangkitan berterusan. Kajian ini bertujuan untuk mengenal pasti perbezaan dari segi pembentukan biofilem, ekspresi gen berkaitan biofilem, dan profil proteomik antara PS_UMC083, NI_UMC082 dan RS_UMC114 *B. pseudomallei* yang berkemungkinan menyumbang kepada mekanisme adaptasi dan jangkitan berterusan. Kuantifikasi biofilem dilakukan menggunakan ujian kristal violet, manakala ekspresi gen biofilem dianalisis melalui qPCR terhadap gen sasaran biofilem, dan profil proteomik bakteria ditentukan menggunakan pendekatan kromatografi cecair–spektrometri jisim (LC-MS) serta analisis hiliran. Berdasarkan lengkung pertumbuhan bakteria, fasa log pertengahan bagi ketiga-tiga strain adalah pada jam 16. Strain-strain tersebut menunjukkan pertumbuhan biofilem yang signifikan ($p<0.05$) pada semua titik masa (24, 48 dan 72 jam), di mana PS_UMC083 menunjukkan pertumbuhan biofilem paling rendah pada semua selang masa (24 jam, 1.150±0.006; 48 jam, 1.415±0.077; dan 72 jam, 4.210±0.353). Strain RS_UMC114 pula mempunyai jumlah biofilem tertinggi pada 48 jam (3.482±0.372) dan 72 jam (10.51±0.641) pada OD_{570} berbanding dengan PS_UMC083 serta NI_UMC082 (48 jam; 2.075±0.201 dan 72 jam; 7.133±0.195). Hasil analisis reaksi berantai polimerase kuantitatif (qPCR) menunjukkan enam gen biofilem (*bpsl1607, bpsl1799, bpss0124, bpss0312, bpss1214* dan *bpss2016*) mengalami penurunan tahap pengungkapan dalam NI_UMC082 dan RS_UMC114 berbanding dengan PS_UMC083. Profil proteomik menunjukkan bahawa strain relaps RS_UMC114 memperlihatkan peningkatan ketara dalam protein virulen (contohnya BipD), pengawal selia pencerobohan (contohnya BsaR), serta protein oksidoreduktase dan tindak balas tekanan (contohnya SodB, DnaK, DnaJ, GrpE), yang mencadangkan fenotip berorientasikan kelangsungan hidup yang telah menyesuaikan diri dengan keadaan hos yang mencabar. Analisis pengayaan laluan KEGG dan protein hab turut menunjukkan bahawa RS_UMC114 diperkaya dengan laluan biosintetik, penyesuaian tekanan, dan metabolisme purin, konsisten dengan strategi kelangsungan jangka panjang. Sebaliknya, NI_UMC082 dicirikan oleh laluan motiliti dan kemotaksis, mencerminkan profil jangkitan akut. Secara keseluruhannya, penemuan ini menunjukkan bahawa protein virulen, oksidoreduktase, dan tindak balas tekanan mungkin menjadi pusat kepada mekanisme relaps *B. pseudomallei*, sekali gus memberikan pandangan baharu tentang adaptasi molekul yang mendasari jangkitan kronik.

ABSTRACT

Melioidosis, an infectious disease found in tropical countries, is caused by *Burkholderia pseudomallei*. *B. pseudomallei* is present in contaminated soil and water and is known to produce several virulence factors, including biofilm, which enhances its ability to withstand antibiotic treatment. Although the treatment of melioidosis primarily depends on antibiotic therapy, the ability of *B. pseudomallei* to persist within the host contributes to chronic infection and the potential for relapse. This study investigates how variations in biofilm formation, biofilm-associated gene expression, and proteomic profiles among three isolates, primary infection (PS_UMC083; ST51), new infection (NI_UMC082; ST1644), and relapse (RS_UMC114; ST51), may underlie bacterial adaptation and persistence. This study aims to characterise differences in biofilm production, gene expression related to biofilm development, and proteomic signatures that could be linked to long-term survival and recurrent infection. Biofilm formation was quantified using the crystal violet assay, biofilm-associated gene expression was assessed by quantitative polymerase chain reaction (qPCR) targeting selected genes, and proteomic profiling was performed using liquid chromatography–mass spectrometry (LC-MS) followed by downstream analyses. Based on the bacterial growth curve, the mid-log phase for all three strains occurred at 16 hours. All strains demonstrated significant biofilm formation ($p<0.05$) at all time points (24, 48, and 72 hours), with PS_UMC083 showing the lowest biofilm formation across all intervals (24 hrs: 1.150±0.006; 48 hrs: 1.415±0.077; 72 hrs: 4.210±0.353). RS_UMC114 exhibited the highest biofilm quantity at 48 hrs (3.482±0.372) and 72 hrs (10.51±0.641) at OD_{570} compared to PS_UMC083 and NI_UMC082 (48 hrs: 2.075±0.201; 72 hrs: 7.133±0.195). qPCR analysis revealed that six biofilm-related genes (*bpsl1607*, *bpsl1799*, *bpss0124*, *bpss0312*, *bpss1214*, and *bpss2016*) were downregulated in NI_UMC082 and RS_UMC114 compared to PS_UMC083. Proteomic profiling revealed that the relapse isolate RS_UMC114 exhibited marked upregulation of virulence proteins (e.g., BipD), invasion regulators (e.g., BsaR), and oxidoreductase/stress response proteins (e.g., SodB, DnaK, DnaJ, GrpE), suggesting a persistence-oriented phenotype adapted to hostile host conditions. KEGG pathway enrichment and hub protein analysis further demonstrated that RS_UMC114 is enriched in biosynthetic, stress adaptation, and purine metabolism pathways, consistent with long-term survival strategies. In contrast, NI_UMC082 was characterised by motility and chemotaxis pathways, reflecting an acute infection profile. Together, these findings indicate that virulence, oxidoreductase, and stress response proteins may be central to relapse in *B. pseudomallei*, providing new insight into the molecular adaptations underpinning chronic infection.

TABLE OF CONTENTS

		Page
DECLARATION		iii
ACKNOWLEDGEMENT		iv
ABSTRAK		v
ABSTRACT		vi
TABLE OF CONTENTS		vii
LIST OF TABLES		xiii
LIST OF ILLUSTRATIONS		xiv
LIST OF ABBREVIATIONS		xiv
CHAPTER I	**INTRODUCTION**	
1.1	Research Background	1
1.2	Problem Statement	2
1.3	Research Justification	3
1.4	Research Question	4
1.5	Research Hypothesis	4
1.6	Objective	4
	1.6.1 Main objective	4
	1.6.2 Specific objective	4
CHAPTER II	**LITERATURE REVIEW**	
2.1	*Burkholderia pseudomallei*: Genus Overview, Characteristics, and Virulence Factors	5
	2.1.1 *Burkholderia* genus	5
	2.1.2 *Burkholderia pseudomallei*	5
2.2	Melioidosis	12
	2.2.1 History of melioidosis	12
	2.2.2 History of melioidosis in Malaysia	12

UNIVERSITI KEBANGSAAN MALAYSIA

	2.2.3	Signs and symptoms of melioidosis	13
	2.2.4	Treatment	14
	2.2.5	*B. pseudomallei* antimicrobial resistance	15
	2.2.6	Risk factors and transmission of melioidosis	16
	2.2.7	Global epidemiology of melioidosis	17
	2.2.8	Epidemiology of melioidosis in Malaysia	18
	2.2.9	*B. pseudomallei* relapse strain identification and characterisation	19
	2.2.10	Malaysian paediatric case distribution	20
2.3		Chronic Melioidosis in a Paediatric Patient: A Case of Relapse and Co-colonisation with Multidrug-Resistant Pathogens	21
2.4		*B. pseudomallei* Proteomics Using LC-MS approach	23
CHAPTER III		**METHODOLOGY**	
3.1		*B. pseudomallei* Clinical Strains Cultivation	28
3.2		*B. pseudomallei* Clinical Strains Identity Confirmation Test	28
	3.2.1	Ashdown agar (phenotypic confirmation)	28
	3.2.2	Polymerase chain reaction and gel electrophoresis (genotypic confirmation)	29
3.3		*B. pseudomallei* Clinical Strains Bacterial Growth Curve	32
3.4		*B. pseudomallei* Clinical Strains Biofilm Formation Quantification	34
3.5		*B. pseudomallei* Clinical Strains Biofilm Gene Expression	35
	3.5.1	Polymerase chain reaction and gel electrophoresis	35
	3.5.2	*B. pseudomallei* RNA extraction	35
	3.5.3	RNA integrity validation using denaturing gel electrophoresis	39
	3.5.4	*B. pseudomallei* cDNA conversion	39
	3.5.5	*B. pseudomallei* quantitative PCR (qPCR)	40
3.6		Proteomics of *B. pseudomallei* Clinical Strains	42
	3.6.1	*B. pseudomallei* protein extraction and Bradford assay	42

UNIVERSITI KEBANGSAAN MALAYSIA

	3.6.2	Sodium dodecyl sulphate-polyacrylamide gel electrophoresis	43
	3.6.3	Liquid chromatography-mass spectrometry and downstream analysis	44
	3.6.4	Comprehensive proteomic analysis of all three *B. pseudomallei* strains	46

CHAPTER IV RESULTS

4.1		*B. pseudomallei* confirmation Test	50
	4.1.1	Phenotypic confirmation of strains PS_UMC114, NI_UMC082 and RS_UMC114 through Ashdown agar cultivation	50
	4.1.2	Genotypic confirmation of strains PS_UMC114, NI_UMC082 and RS_UMC114 through polymerase chain reaction	51
4.2		Bacterial Growth Curve and CFU of Strains PS_UMC083, NI_UMC082 and RS_UMC114	53
4.3		Biofilm Quantification of Strains PS_UMC083, NI_UMC082 and RS_UMC114	56
4.4		Quantification of Biofilm Gene Expression of all Three *B. pseudomallei* Clinical Strains	57
	4.4.1	Biofilm gene confirmation of all three *B. pseudomallei* clinical strains through PCR	57
	4.4.2	qPCR annealing temperature optimisation	59
	4.4.3	RNA integrity validation for cDNA conversion using gel electrophoresis	62
	4.4.4	qPCR gene expression analysis	63
4.5		Proteomics Analysis to Determine Differentially Expressed Proteins in all Three *B. pseudomallei* Clinical Isolates	65
	4.5.1	Bradford assay of all three *B. pseudomallei* strains	65
	4.5.2	SDS PAGE of all three *B. pseudomallei* strains at different protein concentrations	66

UNIVERSITI KEBANGSAAN MALAYSIA

4.5.3	Overview of proteomic profiles of PS_UMC083, NI_UMC082 and RS_UMC114	68
4.5.4	Comparative proteomic analysis	76

CHAPTER V DISCUSSION

5.1	Comparative Analysis of Biofilm Formation Across *B. pseudomallei* Clinical Isolates	108
5.2	Comparative Expression of Biofilm-Related Genes in *B. pseudomallei* Clinical Isolates	109
5.3	Differential Expression of Proteins Across PS_UMC083, NI_UMC082 and RS_UMC114	110
5.3.1	Overview of proteomic characterisation of all three *B. pseudomallei* strains	110
5.3.2	Differential protein expression between NI_UMC082 vs PS_UMC083	111
5.3.3	Differential protein expression between RS_UMC114 vs PS_UMC083	115
5.3.4	Comparative KEGG pathway analysis of *B. pseudomallei* clinical strains	119
5.3.5	Identification and functional characterisation of hub proteins in *B. pseudomallei* clinical isolates	120

CHAPTER VI CONCLUSION AND FUTURE WORKS

6.1	Conclusion	123
6.2	Study Limitations	126
6.3	Future Works	127

REFERENCES 129

UNIVERSITI KEBANGSAAN MALAYSIA

APPENDICES

APPENDIX A	Media, Buffers and Reagent Preparations	141
APPENDIX B	Proteomics Preparation	143
APPENDIX C	Supplementary Data	145
APPENDIX D	Conferences Attended and Manuscripts in Preparation	150

UNIVERSITI KEBANGSAAN MALAYSIA

LIST OF TABLES

Table No.		Page
Table 2.1	Key virulence factors of *B. pseudomallei*: roles and mechanisms	10
Table 2.2	Overview of LC-MS proteomic studies on *B. pseudomallei* isolates: methodologies, analytical tools, and key findings	26
Table 3.1	*B. pseudomallei* genus and species-specific primer list	30
Table 3.2	*B. pseudomallei* biofilm genes primer list	38
Table 3.3	Dilution series and starting concentration for biofilm primers	40
Table 4.1	Morphological observations of clinical strains PS_UMC083, NI_UMC082 and RS_UMC114 on Ashdown agar	50
Table 4.2	Neat protein concentration of all three *B. pseudomallei* strains	65
Table 4.3	Overview of unique proteins identified across all three *B. pseudomallei* clinical strains	69
Table 4.4	List of top 20 proteins with the highest iBAQ intensity across all three *B. pseudomallei* clinical strains	74
Table 4.5	Differentially expressed proteins in comparison group NI_UMC082 vs PS_UMC083 with functional roles or disease pathway associations	84
Table 4.6	Biofilm-associated proteins differentially expressed in comparison group NI_UMC082 vs PS_UMC083, identified based on UniProt annotations and related literature	86
Table 4.7	Differentially expressed proteins in comparison group RS_UMC114 vs PS_UMC083 with functional roles or disease pathway associations	94
Table 4.8	Biofilm-associated proteins differentially expressed in comparison group RS_UMC114 vs PS_UMC083, identified based on UniProt annotations and related literature	97
Table 4.9	Regulatory pathways enriched across infection stages and regulatory profiles of *B. pseudomallei* clinical strains	99
Table 4.10	Regulatory pathways associated with persistence and biofilm formation enriched across infection stages and regulatory profiles of *B. pseudomallei* clinical strains	102

UNIVERSITI KEBANGSAAN MALAYSIA

Table 4.11 High-degree hub proteins from group-specific protein–protein interaction networks 105

UNIVERSITI KEBANGSAAN MALAYSIA

LIST OF ILLUSTRATIONS

Figure No.		Page
Figure 2.1	Microscopic observation of *B. pseudomallei* on a Gram stain	6
Figure 2.2	Genomic reconstruction of chromosome 1 and chromosome 2 of *B. pseudomallei* strain K96243	7
Figure 2.3	Global distribution of melioidosis cases in humans, 1911-2020	17
Figure 2.4	The major states reporting melioidosis cases are shown on the map of Malaysia	18
Figure 2.5	Progression of the Malaysian paediatric melioidosis case study	22
Figure 3.1	Flowchart of phenotypic and genotypic confirmation of the clinical strains	31
Figure 3.2	Miles and Misra dilution method	33
Figure 3.3	Experimental workflow for bacterial growth curve and CFU quantification	33
Figure 3.4	Overall project methodology flowchart	49
Figure 4.1	PCR-Based genotypic confirmation of *B. pseudomallei* clinical isolates (PS_UMC083, NI_UMC082, RS_UMC114) visualized via gel electrophoresis	52
Figure 4.2	Growth curve of *B. pseudomallei* strains PS_UMC083, NI_UMC082 and RS_UMC114 at 37 ^{o}C 180 rpm over 24 hours	54
Figure 4.3	Comparative CFU growth curve of strains PS_UMC083, NI_UMC082, and RS_UMC114 over 24 hours	55
Figure 4.4	Biofilm quantification of *B. pseudomallei* clinical strains PS_UMC083, NI_UMC082, and RS_UMC114 at 24, 48, and 72 hours, measured at OD_{570}	56
Figure 4.5	Biofilm gene confirmation of PS_UMC083, NI_UMC082, and RS_UMC114 visualized via gel electrophoresis	58
Figure 4.6	Optimisation of PCR annealing temperatures for quantitative gene expression analysis in *B. pseudomallei*	61
Figure 4.7	Gel electrophoresis of PS_UMC083, NI_UMC082, and RS_UMC114 RNA samples for RNA integrity validation prior to cDNA conversion	62

UNIVERSITI KEBANGSAAN MALAYSIA

Figure 4.8	qPCR gene expression analysis of eight biofilm-related genes in *B. pseudomallei* strains NI_UMC082 and RS_UMC114, relative to PS_UMC083 after 16 hours of culture	64
Figure 4.9	SDS-PAGE profile of total soluble protein extracts from PS_UMC083, NI_UMC082, and RS_UMC114 at varying concentrations	67
Figure 4.10	Venn diagram of total proteins identified across strains PS_UMC083, NI_UMC082, and RS_UMC114	68
Figure 4.11	Heatmaps of differentially expressed proteins between NI_UMC082 and PS_UMC083	78
Figure 4.12	Functional classification of the differentially expressed upregulated proteins between NI_UMC082 and PS_UMC083	81
Figure 4.13	STRING prediction of the protein–protein interaction (PPI) networks for the differentially expressed upregulated (a) and downregulated (b) proteins between NI_UMC082 and PS_UMC083	82
Figure 4.14	Heatmaps of differentially expressed proteins between RS_UMC114 and PS_UMC083	88
Figure 4.15	Functional classification of the differentially expressed upregulated proteins between RS_UMC114 and PS_UMC083	91
Figure 4.16	STRING prediction of the protein–protein interaction (PPI) networks for the differentially expressed upregulated (a) and downregulated (b) proteins between RS_UMC114 and PS_UMC083	92
Figure 4.17	Protein–protein interaction (PPI) network of hub proteins identified across all experimental groups	106
Figure 4.18	KEGG pathways enriched among hub proteins in comparison group RS_UMC114 vs PS_UMC083	107

UNIVERSITI KEBANGSAAN MALAYSIA

LIST OF ABBREVIATIONS

ABR	Antibiotic resistance
AMK	Amikacin
AMP	Ampicillin
AMP	Adenosine Monophosphate
AMR	Antimicrobial resistance
ANOVA	Analysis of Variance
AZM	Azithromycin
CAP	Chloramphenicol
CAZ	Ceftazidime
CDC	Centers for Disease Control
c-di-GMP	Cyclic diguanylic acid
CDNA	Complementary DNA
CFU	Colony forming unit
dH_2O	Distilled water
DMSO	Dimethyl sulfoxide
DNA	Deoxyribonucleic acid.
DOX	Doxycycline
DTT	Dithiothreitol
e.g.	(Exempligratia): for example
EB	Electrophoresis buffer
EDTA	Ethylenediaminetetraacetic acid
EPS	Exopolysaccharides
et al.	(Et alia): and others
FDR	False discovery rate
GEN	Gentamicin
HPLC	High-performance liquid chromatography
LB	Luria Bertani
LDH	Lactate dehydrogenase
LC-MS	Liquid chromatography- Mass Spectrometry
LFQ	Label-free quantification
LPS	Lipopolysaccharides
MDR	Multidrug resistance
MGVI	Malaysian Genomic and Vaccine Institute

UNIVERSITI KEBANGSAAN MALAYSIA

min	Minute
MLST	Multi-locust sequence typing
MRP	Meropenem
MRSA	Methicillin-resistant *Staphylococcus aureus*
MS	Mass spectrometry
NA	Nutrient agar
OD	Optical density
PANTHER	Protein Analysis Through Evolutionary Relationships
PBS	Phosphate-buffered saline
PCN	Penicillin
PCR	Polymerase chain reaction
PPI	Protein-protein interaction
PTM	Post-translational modifications
QS	Quorum sensing
RNA	Ribonucleic acid
ROS	Reactive oxygen species
RSLC	Rapid separation liquid chromatography
SD	Standard deviation
SDS-PAGE	Sodium dodecyl sulphate-polyacrylamide gel electrophoresis
sec	Seconds
ST	Sequence type
STRING	Search Tool for the Retrieval of Interacting Genes/Proteins
TAE	Tris-acetate-ethylenediaminetetraacetic acid
TE	Tris-ethylenediaminetetraacetic acid
TFA	Trifluoroacetic acid
TMP-SMX	Trimethoprim-sulfamethoxazole
UMMC	Universiti Malaya Medical Centre
USA	United States of America
USAMRU	United States of America Medical Research Unit

UNIVERSITI KEBANGSAAN MALAYSIA

CHAPTER I

INTRODUCTION

1.1 Research Background

Burkholderia pseudomallei causes melioidosis, a potentially life-threatening disease endemic in Southeast Asia, including Malaysia (Allwood et al. 2011). Treatment for melioidosis relies solely on antibiotics, though there are many cases of persistence and relapse where the antibiotics fail to eradicate the bacteria, leading to chronic melioidosis (Wiersinga et al. 2018). Prolonged antibiotic treatment can halt the infection; however, 2.6% - 19% of patients in Malaysia still experience clinical recurrence of melioidosis (Nathan et al. 2018). New infection strains may cause recurrent cases of melioidosis, and relapse cases can occur when *B. pseudomallei* strains inhabit the host cells, evading host-immune response and antibiotic treatment.

While prolonged antibiotic treatment can control the infection, the persistence of *B. pseudomallei* within host cells poses significant challenges, leading to both recurrent and relapsed cases. This is particularly concerning in chronic paediatric melioidosis patients, where relapse can occur even after initial treatment. A recent study by Mariappan et al. (2018) has discovered notable differences between a primary (PS_UMC083), new infection (NI_UMC082) and relapse (RS_UMC114) isolates in a chronic paediatric melioidosis patient with cystic fibrosis. These variances include differences in strain type, where both PS_UMC083 and RS_UMC114 shared the same sequence type (ST) (ST51), while NI_UMC082 is of a different ST (ST1644). In addition to differences in sequence types, the strains also exhibited distinct phenotypic characteristics. Notably, resistance to key antibiotics, including amoxicillin-clavulanate, co-trimoxazole, and doxycycline, was observed, along with the coexistence of other bacterial pathogens, further complicating disease management in this patient.

Based on these observations, to gain a deeper understanding of the relapse mechanisms in *B. pseudomallei* chronic infections, it is crucial to investigate biofilm formation and gene expression, and proteomics profiles across PS_UMC083, NI_UMC082 and RS_UMC114, to elucidate their similarities and differences.

Biofilm formation and gene expression were quantified in all three *B. pseudomallei* clinical strains to examine differences in biofilm production and gene expression levels between PS_UMC083, NI_UMC082 and RS_UMC114. Given the established link between biofilm formation and relapse, as reported by Limmathurotsakul et al. (2014), investigating biofilm production could provide valuable insights into its role during relapse. Additionally, analysing biofilm-associated gene expression may uncover the regulation of these genes in relapse strains that have not been previously explored. Furthermore, liquid chromatography-mass spectrometry (LC-MS) was utilised to analyse the total protein profiles of all three strains, aiming to compare the proteomic profiling. A comparative proteomic analysis was conducted to identify proteins that may be uniquely expressed in PS_UMC083, NI_UMC082 and RS_UMC114, which may help to identify key factors contributing to persistence and adaptation. Discovering differential protein expressions is expected to provide new insights into the pathogenic persistence and relapse of melioidosis. Furthermore, comparing biofilm gene expression with proteomics data offers a thorough understanding of how variations in gene expression may lead to changes in protein production, shedding light on the molecular mechanisms of biofilm formation and its possible involvement in relapse.

1.2 Problem Statement

The mechanisms behind *B. pseudomallei* pathogenic persistence and adaptation during relapse infections remain poorly understood. The bacterium's ability to survive intracellularly and produce biofilms likely contributes to its persistence in relapse cases. However, there is a gap in knowledge on the specific factors involved in the relapse of *B. pseudomallei*, particularly in paediatric populations in Malaysia. This gap is further highlighted by Limmathurotsakul et al. (2014), who identified a link between biofilm formation and the relapse of melioidosis. However, their study did not quantify the

expression of biofilm-related genes or perform proteomic profiling to compare differentially expressed proteins between primary and relapse isolates, leaving many of the underlying factors uncharacterised.

While biofilm formation has been implicated in relapse, emerging evidence also points to genetic alterations that may enhance virulence. For instance, Seng et al. (2023) reported mutations in *tssB-5*, a critical component of the type VI secretion system (T6SS), in relapse-associated strains, suggesting that such mutations may contribute to persistence and pathogenicity during recurrent infections. However, this study emphasised proteomic analysis, which could provide further insight into differential protein expression between primary and relapse isolates. Building on this, Velapatino et al. (2012) identified differentially expressed proteins in primary and relapse isolates of *B. pseudomallei*; however, they did not focus on paediatric patients, nor did they investigate biofilm quantification or the expression of biofilm-related genes, which are key factors in relapse mechanisms.

Given the limited research on paediatric relapse strains and their unique characteristics, there is a significant gap in understanding the factors contributing to relapse. Thus, a more comprehensive investigation of *B. pseudomallei*'s phenotypic and proteomic factors in paediatric relapse, particularly related to biofilm formation and intracellular persistence factors, is urgently needed to improve treatment strategies for these cases.

UNIVERSITI KEBANGSAAN MALAYSIA

1.3 Research Justification

Quantification of biofilm formation and biofilm gene expression, and the elucidation of differential proteomic levels between primary, new infection and relapse isolates may increase our understanding of the relapse mechanisms in chronic melioidosis infections despite antibiotic treatment.

1.4 Research Question

1. What are the differences in biofilm formation quantities between PS_UMC083, NI_UMC082, and RS_UMC114?
2. How does the expression of biofilm-related genes differ between PS_UMC083, NI_UMC082, and RS_UMC114?
3. How does the proteome differ between PS_UMC083, NI_UMC082, and RS_UMC114?

1.5 Research Hypothesis

B. pseudomallei relapse infections arise from distinct molecular adaptations rather than simple persistence of the primary strain. Specifically, variations in biofilm formation, differential regulation of biofilm-associated genes, and altered proteomic profiles are hypothesised to drive pathogenic persistence and relapse potential, despite antibiotic treatment. Identifying these molecular signatures will clarify whether biofilm activity and protein-level changes constitute key mechanisms linking chronic infection to relapse.

1.6 Objective

1.6.1 Main objective

To elucidate the mechanisms of adaptation and pathogenic persistence in *B. pseudomallei* by investigating biofilm formation, biofilm-associated gene expression, and proteomic profiles across clinical isolates PS_UMC083, NI_UMC082, and RS_UMC114.

1.6.2 Specific objective

1) To quantify the biofilm formation between PS_UMC083, NI_UMC082 and RS_UMC114.
2) To quantify the expression of biofilm-related genes between PS_UMC083, NI_UMC082 and RS_UMC114.
3) To determine the *B. pseudomallei* proteins which are differentially expressed in PS_UMC083, NI_UMC082 and RS_UMC114.

UNIVERSITI KEBANGSAAN MALAYSIA

CHAPTER II

LITERATURE REVIEW

2.1 *Burkholderia pseudomallei*: Genus Overview, Characteristics, and Virulence Factors

2.1.1 *Burkholderia* genus

The genus *Burkholderia* was first described in 1950 by Walter H. Burkholder, who identified *Burkholderia cepacia* (originally called *Pseudomonas cepacia*) as the bacterium responsible for onion bulb rot (Burkholder 1950). The genus *Burkholderia* was previously classified as the genus *Pseudomonas*, but it was reclassified due to advancements in research on the genus (Burkholder 1950). Genus *Burkholderia* is very different to genus *Pseudomonas* because they have larger genomes, high metabolic versatility and the ability to thrive in various environments (Mahenthiralingam et al., 2005). *Burkholderia* are closely related to other genera within the family Burkholderiaceae, such as *Paraburkholderia*, *Ralstonia*, and *Cupriavidus* (Estrada-de Los Santos et al. 2013). However, *Burkholderia* species are unique in their potential to cause disease in humans, animals, and plants.

2.1.2 *Burkholderia pseudomallei*

Burkholderia pseudomallei is a major human pathogen and the causative agent of melioidosis (Dance 1991). It also affects animals, causing disease in various species, including mammals, reptiles, and birds. The bacteria have been renamed multiple times since they were first discovered, from *Bacterium whitmori, Malleomyces pseudomallei, Loefflerella pseudomallei, Pfeifferella whitmori, Pseudomonas pseudomallei* and finally, named *B. pseudomallei* in 1992 (Centers for Disease Control 2023).

UNIVERSITI KEBANGSAAN MALAYSIA

a. Characteristics of *B. pseudomallei*

B. pseudomallei is a gram-negative, motile, facultative aerobic, non-spore-forming, rod-shaped bacterium (Figure 2.1). It is commonly found in soil, muddy areas and polluted water (Allwood et al. 2011). During the stationary phase of growth, *B. pseudomallei* cells typically appear as short rod-shaped bacilli, with sizes averaging approximately 1.2 μm (Pitt., 1995). *B. pseudomallei* grows optimally at temperatures ranging from 37 – 42 ˚C and a pH of 6.5 – 7.5 (Chen et al. 2003). *B. pseudomallei* is classified as a tier 1 bioterrorism agent by the Centers for Disease Control and Prevention (CDC) because of its ability to spread via aerosol, contributing to its high infection rate (Butler 2012). Morphologically, *B. pseudomallei* has high phenotypic plasticity and multiple mixed morphologies among clinical strains and can exhibit wrinkled and rough textures and dry or mucoid colonies (Chantratita et al. 2007). *B. pseudomallei* colonies display a purplish colour when grown on Ashdown's agar, a selective medium agar for *B. pseudomallei* growth (Ashdown 1979).

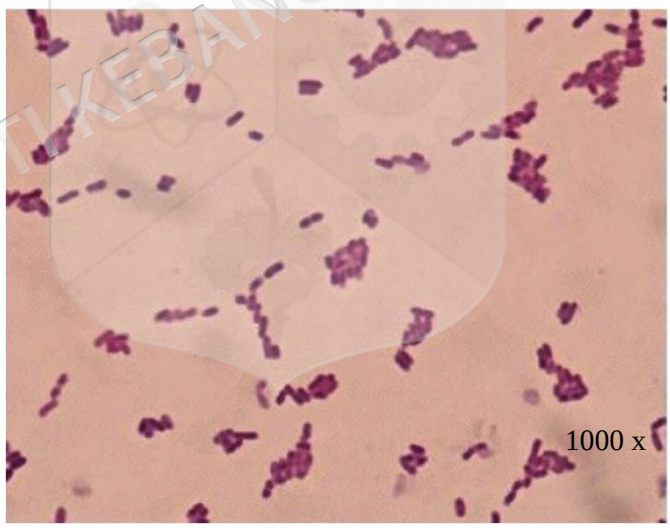

Figure 2.1 Microscopic observation of *B. pseudomallei* on Gram stain

Source: Zainal et al. 2017

B. pseudomallei has two chromosomes, which comprise over 7.2 Mb of genomic content, making it one of the largest genomes among bacterial species (Figure 2.2)

UNIVERSITI KEBANGSAAN MALAYSIA

(Holden et al. 2004). Chromosome one houses the core functions for cell growth, cell metabolism, lipoprotein, protein and RNA production and many other essential functions. Chromosome 2 contains genetic information for secondary metabolism, drug resistance, adaptation, as well as virulence factors (Holden et al. 2004). *B. pseudomallei* also has multiple genomic islands and mobile genetic elements isolates contributing to its genomic plasticity and strain variance among species across different geographical regions (Limmathurotsakul & Peacock 2011). This genomic plasticity greatly affects virulence and antibiotic resistance (ABR) among strains. It plays a vital role in intracellular living, evading host-killing mechanisms, antimicrobial resistance (AMR) and perhaps even relapse (Ghazali et al. 2021).

Genotyping approaches have been developed to support species-level identification and differentiation of *B. pseudomallei* from other *Burkholderia* species. Suppiah et al. (2010) reported the use of conserved and species-specific genetic markers, notably the *groEL* and *mprA* genes, for molecular confirmation. The *groEL* gene serves as a genus-specific marker targeting conserved regions within the *Burkholderia* genus, while *mprA* is uniquely associated with *B. pseudomallei*, enabling precise species-level identification. These molecular tools have enhanced diagnostic accuracy and are widely adopted in clinical and environmental studies involving *B. pseudomallei*.

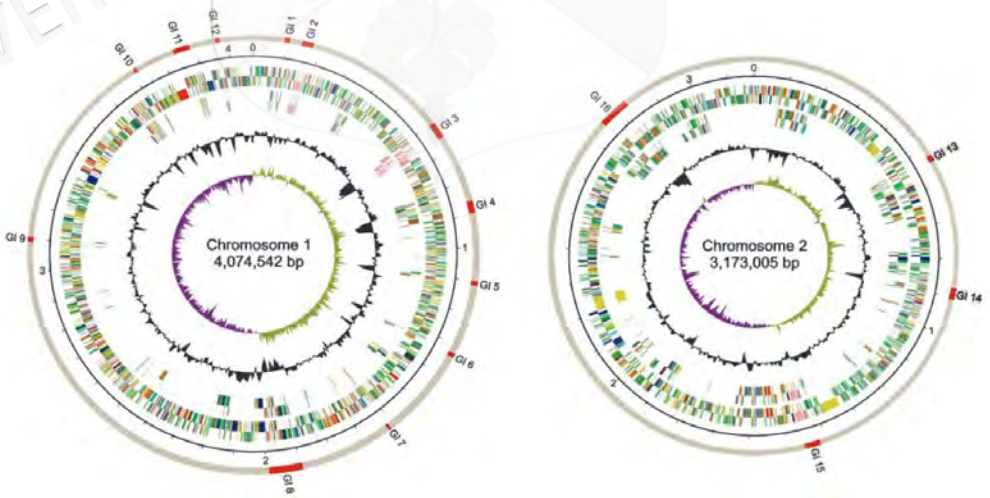

Figure 2.2 Genomic reconstruction of chromosome 1 and chromosome 2 of *B. pseudomallei* strain K96243

Source: Holden et al. 2004

UNIVERSITI KEBANGSAAN MALAYSIA

b. *B. pseudomallei* virulence factors

i. Virulence factors of *B. pseudomallei* and mechanisms of host evasion

B. pseudomallei possesses a variety of virulence factors that support its survival, persistence, and pathogenicity. It is encapsulated and contains lipopolysaccharides (LPS) in its cell wall, which aid in evading host immune defences (Wiersinga et al. 2012). The bacterium is also motile, utilising flagella to move within the host and adhere to surfaces. Adhesins and invasins are also produced by *B. pseudomallei* to facilitate attachment to and invasion of host cells (Cheng et al. 2005). These virulence factors are paramount for the ability of *B. pseudomallei* to initiate an infection and propagate within the host.

B. pseudomallei also uses the type III and T6SS, which contribute to its survival inside host cells and its ability to spread. These systems enable the bacterium to inject effector proteins into host cells, avoiding host-cell killing and allowing the bacterium to replicate within immune cells, such as neutrophils and macrophages (Cullinane et al. 2008; Lennings et al. 2019). *B. pseudomallei* can resist the killing mechanisms triggered by phagocytosis and invade the host cytoplasm, leading to the formation of multinucleated giant cells (MNGCs), further promoting its spread within the body (Lennings et al. 2019).

Another important aspect of *B. pseudomallei* virulence is its production of exoenzymes, including lipases, proteases, and other enzymes, which contribute to tissue damage, immune evasion, and pathogenesis (Mangalea et al. 2017). Along with these factors, *B. pseudomallei* also produces biofilm, which is key for persistence and antibiotic resistance.

ii. *B. pseudomallei* biofilm formation

B. pseudomallei forms biofilms, which play a critical role in its pathogenicity, environmental survival and relapse (Limmathurotsakul et al. 2014). The formation of biofilm aids *B. pseudomallei* in its resistance to harsh environmental conditions such as high temperatures, acidity, and desiccation, ensuring its survival in soil and water (Wiersinga et al. 2012). *B. pseudomallei* biofilm formation, similar to other biofilm-forming bacteria, is formed through a series of five steps (phases I-V) (Kostakioti et al.

UNIVERSITI KEBANGSAAN MALAYSIA

2013). In phase I, planktonic cells attach to a surface; phase II involves colonisation and the initiation of protein, exopolysaccharides (EPS) and extracellular DNA (eDNA) production. The release of extracellular DNA in the formation of biofilm promotes bacterial adhesion in *B. pseudomallei* biofilm formation (Kim et al. 2017). During phase III, the bacteria divide and develop the biofilm, with quorum sensing playing a key role in cell-to-cell communication. This results in the reversible attachment turning into an irreversible attachment and biofilm maturation (phase IV). At this point, the biofilm is at its most robust with a proper EPS shield to reduce the penetrative capabilities of antibiotics. In the final step (phase V), the bacteria disperse in the search for new surfaces to colonise (Kostakioti et al. 2013; Tolker-Nielsen 2015). *B. pseudomallei* EPSs in biofilms act as a shield to prevent antibiotic diffusion, mitigating the effectiveness of the antibiotics (Mangalea et al. 2017).

Quorum sensing (QS) plays a significant role in regulating biofilm formation in *B. pseudomallei*. This signal transduction pathway involves the production of N-acyl-homoserine lactones (AHLs), which coordinate the expression of genes involved in biofilm formation, ABR, and other virulence factors (Truong et al. 2015; Utari et al. 2018). The intracellular signalling molecule cyclic diguanylic acid (c-di-GMP) also plays a key role in biofilm formation, promoting the production of LPS, exoenzymes, and adhesins while inhibiting motility, thus enhancing bacterial adhesion (Fazli et al. 2014; Plumley et al. 2017). EPS production and the regulation of biofilm formation by QS and c-di-GMP contribute to *B. pseudomallei's* resistance to antimicrobial agents and its role in the relapse of melioidosis (Limmathurotsakul et al. 2014). The virulence factors of *B. pseudomallei* are tabulated in Table 2.1, highlighting their role and mechanism in the pathogenicity of *B. pseudomallei* infections.

Recent transcriptomic studies have further expanded our understanding of biofilm regulation in *B. pseudomallei*. Chin et al. (2015) performed a global transcriptional analysis comparing high and low biofilm-producing strains, identifying genes such as *bpsl0618*, *bpsl1705*, *bpsl1607*, *bpsl1799*, *bpss0124*, *bpss0312*, *bpss1214*, and *bpss2016* that were upregulated in high biofilm producers. These genes are involved in diverse cellular functions, including membrane transport, signal transduction, and stress response, although their direct roles in biofilm formation remain to be fully characterised. Their differential expression under biofilm-inducing conditions suggests

UNIVERSITI KEBANGSAAN MALAYSIA

a potential contribution to biofilm phenotype and persistence. In parallel, Chen et al. (2011) explored the regulatory dynamics of the T6SS during *B. pseudomallei* infection and noted that biofilm-inducing conditions modulate T6SS gene expression. Their study employed *dnak* and *16S rRNA* as housekeeping genes for qPCR normalisation, providing a stable reference for transcriptional comparisons.

These studies provide insight into how *B. pseudomallei* may regulate biofilm formation under different conditions, with implications for its survival, virulence, and potential to persist during infection.

UNIVERSITI KEBANGSAAN MALAYSIA

Table 2.1 Key virulence factors of *B. pseudomallei*: roles and mechanisms

Key virulence factors	**Function in pathogenicity**	**Mechanisms of action**	**References**
Biofilm formation	Survival, persistence and AMR	Forms a protective EPS matrix that shields against antibiotics and host defences.	Mangalea et al. 2017
Quorum sensing	Cell-to-cell communication in biofilms	Regulates gene expression, EPS production, and biofilm development via AHLs.	Fazli et al. 2014; Plumley et al. 2017; Truong et al. 2015; Utari et al. 2018
Type III secretion system	Intracellular survival	Injects effector proteins into host cells to evade immune responses and establish infection.	Stevens et al. 2002; Stevens et al. 2003; Stevens et al. 2004
Type VI secretion system	Host cell fusion	Utilises host actin to form MNGCs, aiding bacterial spread and evasion of immune responses.	Lennings et al. 2019
Capsule	Anti-phagocytosis	Prevents opsonisation and recognition by immune cells, aiding in immune evasion.	Reckseidler et al., 2001
Adhesin	Adherence	Binds to host cell surfaces, facilitating colonisation and infection.	Berne et al., 2015
Invasins	Invasion	Facilitates entry into host cells by interacting with host cell receptors.	Lee et al., 2010
Flagella	Motility	Promotes movement within host tissues and aids in surface colonisation.	Rao et al. 2024

UNIVERSITI KEBANGSAAN MALAYSIA

2.2 Melioidosis

2.2.1 History of melioidosis

The term "melioidosis" was first introduced in 1921 by A.T. Stanton and W. Fletcher (Stanton & Fletcher 1921). It is derived from the Greek word *melis*, which refers to "a distemper of asses," combined with the suffixes *-oid* (meaning resemblance) and *-osis* (indicating a condition). Melioidosis, also known as Whitmore disease, was first discovered in Rangoon, Myanmar, in 1911 by Alfred Whitmore and his assistant C.S. Krishnaswami. They described melioidosis as a “glanders-like” disease diagnosed in morphine addicts (Whitmore & Krishnaswami 1912). They identified a novel bacterium that could be isolated from autopsy specimens on potato slopes and peptone agar. As melioidosis was clinically akin to glanders, its relatively fast growth and absence of the Strauss response when injected into guinea pigs allowed the differentiation of this novel bacterium from the organism causing glanders (Whitmore & Krishnaswami 1912). Their postulation that this novel bacterium was closely related to the one causing glanders based on its characteristics was proven correct through recent genomic studies (Godoy et al. 2003; Holden et al. 2004).

2.2.2 History of melioidosis in Malaysia

Melioidosis was discovered in Malaysia in the year 1913 by William Fletcher. He reported cases of melioidosis in guinea pigs and rabbits at the Institute for Medical Research, Kuala Lumpur (Stanton & Fletcher 1925). It has since been an endemic disease in Malaysia. The first clinical case of melioidosis in a patient from Kuala Lumpur was discovered in the year 1917 by Ambrose Thomas Stanton (Stanton and Fletcher 1924). Together, Fletcher and Stanton reported over 39 cases of melioidosis in Malaysia (Thin et al. 1970). Melioidosis cases were not documented throughout the years 1950 to 1960s, possibly due to World War II, and only resurfaced after environmental surveillance and sero-surveillance conducted by the United States of America Medical Research Unit (USAMRU) (Strauss et al. 1967; Strauss et al. 1969a; Strauss et al. 1969b; Strauss et al. 1969c). From the sero-surveillance study, Kedah and Sabah documented the highest seroprevalence. *B. pseudomallei* isolates were also discovered in the soil and water in a few states in Malaysia. (Strauss et al. 1967; Strauss et al. 1969a; Strauss et al. 1969c).

UNIVERSITI KEBANGSAAN MALAYSIA

Cases of animal melioidosis in Malaysia have also been reported since 1921 by Stanton and Fletcher (Stanton & Fletcher 1932). Apart from guinea pigs and rabbits, melioidosis has been reported in livestock and house pets such as cats and dogs (Lim et al. 2015; Mustaffa & Nor, 1994; Naama et al. 2012; Puthucheary 2009). Primates such as orangutans, pig-tailed macaques, spider monkeys and gibbons have also shown positive signs of melioidosis (Vellayan 1994). So far, only one zoonotic transmission case has been reported in 1998 by Idris et al from sheep to humans. As *B. pseudomallei* is highly virulent, zoonotic transmission should not be underestimated. Management of animal melioidosis and control should be tightened to prevent outbreaks from environmental contamination.

2.2.3 Signs and symptoms of melioidosis

Patients infected with *B. pseudomallei* experience either acute or chronic infections and, in some cases, latent infections. Approximately 85% of patients show acute symptoms (Limmathurotsakul et al. 2016), 10% exhibit chronic symptoms, while 5% of cases are latent (Wiersinga et al. 2018). Among these cases, 85%-95% involve adult patients while 5%-15% are paediatric (Sanderson et al. 2014). Immunocompetent patients might not exhibit any symptoms although infected by *B. pseudomallei* and some cases lead to relapse infections after exposure to a new strain or activation of the bacteria latently (Wiersinga et al. 2018). *B. pseudomallei* infections can lie latent in the human body for 19-29 years with a high relapse rate despite continuous antibiotic treatment. Unfortunately, the mechanisms that make *B. pseudomallei* difficult to eradicate in humans despite antibiotic treatment have not been fully understood due to its large genome size and plasticity, which houses multiple redundancies to its pathogenesis (Bzdyl et al. 2022; Limmathurotsakul et al. 2016).

Acute melioidosis exhibits acute septicaemia with a high mortality rate and acute blood infections leading to septic shock (Wiersinga et al. 2018). Acute melioidosis is usually accompanied by a fever and manifests as an acute lung infection and acute bacteraemia, or soft tissue infection. Infections involving non-skeletal tissue that surrounds or supports organs, as well as other structures such as blood vessels, lymph nodes, subcutaneous tissue, muscle, and soft tissue organs (such as the liver or spleen), are referred to as soft tissue infections. Chronic melioidosis, however, has multiple

UNIVERSITI KEBANGSAAN MALAYSIA

infection sites showing caseous or suppurative wounds at the joints, skin, lymph nodes, lungs, heart and brain, manifesting as persistent skin ulcers or abscesses, persistent pneumonia, or a disseminated infection that developed into sepsis. The bacteria can live intracellularly in the reticuloendothelial systems or in macrophages, which can lead to latent, recurrent or relapsed infections (Wiersinga et al. 2018).

Latent infections occur when *B. pseudomallei* remain in a dormant state within host cells, avoiding detection by the immune system and evading the effects of antibiotics for extended periods. These dormant bacteria can become active again when conditions are favourable for bacterial growth (immunocompromised patients), leading to symptoms reappearing (Currie et al. 2000). Recurrent infections result from incomplete eradication of the bacteria during initial antibiotic treatment, with *B. pseudomallei* utilising strategies such as biofilm formation and persistence within host cells to resist antibiotic action (Limmathurotsakul et al. 2014). Recurrent infections may also occur when *B. pseudomallei* of a different strain type infects the patient. Relapse cases occur when the original strain re-emerges after an apparent resolution or negative diagnosis of the primary infection. Mechanisms like biofilm production and intracellular survival play a significant role in the bacteria's persistence (Pinweha et al. 2018). Relapse is of particular concern in paediatric cases, as there is limited research on the proteomic and genomic alterations associated with paediatric relapse strains, leaving significant gaps in our understanding of their pathogenesis and effective management.

UNIVERSITI KEBANGSAAN MALAYSIA

2.2.4 Treatment

Early treatment was largely ineffective, with sulfonamides and other broad-spectrum antibiotics failing due to *B. pseudomallei* innate resistance (Dance 1991). Penicillin (PCN) and chloramphenicol (CAP) also were ineffective, contributing to high mortality, especially in immunocompromised patients (Ciornei et al. 2003). Ceftazidime (CAZ) was introduced in the 1980s, significantly reduced mortality and became the standard treatment for severe cases (Limmathurotsakul et al. 2014). Current treatment involves a two-phase regimen: an initial 10-14-day intensive phase with intravenous antibiotics, CAZ or meropenem (MRP), followed by a 12-20-week eradication phase with oral

antibiotics trimethoprim/sulfamethoxazole (TMP-SMX) combined with doxycycline (DOX) to prevent relapse (Wuthiekanun et al. 2014).

2.2.5 *B. pseudomallei* antimicrobial resistance

B. pseudomallei is resistant to PCN, ampicillin (AMP), first and second-generation cephalosporins and many other antibiotics (Wiersinga et al. 2018). Although resistance or tolerance to CAZ is rare and only occurs in 0.1 to 1.5% of cases in Thailand (Panya et al. 2016; Wuthiekanun et al. 2011) and 0.6 to 2.4% of cases in Malaysia (Ahmad et al. 2013; Hassan et al. 2014), the mortality rate of patients given CAZ is still high. Even treatment of paediatric melioidosis (co-colonised with other bacterial infections) with a combination of CAZ and gentamicin (GEN) or CAZ and amikacin (AMK) or DOX, TMP-SMX and azithromycin (AZM) is ineffective in completely eradicating *B. pseudomallei* (Mariappan et al. 2018). The inefficiency of CAZ in certain cases may be attributed to the existence of transient CAZ-tolerant genes in *B. pseudomallei* (Chattagul et al. 2021). In Northern Australia, *B. pseudomallei* resistance to MRP, CAZ and TMP-SMX has not been reported (Crowe et al. 2014; Currie et al. 2015).

B. pseudomallei also has high phenotypic plasticity and multiple mixed morphologies are commonly found in clinical samples (Chantratita et al. 2007). The changes in *B. pseudomallei* colony morphology have shown implications in facilitating persistence *in vivo* by adapting and changing their surface structures (Chantratita et al. 2007) and have shown higher biofilm formation and AMR *in vitro* (Al-Maleki et al. 2020). *B. pseudomallei* SCVs are also reported to display significantly higher biofilm formation and increased resistance to antibiotics compared to wild-type *B. pseudomallei* (Al-Maleki et al. 2020). Although *B. pseudomallei* is already intrinsically resistant to many antibiotics, both Sawasdidoln et al. (2010) and Anutrakunchai et al. (2018) demonstrated that *B. pseudomallei* isolates showed an increased resistance in biofilm conditions.

Generally, bacteria enter a stationary phase when oxygen and nutrients are depleted, or waste products accumulate in mature biofilms. This reduces the efficacy of growth-dependent antibiotic killing as the bacteria may adapt to be more resistant

UNIVERSITI KEBANGSAAN MALAYSIA

towards the antimicrobials (Stewart et al. 2008). The gradient shift in biofilm occurs where the cells on the surface of the biofilm monopolise nutrients and oxygen from the cells below. This affects growth between bacterial cells throughout the biofilms, which may weaken the efficacy of growth-dependent antibiotic killing (Blanco et al. 2016). Efflux pumps, membrane proteins that transport toxins and other substances from within the cell to the environment (Alav et al. 2018), are also largely responsible for *B. pseudomallei* biofilm-associated AMR. Overexpression of the BpeAB-OprB efflux pumps in *B. pseudomalle*i biofilms increases the natural resistance of bacteria as well as induces multidrug resistance (MDR) towards aminoglycosides and macrolides (Chan et al. 2005).

2.2.6 Risk factors and transmission of melioidosis

B. pseudomallei is an opportunistic pathogen and the risk factors of melioidosis include diabetes mellitus, immunocompromised patients, patients with chronic lung disease, occupations near contaminated soils and waters, as well as vacations in endemic countries (Limmathurotsakul et al. 2010; Nathan et al. 2018). Melioidosis transmission primarily occurs through direct exposure to contaminated soil or water. *B. pseudomallei* can enter the body through cuts, abrasions, inhalation, or ingestion, putting individuals who are frequently in contact with contaminated environments, such as farmers, agricultural workers, and outdoor enthusiasts, at higher risk (Allwood et al. 2011). This mode of transmission is especially relevant in regions with agricultural practices like ploughing and irrigation, which disturb soil that may be contaminated.

Although person-to-person transmission is rare, it can occur, particularly among immunocompromised individuals, such as those with diabetes or chronic kidney disease. There have been occasional reports of person-to-person spread via respiratory droplets, but such cases are uncommon (Centers for Disease Control and Prevention 2024). Overall, while environmental exposure remains the main route of transmission, factors such as underlying health conditions like diabetes, excessive alcohol use, and renal disease can increase the risk of infection once the bacteria enter the body. Infection of *B. pseudomallei* begins as a non-specific wound in the inoculum and this can then lead to septicaemia as well as pulmonary infections (Gassiep et al. 2020; Limmathurotsakul et al. 2016).

UNIVERSITI KEBANGSAAN MALAYSIA

2.2.7 Global epidemiology of melioidosis

Melioidosis is also known as “the great mimicker” as it has a wide range of non-specific symptoms and is easily mistaken for tuberculosis and pneumonia. This makes melioidosis difficult to determine before diagnostic testing (Wiersinga et al. 2018). Cases and deaths of melioidosis are severely under-reported and it is estimated that around 165,000 cases of human melioidosis occur annually, with 89,000 deaths worldwide (Figure 2.3) (Limmathurotsakul et al. 2016). Melioidosis is highest in Southeast Asia and northern Australia, where it is endemic, with up to 50 cases per 100,000 people reported each year. Northeast Thailand accounts for a large number of cases in Southeast Asia (Wiersinga et al. 2018). South Asia also has a substantial portion of cases, with countries like India and Bangladesh accounting for 44% of the total global cases (Limmathurotsakul et al. 2016). Again, cases are underreported because of a lack of proper diagnostic tools and surveillance systems, especially in poorer areas (Limmathurotsakul et al. 2016; Wiersinga et al. 2018). *B. pseudomallei* infections generally do not show any symptoms directly. However, patients can show mild symptoms such as fevers to severe symptoms (joint and brain inflammation as well as low blood pressure) that can lead to death (Limmathurotsakul et al. 2016). Clinical signs can include fevers, loss of weight, coughing and organ abscesses (Foong et al. 2014).

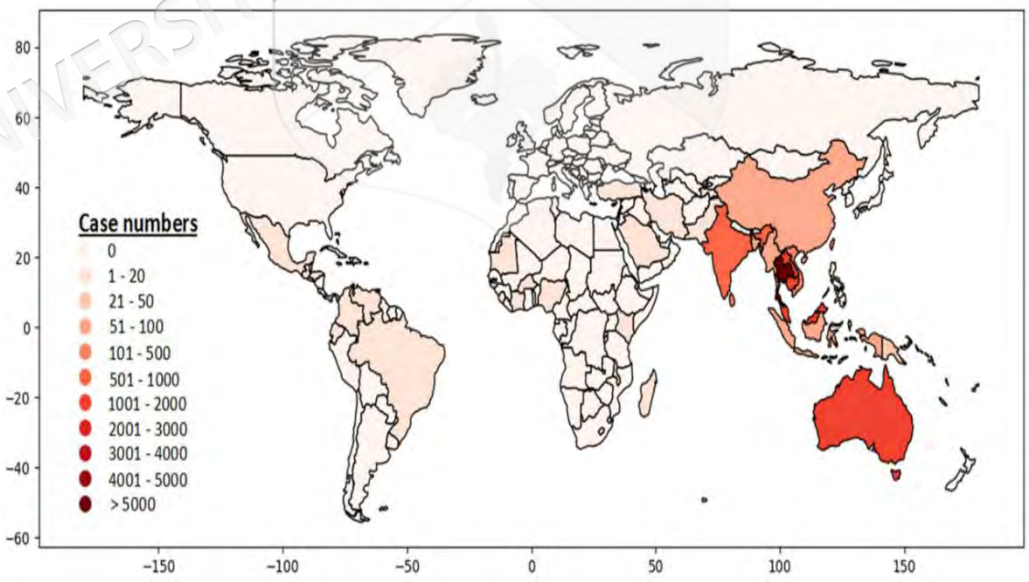

Figure 2.3 Global distribution of melioidosis cases in humans, 1911-2020 (Data obtained from the Microbiology Department at Mahidol Oxford Tropical Medicine Research Unit)

Source: Chowdhury et al. 2022

UNIVERSITI KEBANGSAAN MALAYSIA

2.2.8 Epidemiology of melioidosis in Malaysia

As melioidosis is underreported even in Malaysia, the exact number of cases remains unknown. Incidence across states varies significantly, often influenced by economic activities and environmental conditions. Pahang records an incidence rate of 6.1 cases per 100,000 population, while Kedah has a much higher rate of 16.35 cases per 100,000 population; both regions are heavily involved in agriculture (Hassan et al. 2010; How et al. 2005). In Kelantan, a tertiary hospital reported that 31% of melioidosis patients presented with pneumonia, reflecting the burden of the disease in this state (Kingsley et al. 2016).

In Perak, a five-year retrospective study at Hospital Teluk Intan documented 46 confirmed melioidosis cases, with a mortality rate of 52% and pneumonia as the most common clinical presentation (54.3%) (Tang et al. 2019). Sabah and Sarawak have also reported an increasing number of cases, though precise data is scarce due to limited surveillance in these regions. Figure 2.4 displays the states that have reported melioidosis cases. The majority of cases were reported by hospitals and medical centres in Pahang and Sabah (Nathan et al. 2018).

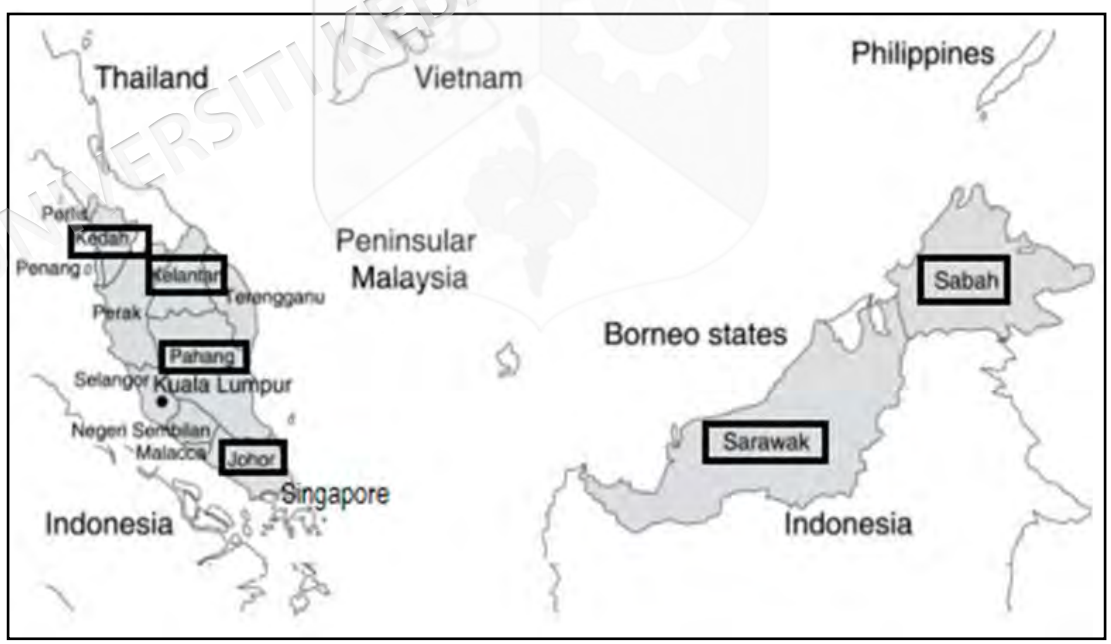

Figure 2.4 The major states reporting melioidosis cases shown on the map of Malaysia. Since the state health authorities were diligent in starting state-level registers for melioidosis, the bulk of case reports come from hospitals and medical centres in Sabah and Pahang.

Source: Nathan et al. 2018

UNIVERSITI KEBANGSAAN MALAYSIA

2.2.9 Relapse strain identification and characterisation in *B. pseudomallei*

Relapse in melioidosis refers to the re-emergence of clinical symptoms and positive cultures for *B. pseudomallei* following apparent resolution of the initial infection. This phenomenon is typically attributed to the persistence of the original infecting strain within host cells, facilitated by mechanisms such as biofilm formation, intracellular survival, and evasion of host immune responses. Unlike reinfection, which involves a genetically distinct strain, relapse is often confirmed through molecular typing techniques such as multi-locus sequence typing (MLST) and pulsed-field gel electrophoresis (PFGE), with relapse isolates frequently sharing the same ST as the primary strain (Hayden et al. 2012; Mariappan et al. 2018).

In a Malaysian paediatric case, both the primary and relapse isolates were identified as ST51, while a subsequent new infection was attributed to ST1644, reinforcing the hypothesis of strain persistence rather than reinfection (Mariappan et al. 2018). This case underscores the clinical relevance of strain-level surveillance, particularly in endemic regions where recurrent melioidosis poses diagnostic and therapeutic challenges.

Recent molecular investigations have provided valuable insights into the mechanisms of relapse in melioidosis. Seng et al. (2023) identified mutations in *tssB-5*, a gene encoding a structural component of the T6SS, in relapse isolates. These mutations are postulated to influence virulence, enhance intracellular persistence, and modulate host-pathogen interactions. In parallel, Velapatino et al. (2012) conducted proteomic profiling on matched primary-relapse isolate pairs and reported differential expression of proteins associated with anaerobic metabolism (ArcA, ArcB, ArcC), nitric oxide detoxification (HmpA), and oxidative stress response (sodB). These

UNIVERSITI KEBANGSAAN MALAYSIA

findings suggest that *B. pseudomallei* may undergo metabolic reprogramming to withstand intracellular stressors and antimicrobial pressure during relapse episodes.

Together, these studies highlight the critical importance of characterising relapse strains to elucidate the molecular basis of chronic infection, persistence, and treatment failure. The integration of genotypic and proteomic approaches offers a multidimensional view of *B. pseudomallei* pathogenesis, particularly in paediatric cases where relapse remains underreported and poorly understood. Such insights are essential for guiding therapeutic strategies, improving diagnostic accuracy, and informing public health interventions in endemic regions.

2.2.10 Malaysian paediatric case distribution

Although melioidosis cases in Malaysia are estimated to occur in greater numbers than reported, *B. pseudomallei* infections in children are only a fraction of confirmed cases. Only four studies (excluding a recent case study) have reported between 13 and 42 culture-confirmed cases (Fong et al.,2015; How et al. 2005; Mohan et al. 2017; Sam & Puthucheary 2006). Paediatric melioidosis has been reported in Pahang (How et al. 2005), Kuala Lumpur (Sam & Puthucheary 2006), Sabah (Fong et al. 2015) and Sarawak (Mohan et al. 2017). The incidence rate of paediatric melioidosis is estimated to be below 5 per 100,000 children in Sabah, Pahang and Sarawak. Paediatric melioidosis in Malaysia has a high fatality rate, with over 24%-59% of culture-confirmed cases leading to fatal outcomes and over 75% in cases with septicaemic shock.

An increase in awareness towards the dangers of melioidosis is warranted for the quick diagnosis of melioidosis for effective antimicrobial treatment of infection for both adult and paediatric cases. The delay in treatment is postulated to increase the fatality rate of the disease and this should be circumvented with proper knowledge and practice, with the dangers of melioidosis in mind. Adults in high occupational hazard workplaces, citizens in endemic areas and healthcare professionals should be made

UNIVERSITI KEBANGSAAN MALAYSIA

more aware of *B. pseudomallei* and melioidosis for quicker infection-to-diagnosis timing for more efficient treatment.

2.3 Chronic Melioidosis in a Paediatric Patient: A Case of Relapse and Co-colonisation with Multidrug-Resistant Pathogens

The samples used in this study were obtained from a paediatric patient with melioidosis throughout different phases of infection (Mariappan et al. 2018). The patient was 14 years old when he was admitted to University Malaya Medical Centre (UMMC). The patient had a history of pneumonia with co-colonisation of other bacteria, and cystic fibrosis and lived in a region of the city that was not endemic to melioidosis. In 2013, the patient tested positive for *B. pseudomallei*. Following treatment with CAZ and GEN, subsequent diagnostic tests confirmed the absence of the pathogen (Figure 2.5). The patient then went on vacation to a melioidosis-endemic state in the year 2014 and was once again diagnosed with *B. pseudomallei*. The patient was treated with CAZ and AMK in the hospital and given DOX, SXT and AZM orally after discharge. Diagnosis for *B. pseudomallei* was negative for 120 weeks. In the year 2015, he was admitted again, and a lung function test showed a decline. He was still negative for *B. pseudomallei*. However, in the year 2016, the diagnosis was positive for *B. pseudomallei*. Despite continuous antibiotic intervention, the patient succumbed to the infection. It is also worth mentioning that the patient suffered co-colonisation of other bacterial species such as *Pseudomonas aeruginosa, B. cepacia, Pseudomonas spp* and methicillin-resistant *Staphylococcus aureus* (MRSA).

Clinical isolates from the years 2013 (primary strain - UMC083), 2014 (new infection strain - UMC082) and 2016 (relapse strain - UMC114) were taken from the patient. MLST was conducted, identifying both the primary and relapse strains to be of the same sequence type (ST51) and the new infection strain to be of a different sequence type (ST1644). All isolates showed different susceptibility patterns (resistant to SXT, intermediate to DOX and susceptible to all other antibiotics).

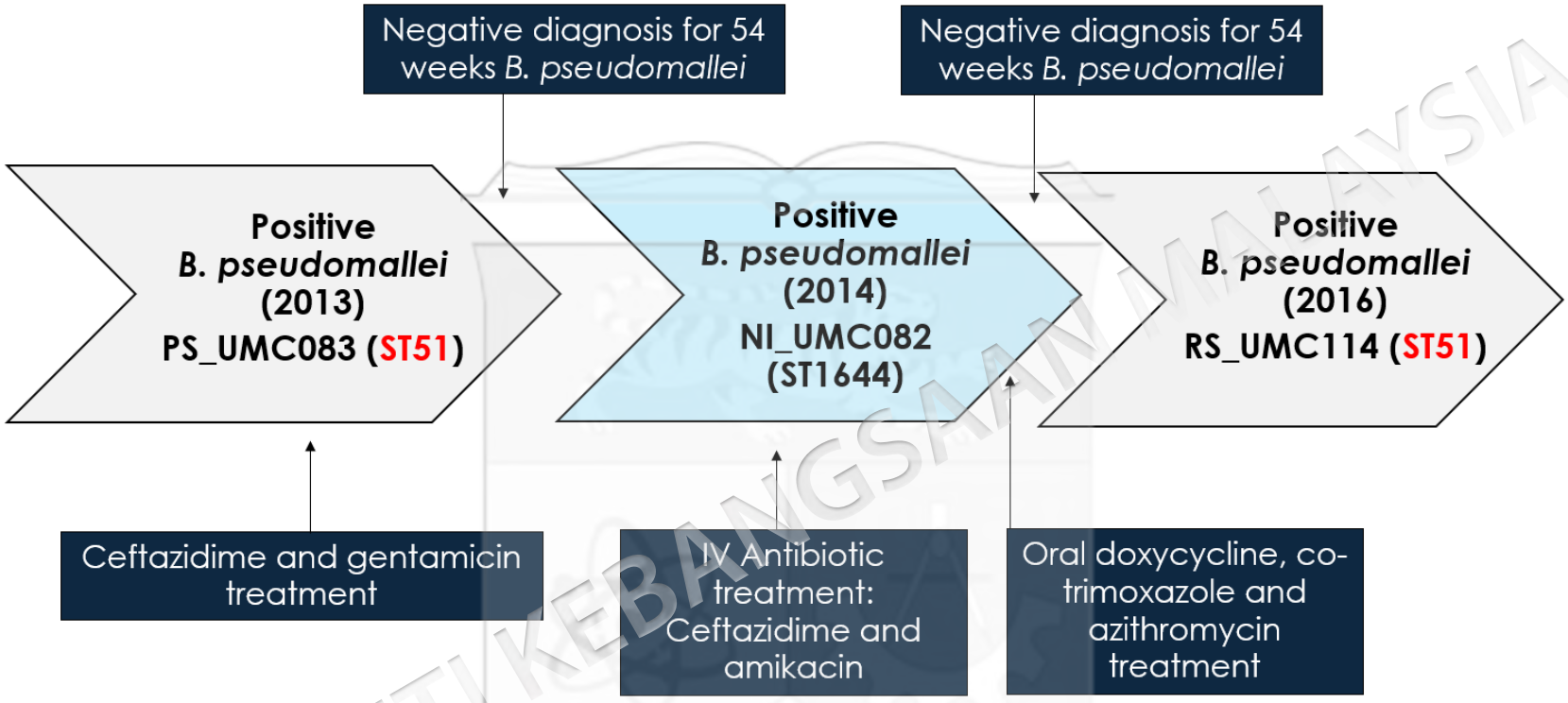

Figure 2.5 Progression of the Malaysian paediatric melioidosis case study. The paediatric case began with the patient being positively diagnosed with a *B. pseudomallei* infection in the year 2013. CAZ and GEN were given via IV and the patient was negative for *B. pseudomallei* for over 54 weeks. The patient then returned from a trip to Sabah (endemic) and was admitted once more in 2014 with a positive diagnosis of *B. pseudomallei*. CAZ and AMK were administered, and the patient was once again diagnosed with *B. pseudomallei* for 70 weeks. DOX, SXT and AZM were given upon discharge to be taken orally. In 2016, the patient was once again admitted and diagnosed positive for *B. pseudomallei.* MLST showed the isolates from the years 2013 and 2016 were of the same ST (ST51) and the isolate from the year 2014 was of ST1644.

Source: Mariappan et al. 2018

UNIVERSITI KEBANGSAAN MALAYSIA

2.4 Proteomic Analysis of *B. pseudomallei* Clinical Isolates via Liquid Chromatography – Mass Spectrometry

B. pseudomallei contains numerous proteins mediating virulence innately or released by its virulence systems (Kang et al. 2015). Identification of these proteins may help elucidate growth and metabolism as well as cellular function and regulation in host cells. Identification of total protein can be used for strain comparison to determine differentially expressed proteins among isolates as well as in primary and relapse isolate pairing (Velapatiño et al. 2012). Liquid chromatography-mass spectrometry (LC-MS) is a tool for identifying proteins in a sample. The advantages of LC-MS compared to other methods are its high sensitivity and selectivity using low sample concentrations (Pitt 2009), accurate quantitative analysis of analytes (Eeckhaut et al. 2009), high throughput analysis for screening a large number of samples in a short amount of time (Plumb et al. 2006), as well as for structural elucidation of samples to determine molecular weight and structure for protein identification (Paauw et al. 2023).

Generally, proteins are extracted either mechanically and/or chemically (Joompa et al. 2017) and are quantified to determine their concentrations. The proteins are then prepped for LC-MS by digestion to break them down into peptides to make them amenable to chromatographic separation and mass spectrometric analysis. LC-MS is then conducted by injecting samples into the liquid chromatograph, separating, and analysing in the mass spectrometer based on their mass-to-charge (m/z) ratio. The data attained is information about the peptide sequences and abundance, which is then be analysed using software linked to databases for identification of proteins. Comparisons of differently expressed proteins between primary and relapse strains to uncover relapse mechanisms can also be carried out through the identification and analysis of total proteins (Velapatiño et al. 2012). Total protein extraction and identification of *B. pseudomallei* also elucidates AMR and virulence proteins involved in its pathogenicity (Paauw et al. 2023; Vander et al. 2015; Welkos et al. 2020) and modulating host immune response (Burtnick et al. 2014).

Velapatino et al. (2012) identified differentially expressed proteins in primary and relapse isolates of *B. pseudomallei*. Total protein was extracted from primary-

UNIVERSITI KEBANGSAAN MALAYSIA

relapse paired isolates and peptides were analysed by LC-MS, where 974 proteins were identified, and 32 proteins were differentially expressed in the primary isolate. Isotope tagging for relative and absolute quantification showed that factors for nitric oxide detoxification (HmpA) and anaerobic growth (ArcA, ArcC and ArcB) were highly expressed in the relapse strain. Oxidoreductase protein sodB was also upregulated in the relapse strain in this study.

Paauw et al. (2023) studied the proteins of six *B. pseudomallei* isolates for potential resistance and virulence. Total protein identification revealed efflux pump-related proteins such as (AmrAB–OprA, BpeAB–OprB, BpeEF–OprC, Pen A) to be synthesised by the bacterium, as well as β-lactamases for inactivation of β-lactam antibiotics. Expression of at least seven of the nine proteins in the bactobolin clusters was identified and capsules and T2SS virulence factors were discovered across all strains. Biofilm protein (Pga) pertinent to biofilm formation was also uncovered.

Welkos et al. (2020) identified bacterial proteins synthesised by murine macrophages upon *B. pseudomallei* infections, where the cells infected with *B. pseudomallei* were lysed and the total proteins were digested and analysed. Downstream analysis identified 160 bacterial proteins, including BimA, TssA, TssB, Hcp1 and TssM. BimA protein is important in the intracellular replication of the bacterium (Jitprasutwit et al. 2023). A summary of all the LCMS-focused techniques experimented on *B. pseudomallei* mentioned in this section is tabulated in Table 2.2.

Burtnick et al. (2014) conducted a comprehensive proteomic analysis of the Type II secretion system (T2SS) in *B. pseudomallei*. They identified 48 proteins that were either missing or significantly reduced in T2SS mutants compared to the wild-type strain. The secretome contained 12 different proteases, two phospholipases, and a chitinase, which are hydrolytic enzymes that may play a role in degrading host tissues and modulating the immune response.

Vander et al. (2015) identified 26 potential Bsa-dependent secreted proteins as possible candidate effectors. These proteins were uncovered by comparing the secreted protein profiles of *B. pseudomallei* Bsa Type III secretion system (T3SS) hypersecreting mutants (lacking bsaP or BipD) with the parent strain and a bsaZ mutant, which is

UNIVERSITI KEBANGSAAN MALAYSIA

unable to secrete effector proteins. The lack of BsaP or BipD regulation resulted in the excessive secretion of BopE, a known Bsa effector protein. The identified proteins, BprD and BapA, were validated as new effectors secreted by the Bsa T3SS, highlighting their potential to contribute to the bacterium's virulence.

Melioidosis relapse cases, particularly in paediatric patients, remain poorly understood, with limited research exploring the underlying proteomics mechanism. Although there are studies on paediatric melioidosis relapse cases, none have investigated the proteomic profile of *B. pseudomallei* in these cases, particularly in Malaysia. Existing research focuses on clinical outcomes and treatment strategies. The molecular mechanisms of relapse at the protein level remain unexplored and this study is the first in Malaysia to address this gap by conducting a proteomic analysis of both primary, new infection and relapse isolates from a paediatric patient.

UNIVERSITI KEBANGSAAN MALAYSIA

Table 2.2 Overview of LC-MS Proteomic Studies on *B. pseudomallei* Isolates: Methodologies, Analytical Tools, and Key Findings

Research aim	**Chromatography setting**	**Software used for analysis**	**Results**	**References**
Proteomic analysis of the *Burkholderia pseudomallei* Type II secretome reveals hydrolytic enzymes, novel proteins and the deubiquitinase TssM	• C-18 medium (2mm)	• MassSieve	• 48 proteins that were either missing or significantly reduced in T2SS mutants • 12 different proteases, two phospholipases, and a chitinase •	Burtnick et al. (2014)
To study the proteins of six *B. pseudomallei* isolates for potential resistance and virulence	• C18 trap column (C18 PepMap, 300 µm ID ×5 mm, 5 µm particle size, 100 Å pore size; Thermo Fisher Scientific), • Column flow rate (300 nL/min)	• PEAKS7.5	• Expression of at least seven of the nine proteins in the bactobolin clusters was identified • Biofilm protein (Pga) was discovered	Paauw et al. (2023)
Quantitative proteomic analysis of *B. pseudomallei* Bsa type III secretion system effectors using hypersecreting mutants	• Acclaim PepMap RSLC nanoViper, C18 column (75 µm, 15 cm) • Column flowrate (300 nL/min)	• Mascot	• Proteins BprD and BapA were validated as new effectors secreted by the Bsa T3SS	Vander et al. (2015)

… to be continued

UNIVERSITI KEBANGSAAN MALAYSIA

… continuation

To identify differently expressed proteins in primary and relapse isolates of *B. pseudomallei*	• The reverse gradient length - 2h per HPLC • Reverse phase nanoflow (300 nL/min) HPLC	• MS data search (ProteinPilot 3.0)	• 974 proteins, and 32 proteins were differently expressed in the primary isolate • Factors for nitric oxide detoxification (HmpA) and factors for anaerobic growth (ArcA, ArcC and ArcB) were highly expressed in the relapse strain.	Velapatino et al. (2012)
To identify bacterial proteins synthesised by murine macrophages upon *B. pseudomallei* infections	• C-18 stationary phase into fused silica capillaries with a flame-pulled tip • Column flowrate (0.25 µl min^{-1})	• MaxQuant software (version 1.2.2.5) • Perseus program (version 1.2.0.17)	• 160 bacterial proteins, including BimA, TssA, TssB, Hcp1 and TssM. The BimA protein is important in the intracellular replication of the bacterium	Welkos et al. (2020)

UNIVERSITI KEBANGSAAN MALAYSIA

CHAPTER III

METHODOLOGY

3.1 *B. pseudomallei* Clinical Strains Cultivation

The *B. pseudomallei* isolates were obtained from a paediatric case study patient (section 2.3) in the years 2013 (PS_UMC083), 2014 (NI_UMC082), and 2016 (RS_UMC114).The *B. pseudomallei* clinical strains were then sub-cultured and stored at −80 ˚C following initial isolation. *B. pseudomallei* reference strain K96243 was included as a positive control in both PCR and qPCR analyses. All strains were retrieved from −80 ˚C storage and subsequently streaked onto nutrient agar (NA) (Oxoid, United Kingdom) for revival prior to downstream applications (Appendix A). Cultures were incubated at 37℃ for 24 hours (Stuart Scientific, Malaysia). For inoculation, a single colony was transferred to a 50 mL Falcon tube (Biologix, Germany) containing 10 mL of Luria–Bertani (LB) medium (Oxoid, United Kingdom) (Appendix A). The bacterial broth was then placed in a shaking incubator (Stuart Scientific, Malaysia) set to 37 ˚C and 180 rpm for 18 hours to allow overnight growth (Mariappan et al., 2017). Upon confirming the identity of the bacterial cultures PS_UMC083, NI_UMC082, and RS_UMC114 (Section 3.2), the broth was prepared for glycerol stock culture (Appendix A).

B. pseudomallei Clinical Strains Identity Confirmation Test

3.2.1 Ashdown agar (phenotypic confirmation)

Ashdown agar, a selective growth medium for *B. pseudomallei*, contains crystal violet and GEN, which suppress the growth of other bacteria. *B. pseudomallei* absorbs the neutral red in the agar, further distinguishing it from other bacterial colonies. The medium is also supplemented with 4% glycerol, which is required for the growth of

certain *B. pseudomallei* strains (Ashdown, 1979). The clinical strains PS_UMC083, NI_UMC082, and RS_UMC114, retrieved from −80 ˚C storage, were immediately streaked onto Ashdown agar (Appendix A) for phenotypic confirmation. The freshly

streaked plates were incubated at 37 ˚C for 72 hours. Single colonies appeared after incubation, and their morphology was observed and documented.

3.2.2 Polymerase chain reaction and gel electrophoresis (genotypic confirmation)

a. DNA extraction (boiling method)

Upon growth on NA agar, several colonies of *B. pseudomallei* were transferred into a 1.5 mL centrifuge tube containing 100 µL of sterile distilled water (dH_2O). The tube was placed in a water bath (Fisherbrand, United Kingdom) at 100 ˚C for 10 minutes to lyse the bacteria. The samples were then centrifuged at 13,000 × g for 1 minute using a microcentrifuge (Hettich, Germany), and the supernatants were transferred to new microcentrifuge tubes for storage at −20 ˚C (Jose et al., 2006).

b. Polymerase chain reaction (PCR)

The *Burkholderia* genus-specific gene (*groEL*) and the *B. pseudomallei* species-specific gene (*mprA*) were tested to confirm that the clinical strains were of *B. pseudomallei* origin (Suppiah et al., 2010). Each PCR reaction was prepared in a total volume of 25 µL. A volume of 5 µL of 5× PCR Master Mix (iDNA, Singapore) was added to the PCR tube, followed by 0.5 µL each of forward and reverse primers (Integrated DNA Technologies, USA), as listed in Table 3.1. The final primer concentration in each reaction was 0.2 µM. A total of 2.5 µL of extracted genomic DNA, ranging between 10–100 ng per reaction, was used as the template. Finally, 16.5 µL of nuclease-free distilled water (dH_2O) was added to complete the reaction mixture. DNA from *B. pseudomallei* K96243 was used as a positive control, while sterilised dH_2O was used in place of genomic DNA for the negative control. The presence of the genes was tested in all three *B. pseudomallei* clinical strains. PCR was conducted for 35 cycles in a thermocycler (Bio-Rad, Singapore) under the following parameters: initial denaturation at 94 ˚C for 5 minutes, followed by 35 cycles of denaturation (94 ˚C for 30 seconds),

UNIVERSITI KEBANGSAAN MALAYSIA

annealing (56 ˚C for 30 seconds), and extension (72 ˚C for 45 seconds), ending with a final extension at 72 ˚C for 2 minutes. The PCR products were stored at −20 ˚C until further use (Suppiah et al., 2010).

Table 3.1 *B. pseudomallei* genus and species-specific primer list

Primer	Sequence	Product size (bp)	Characteristics
***gro1* F**	CTG GAA GAC ATC GCG ATC	139	*Burkholderia* genus-specific
***gro2* R**	CGT CGA TGA TCG TCG TGT T		
***mpr1* F**	TCT CCG ATA GCC GCC TTG	162	*B. pseudomallei*- specific
***mpr2* R**	CGT ATC ACA TCG CAT CGC		

c. Agarose gel electrophoresis

A 1.5% (w/v) agarose gel was prepared by dissolving 0.6 g of agarose (1st Base, Singapore) in 40 mL of 1× TAE buffer (Appendix A) in a conical flask. The mixture was microwaved at medium heat for 50 seconds and shaken, with the process repeated until the agarose was fully dissolved. From this solution, 30 mL was measured into a conical flask and allowed to cool slightly. Subsequent steps were performed in the dark due to the use of photosensitive reagents. A volume of 1.5 µL of EtB-Out Nucleic Acid Staining Solution (Yeastern Biotech, Taiwan), supplied as a 20,000× concentrate, was added directly to the agarose for nucleic acid visualisation, in accordance with the manufacturer's recommendation of a final 1× concentration. The solution was gently mixed and poured into a gel electrophoresis casting chamber (Bio-Rad, Singapore), placed on a flat surface to ensure even distribution. A 15-well comb was inserted, air bubbles were removed, and the gel was left to solidify in the dark for 40 minutes.

Once solidified, the comb was carefully removed, and the gel with its casting chamber was placed into the electrophoresis tank (Bio-Rad, Singapore) with the wells oriented toward the negative terminal. The tank was filled with 1× TAE buffer until the gel was fully submerged. PCR products (Section 3.2.2b) were prepared for loading on a strip of parafilm. The DNA ladder was prepared by mixing 1 µL of loading dye, 1 µL

UNIVERSITI KEBANGSAAN MALAYSIA

of 1× TAE, and 2 µL of a 100 bp DNA ladder, which was then pipetted into the first well. For sample loading, 5 µL of PCR product was combined with 1 µL of 6× loading dye on parafilm, mixed by pipetting, and 5 µL of the mixture was loaded into adjacent wells.

The electrophoresis chamber was closed, and the electrodes were connected to a power supply. The gel was run at 80 V for 1 hour, with DNA migration monitored throughout. The run was stopped once the DNA fragments had migrated through approximately 80 – 90% of the gel. The gel was then carefully removed from the casting chamber and placed in an ultraviolet viewer (Vilber Lourmat, France). DNA bands were observed, and the gel image was documented. To provide a clear overview of the strain identity confirmation process, a flowchart is presented in Figure 3.1.

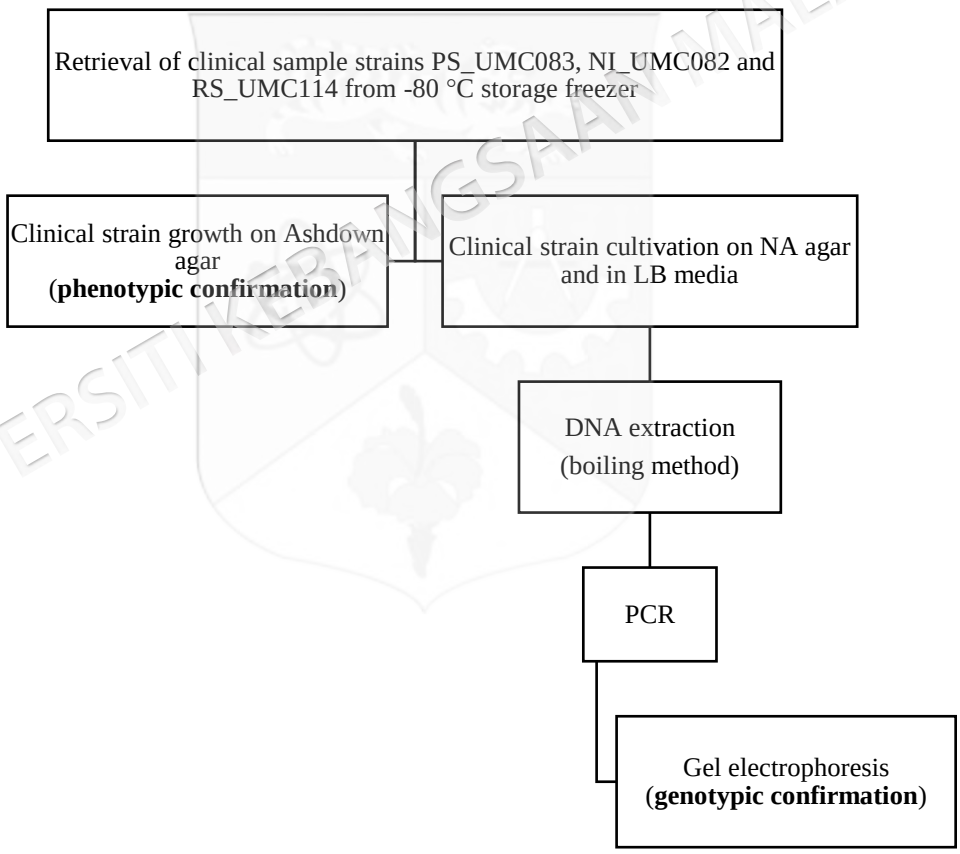

Figure 3.1 Flowchart of phenotypic and genotypic confirmation of the clinical strains. The process begins with strain retrieval from −80 ˚C storage, followed by phenotypic confirmation on Ashdown agar and cultivation on nutrient agar and LB medium. Genomic DNA is extracted using a boiling method and subjected to PCR amplification targeting genus-specific (*groEL*) and species-specific (*mprA*) genes. PCR products are then analysed via agarose gel electrophoresis to confirm strain identity through genotypic profiling.

UNIVERSITI KEBANGSAAN MALAYSIA

3.3 *B. pseudomallei* Clinical Strains Bacterial Growth Curve

The growth curve of *B. pseudomallei* clinical strains was conducted following the protocol described by Mariappan et al. (2017). Freshly cultured strains PS_UMC083, NI_UMC082, and RS_UMC114 were prepared as outlined in Section 3.1. A volume of 1 mL of bacterial broth was pipetted into a cuvette, and the turbidity was measured using a spectrophotometer (AHS Lab Supplies, Malaysia) at OD_{600nm}. The culture was standardised to an absorbance range of OD_{600nm} 0.8–1.0.

A total of 13 Falcon tubes (50 mL) were prepared, each containing 5 mL of LB broth, representing bi-hourly time points over 24 hours starting from 0 hours. The entire experiment was performed in triplicate to ensure reproducibility and accuracy. Next, 10 µL of the standardised bacterial culture was added to each tube, followed by incubation at 37 ˚C and 180 rpm. At 2-hour intervals, absorbance and colony-forming unit (CFU)/mL counts were determined by measuring OD_{600nm}. For CFU analysis, three to six 10-fold serial dilutions were performed using phosphate-buffered saline (PBS), and samples were plated on NA using the Miles–Misra method (Miles et al., 1938) (Figure 3.2). In order to quantify CFU/mL, 10 µL of each diluted sample was pipetted in triplicate onto NA agar plates and incubated at 37 ˚C for 24 hours. OD measurements and CFU/mL counts for all clinical strains were conducted bi-hourly in triplicate. After 24 hours, final CFU/mL values were recorded. The growth curve, plotting OD_{600nm} over time, was generated and used to identify the mid-log phase. A flowchart summarising the methodology of the bacterial growth curve analysis is presented in Figure 3.3.

UNIVERSITI KEBANGSAAN MALAYSIA

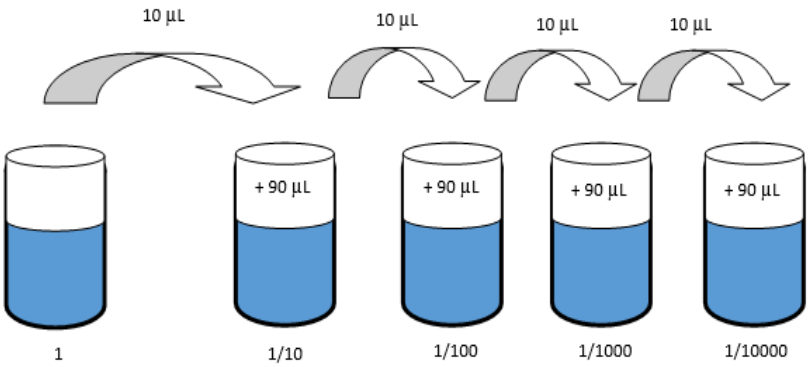

Figure 3.2 Miles and Misra dilution method. A series of three to six 10-fold serial dilutions were prepared using phosphate-buffered saline (PBS). From each dilution, 10 µL aliquots were spotted onto nutrient agar (NA) plates in triplicate

Source: Miles et al. 1938

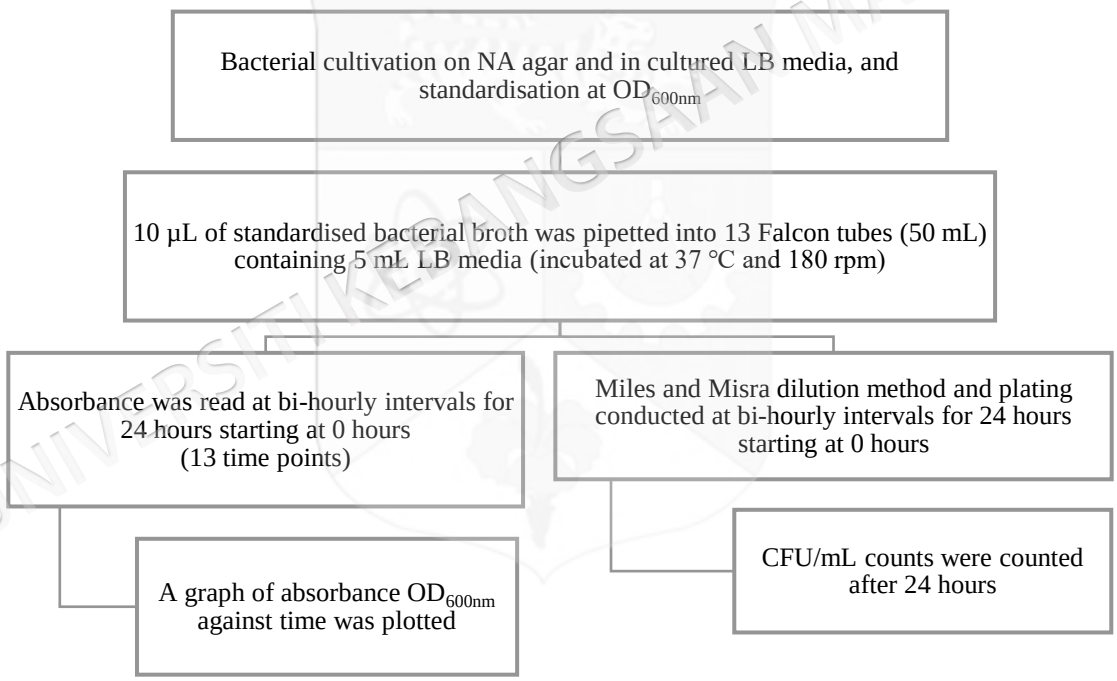

Figure 3.3 Experimental workflow for bacterial growth curve and CFU quantification. Bacterial cultures were first grown on nutrient agar (NA) and in LB broth, then standardised to OD_{600nm}. A 10 µL aliquot of the standardised broth was inoculated into 13 Falcon tubes containing 5 mL LB each and incubated at 37 ˚C with shaking at 180 rpm. Absorbance readings at OD_{600nm} and colony-forming unit (CFU/mL) counts via the Miles and Misra dilution method were taken at bi-hourly intervals over 24 hours. Absorbance values were used to plot a growth curve, while CFU/mL values were determined after 24-hour incubation of plated dilutions.

UNIVERSITI KEBANGSAAN MALAYSIA

3.4 *B. pseudomallei* Clinical Strains Biofilm Formation Quantification

Biofilm formation by *B. pseudomallei* clinical strains was quantified following the protocol described by Mariappan et al. (2017). Bacterial cultures were standardised to an OD_{600nm} of 0.8–1.0 (Section 3.3). Three 96-well plates (BI03, Malaysia) were prepared to represent three time points: 24 hours, 48 hours, and 72 hours. For each strain, 100 µL of LB broth was added to five wells (five replicates), followed by 1 µL of standardised bacterial culture to initiate biofilm growth. Additionally, five wells containing 100 µL of LB broth served as blanks, and another five wells were designated as negative controls. All plates were incubated at 37 ˚C for 24, 48, and 72 hours. The experiment was performed in triplicate, resulting in a total of nine 96-well plates across the three time points.

After 24 hours, the LB broth containing planktonic cells was carefully removed from the 24-hour plates, leaving behind sessile cells and biofilm adhered to the bottom and sides of the wells. The wells were gently washed twice with 150 µL of sterile distilled water (dH_2O) and air-dried for 10 minutes. Subsequently, 100 µL of 0.1% crystal violet was added to each well and incubated at room temperature for 30 minutes. After incubation, the crystal violet was removed, and the wells were washed twice with 150 µL of sterile dH_2O. The wells were then air-dried for another 10 minutes.

To solubilise the bound crystal violet, 150 µL of dimethyl sulfoxide (DMSO) (Merck, Germany) was added to each well. The plates were incubated at room temperature for 30 minutes. The contents of the wells were homogenised by repeated pipette aspiration and dispensing. Absorbance was measured using a microplate reader (Thermo Fisher Scientific, USA) at OD_{570nm}. The true absorbance for each sample was calculated using the following formula:

$$\text{Strain absorbance } (OD_{570nm}) - \text{Blank absorbance } (OD_{570nm}) = \text{True absorbance } (OD_{570nm})$$

A graph was plotted to compare the true absorbance values of each strain. Following this, the LB broth in the 48-hour and 72-hour plates was removed and replenished with fresh LB broth. These plates were then processed using the same protocol after their respective incubation periods.

UNIVERSITI KEBANGSAAN MALAYSIA

3.5 *B. pseudomallei* Clinical Strains Biofilm Gene Expression

3.5.1 Polymerase chain reaction and gel electrophoresis

PCR was performed to confirm the presence of eight biofilm-associated genes and one housekeeping gene in the *B. pseudomallei* test strains (Chen et al., 2011; Chin et al., 2015) (Table 3.2). Genomic DNA was extracted from all three clinical strains and the positive control strain, *B. pseudomallei* K96243, using the boiling method (Section 3.2.2b). For each gene, a 25 µL PCR reaction mixture was prepared in a 200 µL PCR tube.

Each reaction contained 5 µL of 5× PCR Master Mix (iDNA, Singapore), 0.5 µL each of 10 µM forward and reverse primers, and 2.5 µL of DNA template. The final volume of 25 µL was achieved by adding 16.5 µL of sterilised distilled water (dH_2O). Genomic DNA from *B. pseudomallei* K96243 served as the positive control, while sterilised dH_2O was used in place of DNA for the negative control.

PCR amplification was carried out for 35 cycles in a thermocycler (Bio-Rad, Singapore) under the following conditions: initial denaturation at 94℃ for 5 minutes, followed by 35 cycles of denaturation (94 ℃ for 30 seconds), annealing (56 ℃ for 30 seconds), and extension (72 ℃ for 45 seconds), with a final extension at 72 ℃ for 2 minutes. PCR products were stored at −20 ℃ until further use. A 1.5% (w/v) agarose gel electrophoresis was then performed to visualise the DNA bands produced for each strain, following the protocol described in Section 3.2.2c.

3.5.2 *B. pseudomallei* RNA extraction

B. pseudomallei strains were cultivated at 37 ℃ and 180 rpm in a shaking incubator until reaching the mid-log phase. A total of 30 mL of bacterial culture was harvested per strain at this phase, based on the growth curve rather than a fixed optical density. The OD_{600nm} was recorded at the time of harvest. Each strain was then inoculated into three separate 50 mL Falcon tubes, representing three biological replicates, and the cultures were standardised to an OD_{600nm} of 0.8–1.0 (Section 3.3). Total bacterial RNA was extracted using the RNeasy Mini Kit (Qiagen, Netherlands), following the manufacturer's protocol.

UNIVERSITI KEBANGSAAN MALAYSIA

Approximately 4 mL of PS_UMC083 ($1.67 \times 10^9 \pm 1.54 \times 10^8$ cells), 4 mL of NI_UMC082 ($8.6 \times 10^8 \pm 5.0 \times 10^8$ cells), and 5 mL of RS_UMC114 ($8.9 \times 10^8 \pm 5.1 \times 10^8$ cells) cultures, each standardized to OD_{600nm} 0.8–1.0, were transferred into separate 15 mL Falcon tubes and centrifuged at 5000 × g for 3 minutes. The supernatant was discarded, and the pellets were resuspended in 250 µL of PBS. The suspension was transferred to new 1.5 mL microcentrifuge tubes, followed by the addition of 500 µL of RNAprotect Bacteria Reagent. Tubes were vortexed for 5 seconds and incubated at room temperature for 5 minutes. After incubation, samples were centrifuged for 10 minutes at 5000 × g, and the supernatant was removed.

Next, 100 µL of TE buffer containing 15 mg/mL lysozyme (Appendix A) was added to each tube, followed by 10 µL of proteinase K. Tubes were vortexed for 10 seconds and incubated for 10 minutes, with vortexing every 2 minutes. Buffer RLT was prepared by adding 3.5 µL of β-mercaptoethanol to 350 µL of buffer RLT in a separate tube. This mixture was added to the lysed bacterial pellets, and the tubes were vortexed vigorously and centrifuged at maximum speed for 2 minutes. Subsequently, 250 µL of ethanol was added to each tube, and the supernatant was mixed thoroughly by pipetting.

A volume of 700 µL of lysate was transferred to RNeasy Mini spin columns placed in 2 mL collection tubes. Columns were centrifuged for 15 seconds at 8500 × g, and the flow-through was discarded. Spin columns were washed with 350 µL of buffer RW1, centrifuged again for 15 seconds at 8500 × g, and the flow-through was discarded.

For DNase treatment, 10 µL of DNase I stock solution was added to 70 µL of buffer RDD in a new 1.5 mL microcentrifuge tube. The solution was gently mixed by inversion and briefly centrifuged to collect residual liquid. Then, 80 µL of the DNase I incubation mix was added directly to the RNeasy spin column membrane, and the columns were incubated at room temperature for 15 minutes. After incubation, 350 µL of buffer RW1 was added to the spin column and incubated at room temperature for 5 minutes. The column was centrifuged for 15 seconds at 8500 × g, and the flow-through, along with the collection tube, was discarded. The spin column was then placed in a new collection tube and centrifuged again for 15 seconds at 8500 × g, after which the flow-through was discarded.

UNIVERSITI KEBANGSAAN MALAYSIA

Next, 500 µL of buffer RPE was added to the spin column for washing, followed by centrifugation for 2 minutes at 8500 × g. The flow-through and collection tube were discarded, and the spin column was transferred to a new collection tube to remove any residual buffer RPE. The column was centrifuged again at maximum speed for 1 minute. For RNA elution, the spin column was placed in a new 1.5 mL collection tube, and 40 µL of RNase-free water was added directly to the membrane. The tubes were centrifuged for 1 minute at 8500 × g, and the eluted RNA was kept on ice. RNA concentration and purity (A_{260}/A_{280}: 1.9–2.1; A_{260}/A_{230}: 1.8–2.2) were assessed using a Nanodrop spectrophotometer (Thermo Scientific, Canada). The instrument was first blanked with 1 µL of RNase-free water, followed by measurement of 1 µL of RNA sample. Concentration and purity values for each sample were recorded. The extracted RNA was aliquoted into five 200 µL microcentrifuge tubes (8 µL each) and stored at −80 ℃.

UNIVERSITI KEBANGSAAN MALAYSIA

Table 3.2 *B. pseudomallei* biofilm genes primer list

Gene ID	Gene description	Forward Primer	Reverse Primer	Amplicon size	Reference
bpsl0603	Oligosaccharide flippase family protein (membrane protein)	CGAAGCTGTAGTTCGTGAAA	AGAATTTCCTGCTGCTGATG	162	(Chin et al. 2015)
bpsl2026	Spore coat protein U domain-containing protein (surface pilus formation)	TGCAGTAATCCCAGTTCCAT	TGCCGATGTATTTCAGAACG	93	(Chin et al. 2015)
bpsl1607	Nitrous-oxide reductase (denitrification)	CAGAACAATGGGTTTCACGC	TGAGCGCTCTTGATCTTCAC	104	(Chin et al. 2015)
bpsl1799	(Maintains cellular proteostasis)	CCGGTAGAACAGCTTCATCT	TCTATCTGAACATCCGCGAG	92	(Chin et al. 2015)
bpss2016	UDP-N-acetylglucosamine 2-epimerase (biosynthesis of cell-surface polysaccharides)	CACAACCTGTTCAGCGAAGG	GCCGAGAAACGGAAACTGC	147	(Chin et al. 2015)
bpss 0312	LuxR family transcriptional regulator (Quorum sensing)	GCGACTTGCAAGAAGAGCCT	GGAGATCTGATGCCGGTACG	90	(Chin et al. 2015)
bpss 1214	Helix-turn-helix transcriptional regulator (Binds DNA-transcription factor)	ATTTCTCGACGACTGTGGGG	TGGCGGAAGTGTTCGTGTTA	124	(Chin et al. 2015)
bpss 0124	Response regulator transcription factor (transcription factor)	AGCGATGCGACATCCTGATT	GCCTCAAGAACGAAAGCAGC	84	(Chin et al. 2015)
dnak	Housekeeping gene (Bp)(chaperone that prevents protein aggregation and supports the refolding of damaged proteins)	CGCAGATCGAAGTGACCTT	ATCTTCTCGATCTCGGCTTC	136	(Chen et al. 2011)
16s rRNA	Housekeeping gene (*B. pseudomallei*) (component of prokaryotic ribosome)	GGCTAGTCTAACCGCAAGGA	TCCGATACGGCTACCTTGTT	82	(Chen et al. 2011)

UNIVERSITI KEBANGSAAN MALAYSIA

3.5.3 RNA integrity validation using denaturing gel electrophoresis

The integrity of the validated RNA was assessed using the denaturing gel electrophoresis protocol described by Aranda et al. (2012). This protocol was similar to the agarose gel electrophoresis method outlined in Section 3.2.2c, with the key modification of incorporating bleach to denature RNA.

Briefly, a 1.5% (w/v) agarose gel was prepared by dissolving 0.6 g of agarose in 40 mL of 1× TAE buffer (Appendix A) in a conical flask. To this mixture, 1.0% (v/v) Clorox (Clorox, USA) was added and incubated at room temperature for 5 minutes. The solution was microwaved at medium heat for 50 seconds and shaken, with the process repeated until the agarose and bleach were completely dissolved in the buffer. Subsequent steps followed the protocol in Section 3.2.2c, substituting RNA in place of genomic DNA. The gel was visualised under UV transillumination after the RNA bands had migrated to the bottom of the gel.

3.5.4 *B. pseudomallei* cDNA conversion

cDNA synthesis was performed using the PCRBIO UltraScript cDNA Synthesis Kit (PCR Biosystems, United Kingdom), following the manufacturer's instructions. Briefly, the 5× cDNA synthesis mix was thawed and vortexed. The master mix was prepared as follows: 4 µL of 5× cDNA mix was added to a sterile 200 µL PCR tube, followed by 1 µL of 20× UltraScript. Approximately 400 ng of sample RNA was calculated and added. The final reaction volume of 20 µL was achieved using RNase-free water. The thermocycler was programmed at 55 ˚C for 30 minutes, 85 ˚C for 10 minutes, and then held at 12 ˚C indefinitely. The reaction tube was placed in the thermocycler, and the run was completed. The resulting cDNA product was stored at −20 ˚C until further use

UNIVERSITI KEBANGSAAN MALAYSIA

3.5.5 *B. pseudomallei* quantitative polymerase chain reaction (QPCR)

a. Primer efficiency testing and standard curve

Primer efficiency testing and standard curve generation for qPCR were performed using the QuantiNova SYBR Green PCR Kit (Qiagen, Netherlands) on the CFX Connect Real-Time PCR Detection System (Bio-Rad, Singapore). The 2× QuantiNova SYBR Green PCR Master Mix, genomic DNA (gDNA), primers (Table 3.2), and RNase-free water were thawed prior to use.

Each reaction mixture (20 µL total volume) was prepared in 200 µL qPCR-compatible tubes (low profile, thin-walled, polypropylene, clear; Bio-Rad, Singapore) under sterile conditions in a laminar flow hood using sterilised pipettes and tips. The reaction components included 10 µL of 2× QuantiNova SYBR Green PCR Master Mix, 0.5 µL each of 10 µM forward and reverse primers, 7 µL of RNase-free water, and 2 µL of *B. pseudomallei* gDNA. For the negative control, gDNA was replaced with RNase-free water. Serial dilutions comprising six dilution points were prepared for each primer to generate the qPCR standard curve (Table 3.3).

Table 3.3 Dilution series and starting concentration for biofilm primers

Primer	Starting DNA amount	Dilution factors
bpss2016	50 ng	10x
bpsl2026	100 ng	5x
bpsl1799	100 ng	5x
bpsl0603	100 ng	5x
bpss0124	100 ng	5x
16s rRNA	100 ng	5x
bpss1214	100 ng	5x
bpsl1607	100 ng	3x
bpss0312	100 ng	3x

UNIVERSITI KEBANGSAAN MALAYSIA

Each reaction sample tube, along with the negative controls, was run in triplicate. The real-time cycler (Bio-Rad, Singapore) was programmed with the following conditions: (i) initial activation at 95 ˚C for 2 minutes, (ii) denaturation at 95 ˚C for 5 seconds, and (iii) combined annealing/extension at 56 ˚C for 10 seconds, during which data acquisition occurred. The qPCR was run for a total of 40 cycles.

The PCR tubes were placed in the real-time cycler, and the cycling program was initiated. Melting curve analysis and standard curve generation were performed to evaluate primer efficiency. Standard curve parameters were repeated until they met the following criteria: efficiency (E) between 90% and 110%, an R^2 value ≥ 0.98, and a slope ranging from −3.1 to −3.6.

b. Quantitative PCR (qPCR)

qPCR was performed using the QuantiNova SYBR Green PCR Kit (Qiagen, Netherlands) on the CFX Connect Real-Time PCR Detection System (Bio-Rad, Singapore) to quantify the expression of eight biofilm-associated genes in all three *B. pseudomallei* strains. To control for variation in RNA concentration, cycle threshold (Ct) values were normalised against *B. pseudomallei* 16S rRNA, which served as the housekeeping gene. Reaction volumes were prepared in triplicate, following the dilution factors and volumes described in Section 3.5.5a, with 1 ng of cDNA used per reaction. For the negative control, cDNA was replaced with RNase-free water.

The real-time cycler was programmed with the following conditions: (i) initial activation at 95 ˚C for 2 minutes, (ii) denaturation at 95 ˚C for 5 seconds, and (iii) combined annealing/extension at 60 ˚C for 10 seconds, repeated for 40 cycles. Data acquisition occurred during the annealing/extension step. The 200 µL qPCR tubes containing the reactions were placed in the cycler, and the program was initiated. Upon completion, melting curve analysis was performed, and relative abundance was determined using the standard curve.

The relative gene expression was calculated using the Pfaffl method (Pfaffl 2001), where the primary strain (PS_UMC083) was set as the control group because it represents

the earliest isolate from the patient prior to any subsequent NI_UMC082 and RS_UMC114 strains. By comparing NI_UMC082 and RS_UMC114 to PS_UMC083, it is possible to evaluate potential shifts or mutations in biofilm gene expression that may have occurred during the course of infection and host adaptation. This approach provides a more clinically relevant benchmark than using a reference strain like *B. pseudomallei* K96243, which, although well-characterised, does not share the same host origin, infection timeline, or environmental pressures as the patient-derived isolates.

3.6 Proteomics of *B. pseudomallei* Clinical Strains

3.6.1 *B. pseudomallei* protein extraction and Bradford assay

Total protein extraction was carried out following the method described by Joompa et al. (2017). The bacterial strains were cultured and standardised to an OD_{600nm} of 0.8 – 1.0 (Section 3.3). Subsequently, 4 mL of standardised culture from PS_UMC083 and NI_UMC082, and 5 mL from RS_UMC114, were transferred into three separate 15 mL Falcon tubes in triplicate. The tubes were centrifuged at 4000 rpm for 10 minutes, after which the supernatant was discarded and the pellets were resuspended in 500 µL of PBS buffer.

The protease inhibitor cocktail set 2 (Calbiochem, Germany) was freshly prepared according to the manufacturer's instructions. Briefly, the cocktail was reconstituted with 1 mL of DMSO and mixed gently, followed by the addition of 4 mL of sterilised dH_2O. The reconstituted solution was aliquoted into four microcentrifuge tubes (1.25 mL each) and stored at −20 ˚C.

A volume of 10 µL of protease inhibitor cocktail set 2 was added to the tubes containing bacterial pellets. The tubes were then sonicated on ice at 22% amplitude with 10-second pulse intervals for 10 minutes to ensure complete lysis of *B. pseudomallei* cells and release of intracellular proteins. The lysate was transferred to a fresh 1.5 mL microcentrifuge tube and centrifuged at 10,000 rpm for 30 minutes. This step separated soluble proteins from insoluble cellular debris, consistent with Joompa et al. (2017), who demonstrated that high-speed centrifugation effectively retains total soluble proteins in the supernatant.

The supernatant was collected and transferred to a new 1.5 mL microcentrifuge tube. Although the pellet may contain residual proteins bound to debris, these are typically minimal and redundant, with the majority of intracellular proteins recovered in the supernatant. This approach ensures compatibility with downstream LC-MS/MS analysis and aligns with established proteomic workflows. Protein concentration in the supernatant was determined using the Bradford assay (Appendix B). Absorbance values were plotted, and protein amounts were calculated. The samples were subsequently sent to the Malaysian Genomic and Vaccine Institute (MGVI), Selangor, Malaysia, for LC-MS/MS analysis (Section 3.6.3).

3.6.2 Sodium dodecyl sulphate-polyacrylamide gel electrophoresis (SDS-PAGE)

a. SDS-PAGE gel and electrophoresis preparation

The short glass plate and spacer plate for SDS-PAGE (Bio-Rad, Singapore) were cleaned with 70% alcohol and dried. The plates were assembled, placed into a plate holder, and clamped securely, ensuring the bottom was even. The holder was positioned in a stand and clamped tightly to prevent leakage. To check for leaks, sterilised distilled water (dH_2O) was pipetted into the space between the plates, poured out, and the gap was dried with filter paper.

The resolving gel was prepared (Appendix B) and poured into the glass plates until 1.5 – 2.0 cm from the top of the short plate. Sterilised dH_2O was layered on top of the gel to remove bubbles and level the surface. The gel was left to solidify for 45 minutes. After solidification, the water was removed and the surface was dried with filter paper. The stacking gel was then prepared (Appendix B) and carefully poured onto the resolving gel. A 10-well comb was inserted, ensuring no bubbles were formed, and the gel was left to solidify for 45 – 60 minutes.

Once solidified, the comb was carefully removed. The plates were detached from the casting holder and assembled into the electrophoresis holder, which was then placed into the electrophoresis tank. The 1× electrophoresis buffer (EB) (Appendix B) was poured into the

upper buffer chamber, and the system was checked for leaks. An additional 1× EB buffer was added to the sides of the tank and the lower buffer chamber.

When the apparatus was secure and no leakage was observed, 20 µL of a 100 kDa protein marker (1st Base, Singapore) was loaded into the first well, followed by 20 µL of protein samples into subsequent wells. Protein samples were prepared at concentrations of 10 µg, 15 µg, 20 µg, 25 µg, 30 µg, 35 µg, 40 µg, 45 µg, and 50 µg (Appendix B). The lid was placed on the tank, and electrophoresis was run at 100 V for 10 minutes, followed by 150 V until the dye front migrated to the bottom of the gel. Electrophoresis was stopped once the samples reached the bottom, and the gel was processed for staining.

b. Coomassie brilliant blue gel stain

The gel plates were carefully removed from the electrophoresis tank, and the EB buffer from the upper chamber was discarded. The plates were unclamped, and the short plate was gently lifted. The stacking gel was removed and discarded, while the resolving gel was transferred to a container containing 300 mL of dH_2O. The gel was immersed and shaken gently on a low-speed shaker for 5 minutes. The water was discarded, and this washing step was repeated twice.

Next, 15 mL of Coomassie Brilliant Blue Stain One (Bio-Rad, Malaysia) was added to the container to fully cover the gel. The gel was stained with gentle shaking for 60 minutes. The staining solution was then removed, and the gel was rinsed with dH_2O for 5 minutes on a low-speed shaker. The rinse water was discarded, and the process was repeated four times. Following rinsing, protein bands were visualised and documented using a gel documentation system (Bio-Rad, Singapore).

UNIVERSITI KEBANGSAAN MALAYSIA

3.6.3 Liquid chromatography-mass spectrometry (LC-MS) and downstream analysis

a. In-solution protein digestion

Proteins were digested into peptides to improve identification, sequence coverage, and quantification. Briefly, 50 µg of total protein was resuspended in 50 µL of 50 mM ammonium bicarbonate (Sigma-Aldrich, USA). To this, 50 µL of 0.1% Rapigest™ SF (Waters) was added, followed by vortexing. The sample was concentrated to half its volume using a speed vacuum concentrator for 20–30 minutes and subsequently heated at 80 ˚C for 15 minutes in a thermomixer.

Next, 2.5 µL of 100 mM DTT (Sigma-Aldrich, USA) was added, and the mixture was incubated at 60 ˚C for 30 minutes. The microcentrifuge tube was wrapped in aluminium foil, and 2.5 µL of 200 mM iodoacetamide (Sigma-Aldrich, USA) was added, followed by incubation at room temperature for 45 minutes.

Following this, 2.0 µL (1.0 µg/µL) of Trypsin-LysC enzyme (Mass Spec Grade, Promega, USA) was introduced to the mixture, which was incubated overnight at 37 ˚C. To terminate digestion, 1.0 µL of concentrated trifluoroacetic acid (TFA; Sigma-Aldrich, USA) was added, and the sample was incubated at 37 ˚C for an additional 20 minutes. Finally, the sample was centrifuged at 14,000 rpm for 20 minutes, and the supernatant containing digested peptides was collected and stored at −80 ˚C for subsequent analysis.

b. Liquid chromatography-mass spectrometry analysis

Peptide separation was performed using the Dionex Ultimate 3000 RSLCnano system (Thermo Fisher Scientific, Canada), and mass spectrometry analysis was conducted with the Orbitrap Fusion mass spectrometer (Thermo Fisher Scientific, Canada). For peptide separation, samples were loaded onto an EASY-Spray Acclaim PepMap™ column (C18, 100 Å, 2 µm particle size, 50 µm inner diameter × 15 cm) and eluted at a flow rate of 250 nL/min. Mobile phase buffer A consisted of deionised water with 0.1% formic acid, while buffer B contained acetonitrile with 0.1% formic acid. The elution process lasted 101 minutes, with the following gradient of buffer B: 5–40% over 91 minutes, increased to 85% in 2 minutes, held at 85% for 3 minutes, then returned to 5% in 1 minute and maintained at

UNIVERSITI KEBANGSAAN MALAYSIA

5% for 4 minutes. Peptides were subsequently analysed on the Orbitrap Fusion mass spectrometer.

Data were processed using Proteome Discoverer™ software (Version 2.1) with a *B. pseudomallei* protein database (Tax ID: 272560) from UniProt. The analysis allowed up to two missed cleavages, with MS1 tolerance set at 10 ppm and MS2 tolerance at 0.6 Da. Post-translational modifications (PTMs) detection included oxidation of methionine (M), N-terminal acetylation, and carbamidomethylation of cysteine (C). Protein identifications were validated using the Percolator® algorithm, applying a 5% false discovery rate (FDR) cut-off to ensure reliable results.

3.6.4 Comprehensive proteomic analysis of all three *B. pseudomallei* strains

a. Overview analysis of proteomic profiles of all three strains

A comprehensive proteomic analysis was conducted to identify and quantify proteins in *B. pseudomallei*. Protein identification was performed using MaxQuant v2.0.1.0, a widely used software for label-free and quantitative proteomics (Cox et al. 2014; Tyanova et al. 2016). The raw LC-MS data were analysed against a reference protein database for *B. pseudomallei* (Taxonomy ID: 28450), generating a list of identified proteins and their relative intensities. This provided a detailed overview of the proteome while ensuring accuracy and reliability in the identification and quantification process.

The identified proteins were then analysed in Perseus v1.6.15.0 for statistical and biological interpretation (Tyanova et al. 2016). To ensure data quality, contaminants, reverse hits, and low-confidence identifications were filtered out. An overview of the proteomic profiles of all three *B. pseudomallei* clinical strains was then analysed and a Venn diagram was used to visualise the relationship between all three strains.

The proteins were then filtered according to the highest iBAQ (intensity-based absolute quantification) intensity across all three *B. pseudomallei* strains and the top 20 proteins with the highest iBAQ values were identified. The iBAQ method offers a reliable estimate of absolute protein abundance by normalising summed peptide intensities against the number of theoretically observable peptides. Selecting the top 20 ranked proteins

UNIVERSITI KEBANGSAAN MALAYSIA

highlights highly expressed proteins that may play critical roles in virulence, persistence, and host-pathogen interactions.

Then, the dataset underwent filtration, and missing values were imputed to maintain consistency and avoid loss of important data during analysis. A stringent criterion was applied, requiring each protein to be present in at least 70% of the nine replicates in at least one group, meaning it had to be detected in at least seven out of nine replicates in at least one group to ensure consistency. Missing values were imputed based on their normal distribution across replicates to simulate low-abundance proteins below the detection limit.

b. Differentially expressed protein analysis

Differential expression analysis was then carried out using one-way ANOVA, followed by post hoc testing to identify proteins that were significantly upregulated or downregulated between the groups. The statistical threshold for significance was set at a p-value < 0.05. Fold change was then calculated and a cut-off of > 1.5 for both upregulated and downregulated proteins was applied. The data was then grouped into two comparison groups: i) PS_UMC083 compared to NI_UMC082 and ii) PS_UMC083 compared to RS_UMC114 (82 vs 114?). A heat map of differentially regulated proteins was generated using the Prism 8 software for both comparison groups.

Functional annotation and interaction analysis were then conducted for upregulated and downregulated proteins in both comparison groups using PANTHER (Protein Analysis Through Evolutionary Relationships) (https://pantherdb.org/) and STRING (Search Tool for the Retrieval of Interacting Genes/Proteins) (https://string-db.org/). PANTHER was used to determine the classification of proteins into molecular functions, biological processes, and cellular components, providing insights into their functional roles within the cell. STRING v11.5 was used to construct protein-protein interaction (PPI) networks (selecting *B. pseudomallei* as the reference organism and applying a medium confidence threshold (combined score ≥ 0.4). STRING integrates experimental data, curated databases, co-expression profiles, and computational predictions to generate comprehensive interaction maps across thousands of organisms (Szklarczyk et al., 2025). This highlighted how the

UNIVERSITI KEBANGSAAN MALAYSIA

proteins may interact and work together within important biological pathways. Based on this, proteins of interest were elucidated.

c. KEGG pathway enrichment and hub protein bioinformatics analysis

KEGG pathway enrichment analysis was further performed using STRING's built-in functional annotation tool, with significance defined at FDR ≤ 0.05, to functionally interpret differentially expressed proteins across multiple clinical strain comparisons. Annotated locus tags were submitted to KOBAS 3.0 (http://kobas.cbi.pku.edu.cn/kobas3/download/), using *B. pseudomallei* K96243 as the reference organism (Bu et al., 2021). Enrichment was assessed using the hypergeometric test with Benjamini–Hochberg correction for multiple testing. Pathways with corrected p-values < 0.05 were considered statistically significant.

Then after, hub proteins were defined as nodes with a degree ≥ 10, indicating high connectivity and potential regulatory importance. Group-specific networks were subsequently generated for comparison. The KEGG pathway enrichment analysis of identified hub proteins was further performed using STRING's built-in functional annotation tool, with significance defined at FDR ≤ 0.05, to functionally interpret expressed hub proteins. Following that, network diagrams were exported with node colour indicating regulation status and layout optimised to emphasise clustering.

UNIVERSITI KEBANGSAAN MALAYSIA

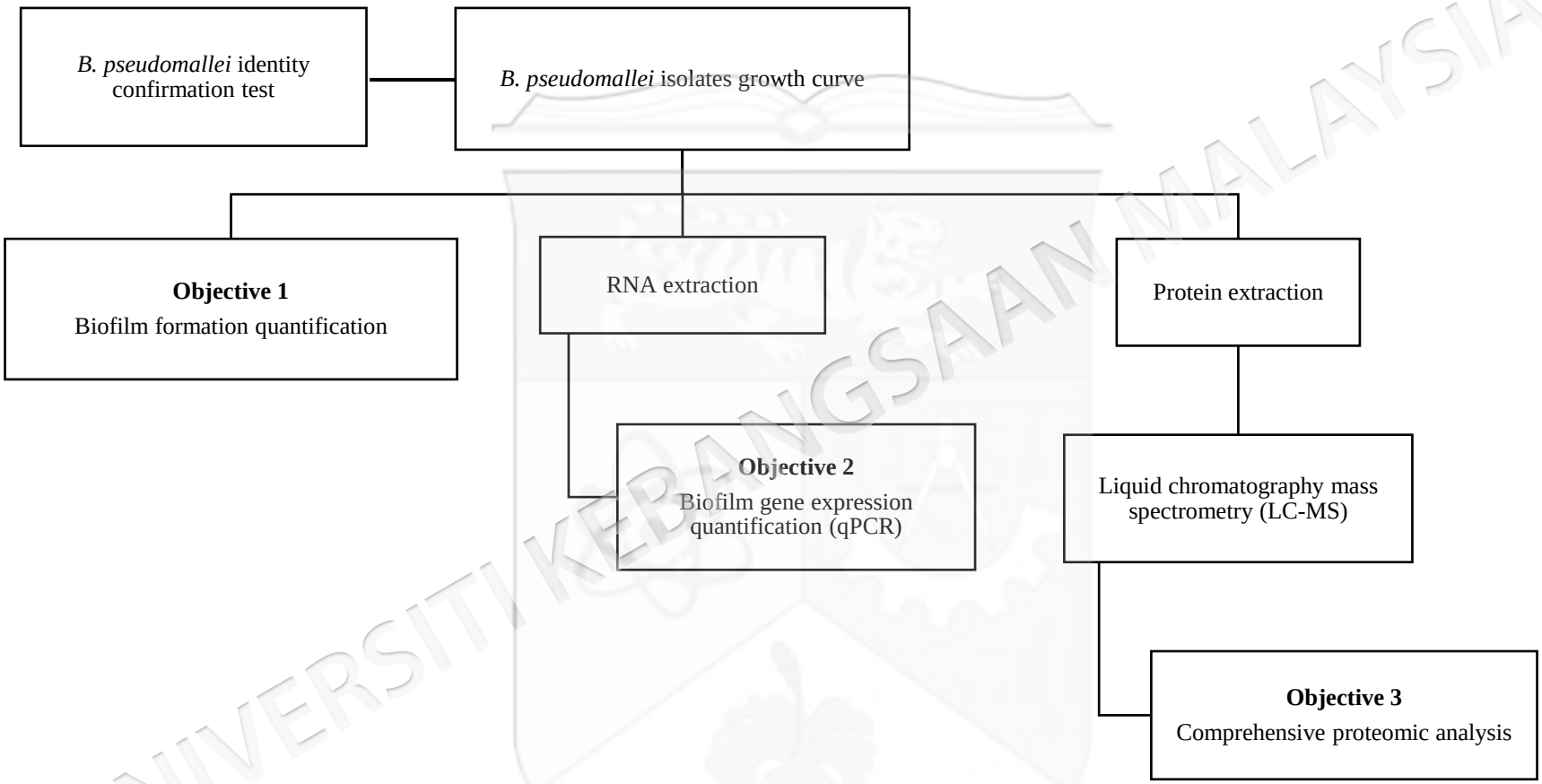

Figure 3.4 Overall project methodology flowchart. The workflow starts with *B. pseudomallei* identity confirmation test. Once the identity of the clinical strains was confirmed, growth curve analysis was conducted for all three *B. pseudomallei* clinical isolates. It is then divided into three main objectives: (1) Biofilm formation quantification (2) RNA extraction, followed by biofilm gene expression quantification, and (3) protein extraction, LC-MS analysis and comprehensive proteomic analysis

UNIVERSITI KEBANGSAAN MALAYSIA

CHAPTER IV

RESULTS

4.1 *B. pseudomallei* Confirmation Test

4.1.1 Phenotypic confirmation of strains PS_UMC083, NI_UMC082 and RS_UMC114 through Ashdown agar cultivation

The morphological observations of *B. pseudomallei* strain PS_UMC083, NI_UMC082, and RS_UMC114 streaked on Ashdown agar (Table 4.1) show the phenotypes of each clinical strain. PS_UMC083 colonies appeared dark purple, dry and slightly wrinkled. Similarly, NI_UMC082 displayed comparable characteristics, with colonies that were dark purple, dry, and slightly wrinkled, showing no discernible differences from PS_UMC083. RS_UMC114 colonies were also dark purple and dry, but exhibited a morphological variation with very wrinkled surfaces. This distinguished it from both PS_UMC083 and NI_UMC082 colonies.

Table 4.1 Morphological observations of clinical strains PS_UMC083, NI_UMC082 and RS_UMC114 on Ashdown agar after 72 hours

Clinical strain	Morphological observation	Colony characteristics
PS_UMC083		• Dark purple • Dry • Slightly wrinkled

… to be continued

… continuation

NI_UMC082	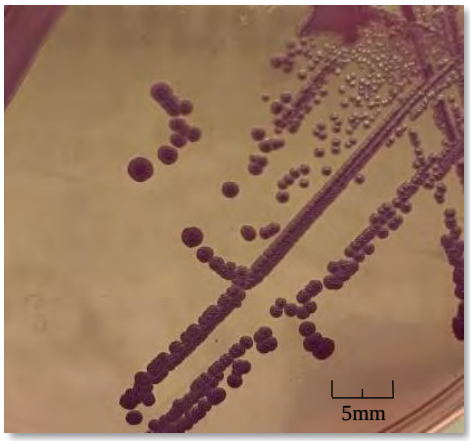	• Dark purple • Dry • Slightly wrinkled
RS_UMC114	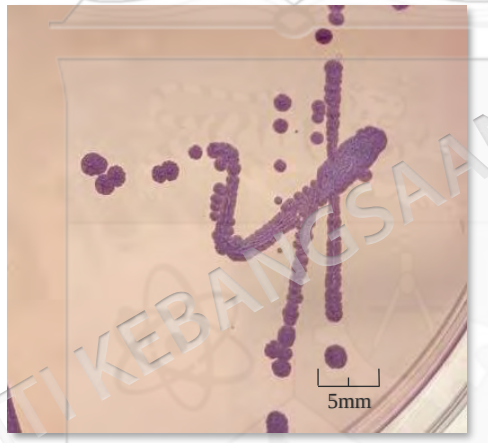	• Dark purple • Dry • Very wrinkled

UNIVERSITI KEBANGSAAN MALAYSIA

4.1.2 Genotypic confirmation of strains PS_UMC114, NI_UMC082 and RS_UMC114 through polymerase chain reaction

Polymerase chain reaction (PCR) was conducted for genomic identification of the three clinical strains. Genes *groEL* and *mprA* were selected due to their specificity for *B. pseudomallei*, with *groEL* encoding a heat shock protein that is highly conserved across species within the genus *Burkholderia*, and *mprA* encoding a transcriptional regulator involved in AMR mechanisms. The amplification of these genes serves as a reliable method for confirming the identity of the clinical isolates, as both *groEL* and *mprA* are well-established genetic markers for *B. pseudomallei*.

Successful amplification of both genes in all three strains (PS_UMC083, NI_UMC082, and RS_UMC114) confirmed their identity as *B. pseudomallei*. The expected product sizes of 139 bp and 162 bp for *groEL* and *mprA* , respectively, were observed in each strain, indicating that the PCR reaction was specific and efficient. The positive control used DNA from *B. pseudomallei* reference strain K96243, produced products of the expected sizes, while the negative control showed no visible bands. The PCR products of *groEL*, *mprA* and positive control *B. pseudomallei* strain K96243 were not sent for sequencing, as species-specific primers previously validated in the literature were used (Suppiah et al. 2010), and the presence of distinct, correctly sized amplicons was sufficient to confirm strain identity for the scope of this study. Figure 4.1 depicts the gel image of the PCR results, clearly indicating the bands that were prominently seen, along with the product sizes.

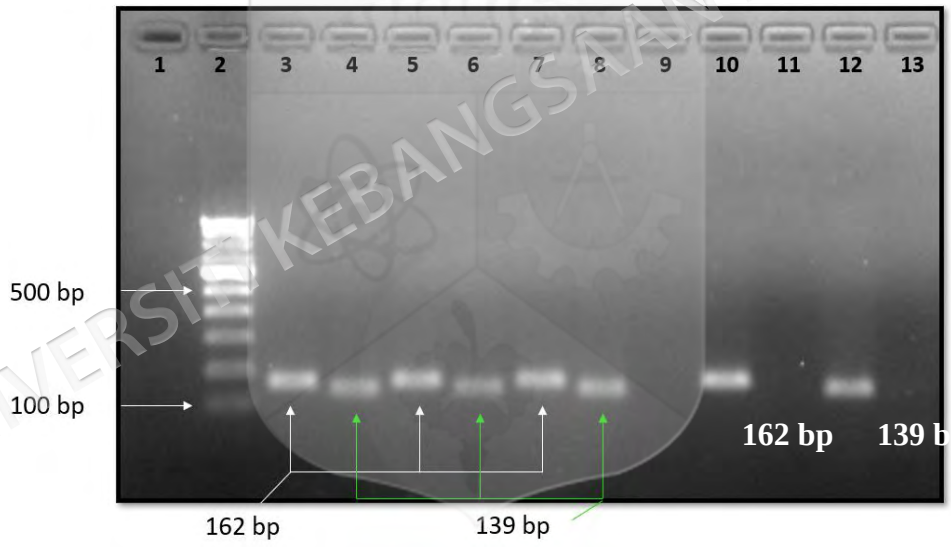

Figure 4.1 PCR-Based Genotypic Confirmation of *B. pseudomallei* Clinical Isolates (PS_UMC083, NI_UMC082, RS_UMC114) via Gel Electrophoresis. Amplification of *groEL* (139 bp), *mprA* (162 bp). Lane 2, 100 bp ladder (Favorgen); lane 3, amplification of *mprA* in PS_UMC083; lane 4, amplification of *groEL* in PS_UMC083; lane 5 amplification of *mprA* in NI_UMC082; lane 6 amplification of *groEL* in NI_UMC082; lane 7 amplification of *mprA* in RS_UMC114; lane 8, amplification of *groEL* in RS_UMC114; lane 9, no sample loaded; lane 10, positive control for *mprA* (refernce strain *B. pseudomallei* K96243) ; lane 12 positive control for *groEL* (reference strain *B. pseudomallei* K96243); lane 11 negative control *mprA* ; lane 13 negative control *groEL*.

UNIVERSITI KEBANGSAAN MALAYSIA

4.2 Bacterial Growth Curve and CFU of Strains PS_UMC083, NI_UMC082 and RS_UMC114

The growth curves of strains PS_UMC083, NI_UMC082, and RS_UMC114 were compared over 24 hours by measuring absorbance at OD_{600nm}, providing an overview of bacterial proliferation for each strain. Both PS_UMC083 and NI_UMC082 exhibited similar growth patterns, with a steady increase in absorbance reaching a peak near 1.6 OD_{600nm} at the 24-hour mark. This indicates slow but robust bacterial growth, with both strains entering the stationary phase around the same time.

However, RS_UMC114 displayed a delayed growth phase, with a slower initial increase in absorbance. While RS_UMC114 experienced a slower start, it eventually reached similar growth levels as PS_UMC083 and NI_UMC082 by the 24-hour mark. This shows that the relapse strain, though delayed in its early growth, could reach comparable final growth levels. The mid-log phase of time for all three clinical strains was found to be around 16 hours, a key point when the strains were actively dividing and exhibiting exponential growth. The 16-hour time point was selected as the mid-log phase due to the consistent and significant increase in absorbance observed across all strains throughout the 24-hour even after the supposed plateau of strain NI_UMC082. This growth trend is visually represented in Figure 4.2, which illustrates the comparative growth curves of the strains over time.

The CFU/mL of clinical strains PS_UMC083, NI_UMC082, and RS_UMC114 were also measured over the same 24-hour time period. PS_UMC083 started with 8.7×10^4 CFU/mL at hour 0 and showed a steady increase, reaching 1.00×10^9 CFU/mL by hour 24, with its highest growth at hour 16. NI_UMC082 began with 7.6×10^4 CFU/mL and grew slower than PS_UMC083, reaching 1.00×10^9 CFU/mL at hour 12, peaking at hour 20, and then dropping slightly by hour 24. RS_UMC114 started at 9.6×10^4 CFU/mL, and grew quickly, peaking at 1.8×10^9 CFU/mL at hour 14, but then its growth slowed down and dropped to 2.6×10^8 CFU/mL by hour 24. Overall, PS_UMC083 had the most consistent and highest growth, while NI_UMC082 grew slower and RS_UMC114 had a quick peak followed by a decline. These CFU dynamics are illustrated in Figure 4.3, which captures the comparative growth trajectories of the three strains over time.

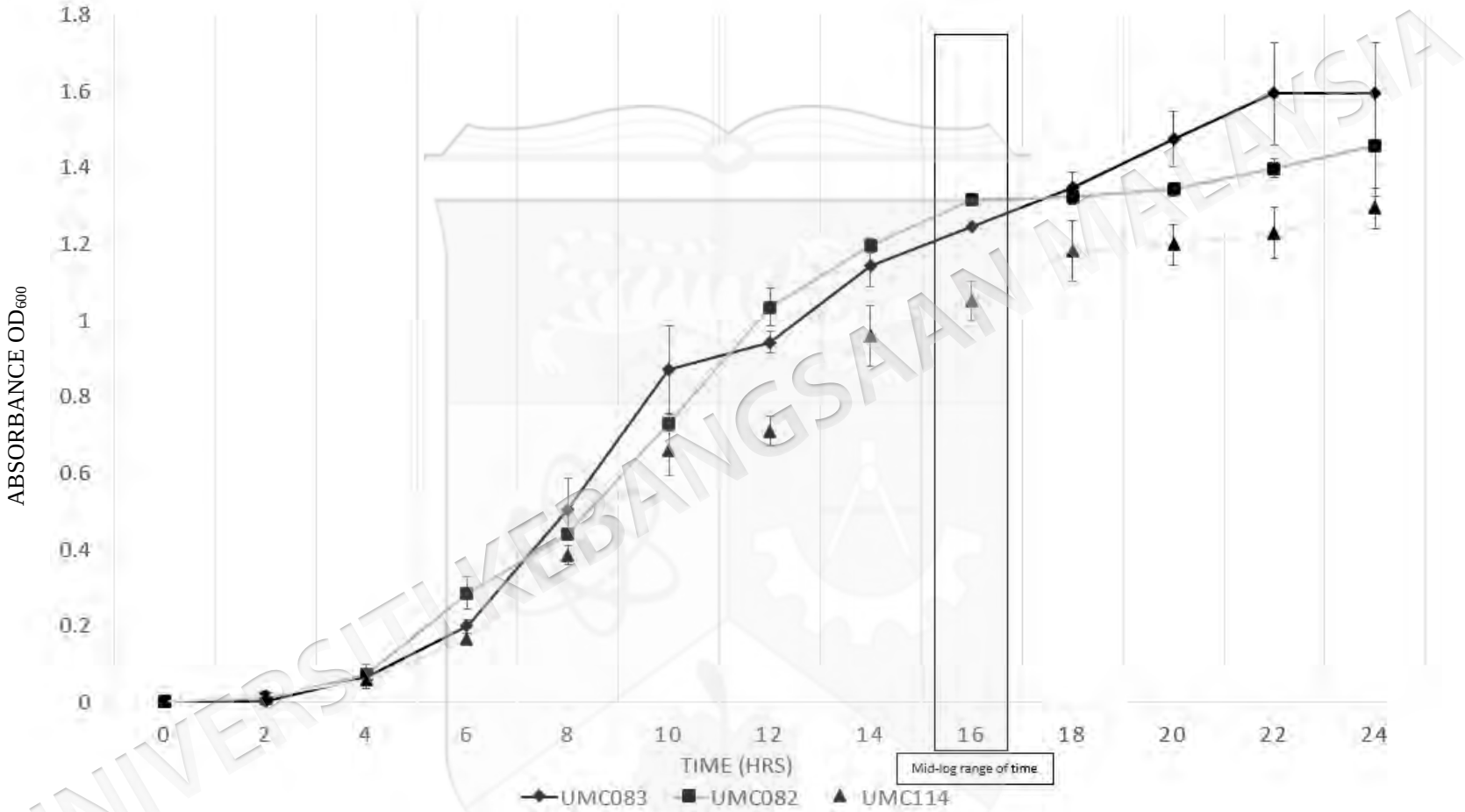

Figure 4.2 Growth curve of *B. pseudomallei* strains PS_UMC083, NI_UMC082 and RS_UMC114 at 37 ºC 180 rpm over 24 hours. Bacterial growth was monitored at bi-hourly intervals using optical density (OD_{600nm}) measurements. All three strains exhibited similar lag phases, with mid-log phase observed at 16 hours. RS_UMC114 demonstrated a slightly accelerated growth rate compared to PS_UMC083 and NI_UMC082 , suggesting potential metabolic adaptation. Data represent the mean ± SD of three biological replicates.

UNIVERSITI KEBANGSAAN MALAYSIA

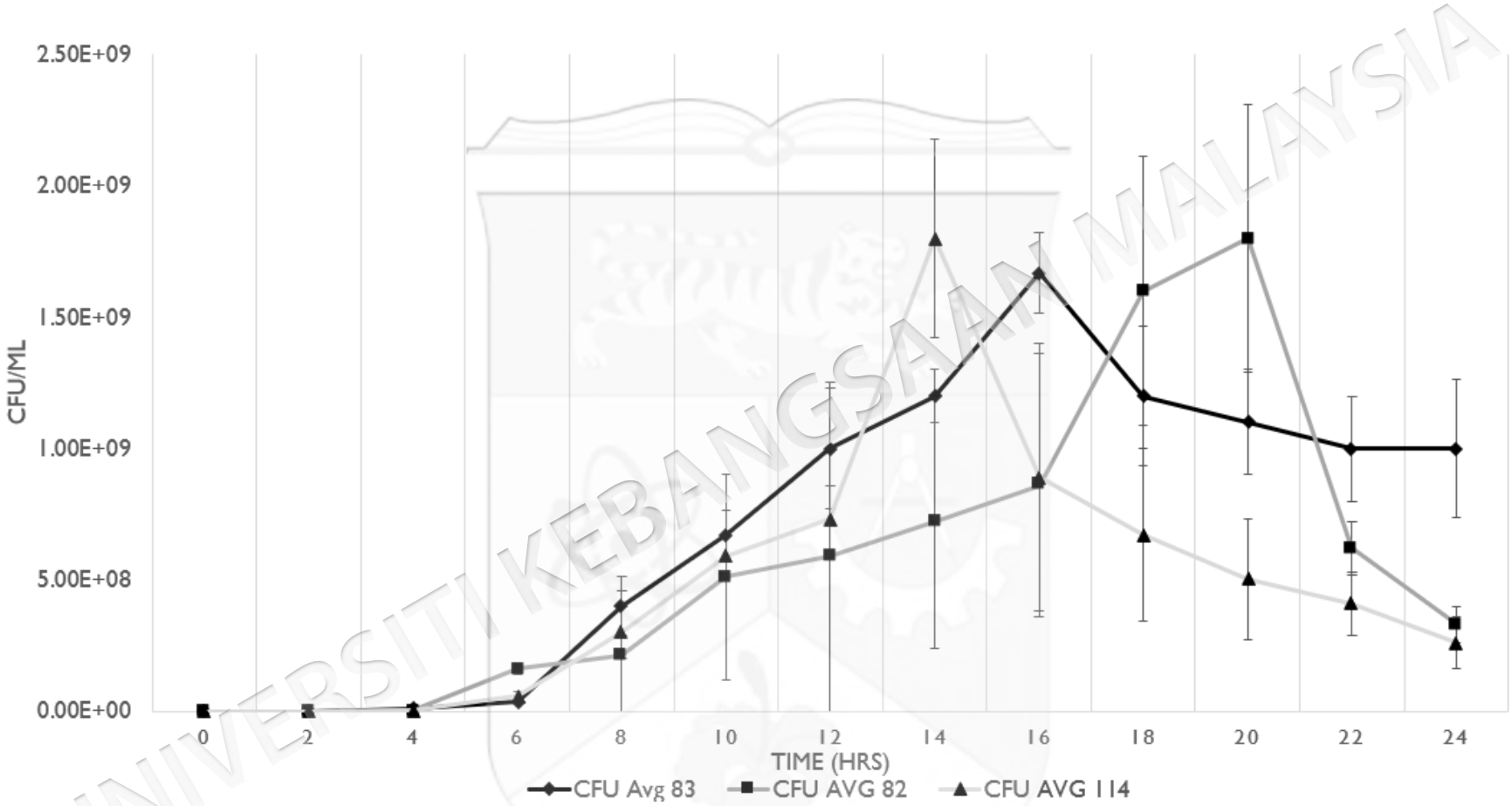

Figure 4.3 Comparative CFU growth curve of *B. pseudomallei* clinical strains PS_UMC083, NI_UMC082, and RS_UMC114 over 24 hours. Colony-forming unit (CFU/mL) measurements were taken at bi-hourly intervals to assess bacterial proliferation. The highest CFU/mL values recorded for each strain were: PS_UMC083 – 1.67E+09 (±1.54E+08), NI_UMC082 – 1.8E+09 (±5.1E+08), and RS_UMC114 – 1.8E+09 (±3.8E+08), with RS_UMC114 showing the greatest overall growth. Data points represent mean values with error bars indicating standard deviation across three biological replicates.

UNIVERSITI KEBANGSAAN MALAYSIA

4.3 Biofilm Quantification of Strains PS_UMC114, NI_UMC082 and RS_UMC114

Biofilm formation was quantified for all three clinical *B. pseudomallei* strains, PS_UMC083, NI_UMC082, and RS_UMC114, at 24, 48, and 72 hours using crystal violet staining (Figure 4.4). Upon 24 hours of incubation, all strains produced comparable amounts of biofilm. However, PS_UMC083 consistently exhibited the lowest biofilm quantity across all time intervals, with absorbance (OD_{570nm}) values of 1.150 ± 0.006 at 24 hours, 1.415 ± 0.077 at 48 hours, and 4.210 ± 0.353 at 72 hours. RS_UMC114 showed the highest biofilm production at both 48 hours (3.482 ± 0.372) and 72 hours (10.51 ± 0.641), followed by NI_UMC082 with 2.075 ± 0.201 and 7.133 ± 0.195, respectively. Statistically significant differences in biofilm production were observed between consecutive time points (24 h vs. 48 h, and 48 h vs. 72 h; $p < 0.05$), as well as between strains at each time point ($p < 0.05$).

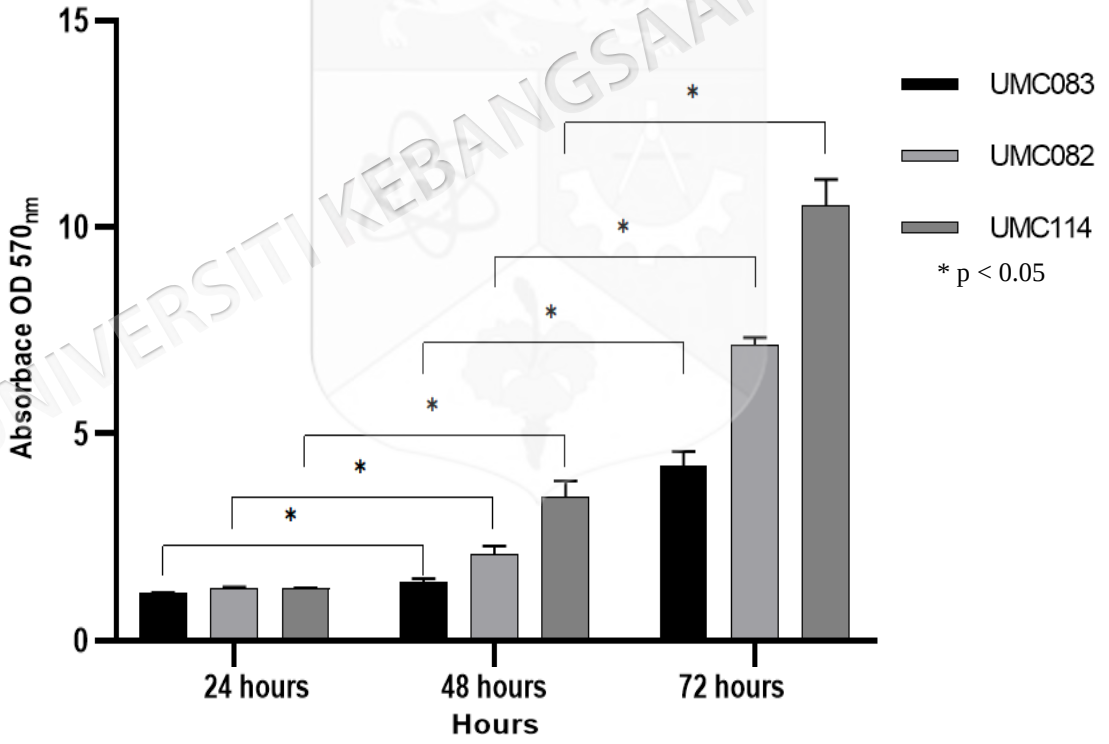

Figure 4.4 Biofilm quantification of *B. pseudomallei* clinical strains PS_UMC083, NI_UMC082, and RS_UMC114 at 24, 48, and 72 hours, measured by OD_{570nm}. Biofilm biomass was quantified via crystal violet staining and OD_{570nm} measurement. All strains showed a significant time-dependent increase in biofilm production ($p < 0.05$), with RS_UMC114 exhibiting the highest levels at 48 and 72 hours, and PS_UMC083 consistently produced the least across all time points.

UNIVERSITI KEBANGSAAN MALAYSIA

4.4 Quantification of Biofilm Gene Expression of all Three *B. pseudomallei* Clinical Strains

4.4.1 Biofilm gene confirmation of all three *B. pseudomallei* clinical strains through PCR

PCR successfully amplified all target biofilm-related genes *bpsl0603*, *bpsl2026*, *bpss2016*, *bpss0312*, *bpss1214*, *bpss0124*, *bpsl1607*, *bpsl1799*, along with the housekeeping gene *16s rRNA*, in all three *B. pseudomallei* clinical strains (Figure 4.5). Amplification in the positive control, using DNA from the *B. pseudomallei* reference strain K96243, yielded products at the expected amplicon sizes for each target gene, confirming the viability of the PCR conditions and reagents.

The observed amplicon sizes were as follows: *bpsl0603* (162 bp), *bpsl2026* (93 bp), *bpss2016* (147 bp), *bpss0312* (90 bp), *bpss1214* (124 bp), *bpss0124* (84 bp), *bpsl1607* (104 bp), *bpsl1799* (92 bp), and *16s rRNA* (82 bp). No amplification was observed in the negative control, confirming the absence of contamination. Furthermore, no non-specific amplification was detected, validating the specificity of the primers used in this study. These results confirm the presence of the selected biofilm-related genes in all three clinical strains.

UNIVERSITI KEBANGSAAN MALAYSIA

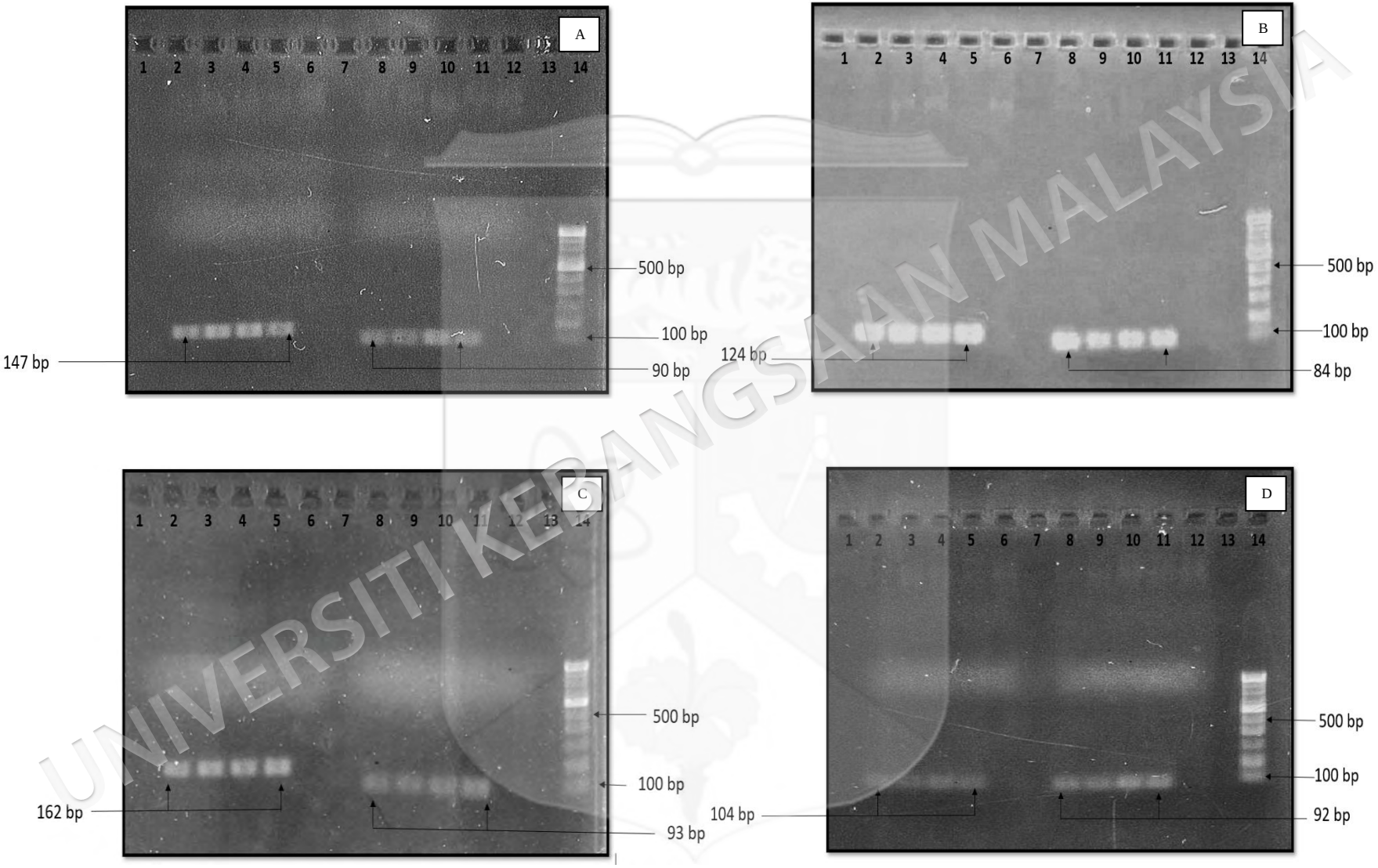

UNIVERSITI KEBANGSAAN MALAYSIA

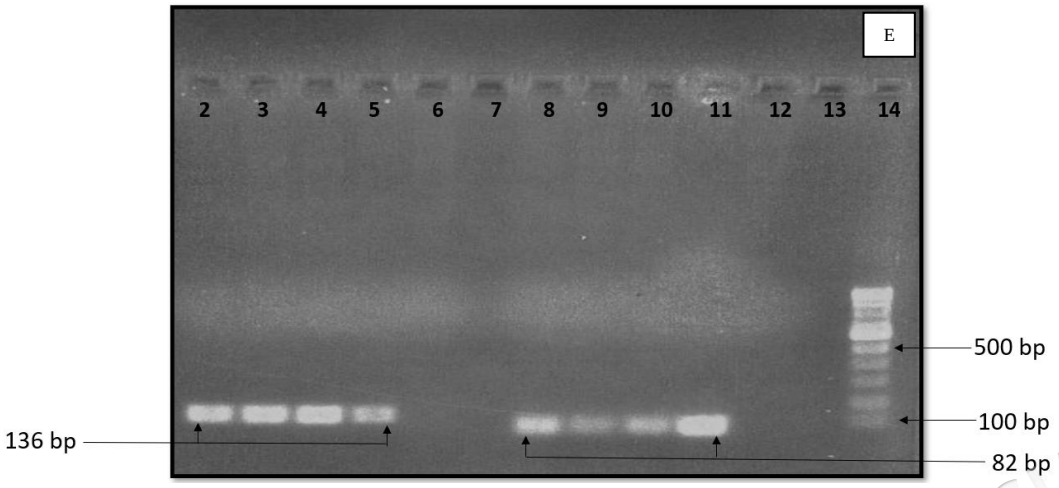

Figure 4.5 Biofilm gene confirmation of PS_UMC083, NI_UMC082, and RS_UMC114 visualised via gel electrophoresis. Gel electrophoresis was used to confirm biofilm genes present across all three clinical strains: (A) Genes *bpss2016* (lanes 2-5) and *bpss0312* (lanes 8-11); (B) genes *bpss1214* (lanes 2-5) and *bpss0124* (lanes 8-11); (C) genes *bpsl0603* (lanes 2-5) and *bpsl2026* (lanes 8-11); (D) genes *bpsl1607* (lanes 2-5) and *bpsl1799* (lanes 8-11); (E) genes *dnak* (lanes 2-5) and *16s rRNA* (lanes 8-11). Lane 2 - PS_UMC083; lane 3 - NI_UMC082; lane 4 - RS_UMC114; lane 5 - *B. pseudomallei* K96243 (positive control); lane 6 – dH_2O (negative control); lane 8 - PS_UMC083; lane 9 - NI_UMC082; lane 10 - RS_UMC114; lane 11 - K9 (positive control); lane 12 - dH_2O (negative control); lane 14 - 100 bp ladder (Favorgen)

4.4.2 Quantitative polymerase chain reaction annealing temperature optimisation

To optimise the annealing temperature for quantitative PCR (qPCR) assays, amplification of the target genes *bpsl0603*, *bpsl2026*, *bpss2016*, *bpss0312*, *bpss1214*, *bpss0124*, *bpsl1607*, *bpsl1799*, *dnak*, and *16s rRNA* was tested at two different annealing temperatures (56 ˚C and 58 ˚C) (Figure 4.6). Although primers were sourced from published studies, temperature optimisation was necessary due to potential variations in laboratory conditions, reaction setups, and reagent kits, all of which can influence primer specificity and amplification efficiency. This step was essential to ensure reliable and reproducible results under the specific parameters of this study.

PCR successfully amplified all target genes at both temperatures, with the positive control (DNA from *B. pseudomallei* strain K96243) producing bands at the expected amplicon sizes. No amplification was observed in the negative control, and no non-specific bands were detected, confirming the specificity of the primers. At 56 ˚C, clear and distinct bands were observed for all tested biofilm-related genes, indicating efficient amplification. In contrast, at 58 ˚C, bands for *bpsl1607* and *bpsl1799* appeared faded, suggesting reduced amplification efficiency at the higher temperature. These observations indicate that 56 ˚C is the more suitable annealing temperature for these qPCR assays, as it provides optimal amplification without compromising specificity across the target gene set.

UNIVERSITI KEBANGSAAN MALAYSIA

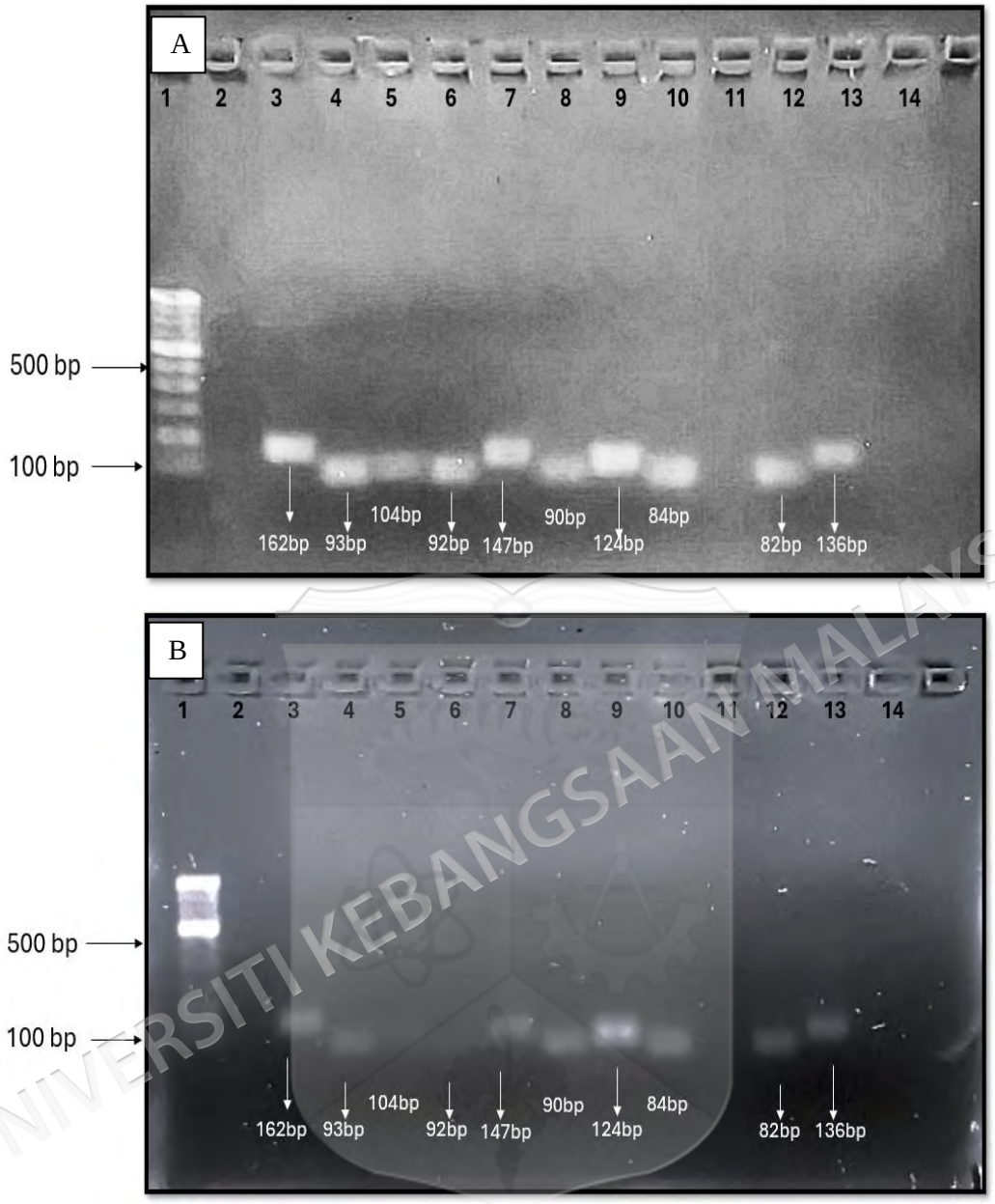

UNIVERSITI KEBANGSAAN MALAYSIA

Figure 4.6 Optimisation of PCR annealing temperatures for quantitative gene expression analysis in *B. pseudomallei*. Gel electrophoresis was used to observe the amplification of DNA samples of *B. pseudomallei* strain K96243 in two different annealing temperatures: (A) 56 ˚C; (B) 58 ˚C. Lane 1, 100 bp ladder (Favorgen); lane 3, amplification of *bpsl0603*; lane 4, amplification of *bpsl2026*; lane 5 amplification of *bpsl1607*; lane 6 amplification of *bpsl1799*; lane 7 amplification of *bpss2016*; lane 8, amplification of *bpss0312*; lane 9, amplification of *bpss1214*; lane 10, amplification of *bpss0124*; lane 12, amplification of *16s rRNA* (positive control); lane 13, amplification of *dnak* (positive control); Lane 14, negative control.

4.4.3 RNA integrity validation for cDNA conversion using gel electrophoresis

RNA integrity validation was performed to assess the quality of RNA extracted from PS_UMC083, NI_UMC082, and RS_UMC114, ensuring its suitability for downstream qPCR analysis (Figure 4.7). Gel electrophoresis revealed distinct, sharp bands corresponding to the 23S and 16S ribosomal RNA (rRNA) in all three *B. pseudomallei* strains, indicating high-quality RNA suitable for cDNA synthesis. The 23S rRNA band appeared as the upper, more intense band, while the 16S rRNA band was slightly lower and less intense, which is consistent with expected bacterial rRNA profiles.

No smearing or additional degraded fragments were observed, confirming RNA integrity and the success of the extraction process. These results validate the quality of the RNA samples and support their reliability for subsequent qPCR analysis.

Figure 4.7 Gel electrophoresis of PS_UMC083, NI_UMC082, and RS_UMC114 RNA samples for RNA integrity validation prior to cDNA conversion. The gel electrophoresis image shows the integrity of RNA extracted from all three clinical strains of *B. pseudomallei* (PS_UMC083, NI_UMC082, RS_UMC114). Lane 1 – 100 bp ladder (Favorgen); Lane 3 – PS_UMC083A; Lane 4 – PS_UMC083C; Lane 5 – PS_UMC083D; Lane 7 – NI_UMC082A; Lane 8 – NI_UMC082B; Lane 9 – NI_UMC082C; Lane 11 – RS_UMC114C; Lane 12 – RS_UMC114D; Lane 13 – RS_UMC114E. Clear, intact rRNA (23S rRNA and 16S rRNA) bands were observed for each strain, confirming that the RNA was of sufficient quality and suitable for cDNA synthesis and subsequent qPCR analysis

UNIVERSITI KEBANGSAAN MALAYSIA

4.4.4 qPCR gene expression analysis

To evaluate the gene expression levels of biofilm-related genes in the clinical strains, qPCR was performed. RNA samples used for qPCR were obtained from cultures grown to mid-log phase after 16 hours of incubation. The cycle threshold (Ct) value of each gene replicate was first normalised to the housekeeping gene (*16S rRNA*), relative to its corresponding replicate. Fold changes in gene expression for NI_UMC082 and RS_UMC114 were then calculated relative to PS_UMC083, to assess upregulation or downregulation of the target genes.

PS_UMC083 was selected as the baseline for comparison to ensure clinical relevance, as it had undergone the same antibiotic treatment and host immune response as the subsequent isolates. Using this strain provided a more accurate and meaningful assessment of gene expression changes associated with bacterial adaptation, persistence, and relapse within the same host environment. In contrast, reference strain *B. pseudomallei* K96243 lacks this clinical context and could introduce confounding variables.

This comparative approach enabled a more clinically relevant evaluation of transcriptional changes across the infection timeline. Based on this framework, the qPCR results revealed distinct expression patterns among the biofilm-related genes in the patient-derived isolates. Fold change values for each gene are indicated in brackets, corresponding to the respective strain and gene. Both NI_UMC082 and RS_UMC114 exhibited similar overall patterns, with most biofilm-related genes being downregulated.

Notably, *bpss1214* was more downregulated in RS_UMC114 (fold change = -3.4) compared to NI_UMC082 (fold change =-2.6). Only *bpsl0603* (fold change = 0.5) and *bpsl2026* (fold change = 0.5) were upregulated in RS_UMC114, although these changes were not statistically significant when compared to the PS_UMC083. In NI_UMC082, *bpsl0603* (fold change = -0.6) and *bpss0124* (fold change = -2.4) showed the lowest fold changes, while in RS_UMC114, the lowest expression levels were observed for *bpsl1607* (fold change = -1.3) and *bpss0312* (fold change = -1.6). These transcriptional profiles are illustrated in Figure 4.8, which presents the qPCR results across the selected biofilm-related genes.

UNIVERSITI KEBANGSAAN MALAYSIA

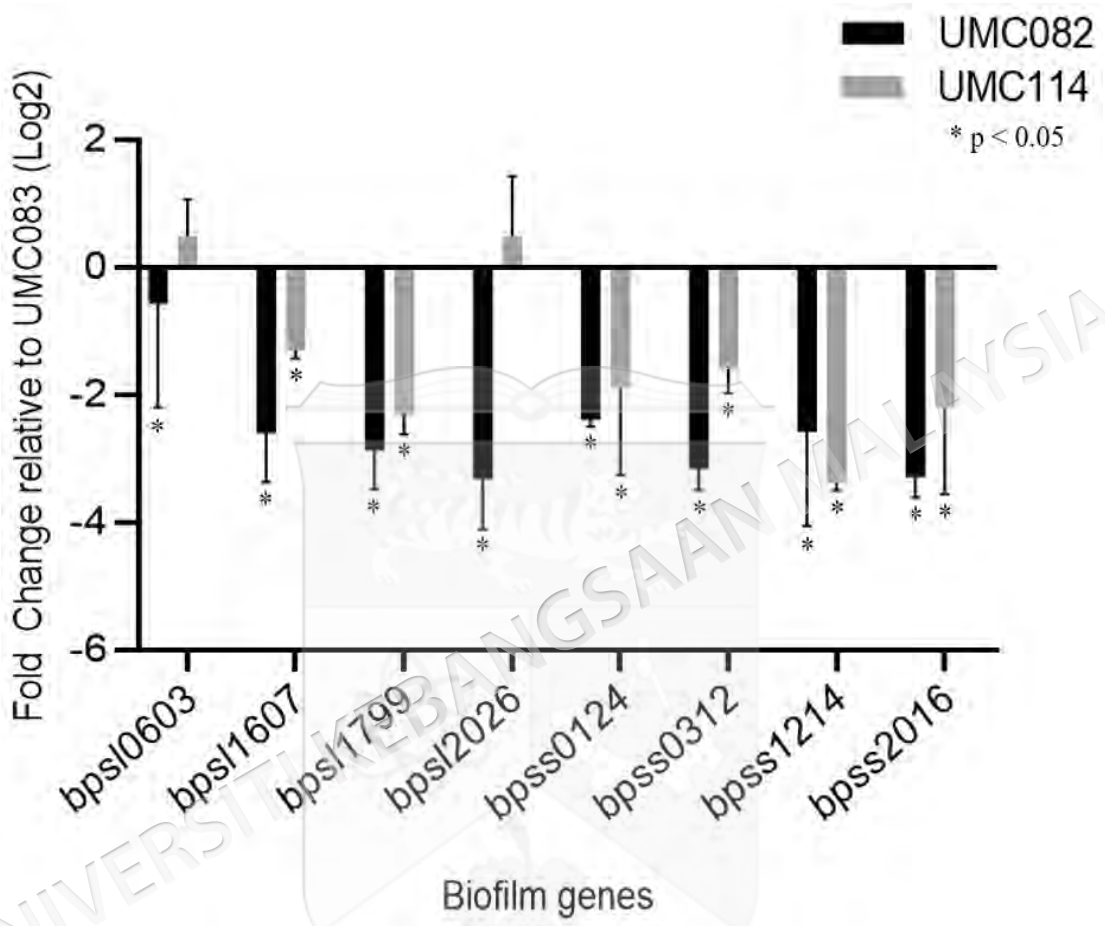

Figure 4.8 qPCR gene expression analysis of eight biofilm-related genes in *B. pseudomallei* strains NI_UMC082 and RS_UMC114, relative to PS_UMC083 after 16 hours of culture. The fold change in gene expression was normalised to the housekeeping gene, 16S rRNA, and compared across the strains to determine differential gene expression. The analysis revealed downregulation of most biofilm-related genes in both NI_UMC082 and RS_UMC114, with NI_UMC082 showing more significant downregulation. Notably, genes BPSL0603 and BPSL2026 in RS_UMC114 were upregulated, although this upregulation was not statistically significant compared to PS_UMC083.

UNIVERSITI KEBANGSAAN MALAYSIA

4.5 Proteomics Analysis to Determine Differentially Expressed Proteins in all Three *B. pseudomallei* Clinical Isolates

4.5.1 Bradford assay of all three *B. pseudomallei* strains

The protein concentrations of the *B. pseudomallei* clinical strains were measured using the Bradford assay, a commonly employed assay to quantify protein concentrations (Table 4.2). The concentrations of protein in the clinical strain samples varied, with PS_UMC083 showing the highest protein concentrations among the three strains. Specifically, PS_UMC083A had a concentration of 31.61 µg/µL, while PS_UMC083B and PS_UMC083C had concentrations of 25.06 µg/µL and 25.16 µg/µL, respectively.

In comparison, NI_UMC082 exhibited lower protein concentrations, with NI_UMC082A having the highest concentration of 17.53 µg/µL, followed by NI_UMC082B (18.65 µg/µL) and NI_UMC082C (15.26 µg/µL). Similarly, RS_UMC114 also displayed relatively lower protein concentrations, with RS_UMC114A showing 21.03 µg/µL, RS_UMC114B at 22.83 µg/µL, and RS_UMC114C having the lowest protein concentration of 12.74 µg/µL

Table 4.2 Neat protein concentration of all three *B. pseudomallei* strains.

Sample ID	Neat concentration (ug/uL)
PS_UMC083A	31.61
PS_UMC083B	25.06
PS_UMC083C	25.16
NI_UMC082A	17.53
NI_UMC082B	18.65
NI_UMC082C	15.26
RS_UMC114A	21.03
RS_UMC114B	22.83
RS_UMC114C	12.74

UNIVERSITI KEBANGSAAN MALAYSIA

4.5.2 SDS-PAGE analysis of extracted proteins from PS_UMC083, NI_UMC082 and RS_UMC114 across varying concentrations

SDS-PAGE was performed to validate the protein extraction method for total proteins from *B. pseudomallei*. The amount of protein loaded onto the gel for each strain was quantified using the Bradford assay. Based on this, 20, 40, 60, 80, and 100 µg of protein were loaded for analysis. Equal volumes of protein lysates were standardised across all samples to ensure consistent comparison of band intensity and migration profiles.

The resulting gels displayed band patterns ranging from below 15 kDa to above 100 kDa, indicating successful separation based on molecular weight (Figure 4.9). Prominent bands were observed around the 60 – 50 kDa and 35 kDa regions, suggesting the presence of several abundant proteins within these molecular weight ranges. In contrast, bands corresponding to the 23 kDa region appeared faint, indicating that proteins in this range may be expressed at lower levels or are less stable during the extraction process.

The gel profiles confirmed that the protein extraction protocol was effective in isolating a broad spectrum of soluble proteins, with good resolution across a wide range of molecular weights.

UNIVERSITI KEBANGSAAN MALAYSIA

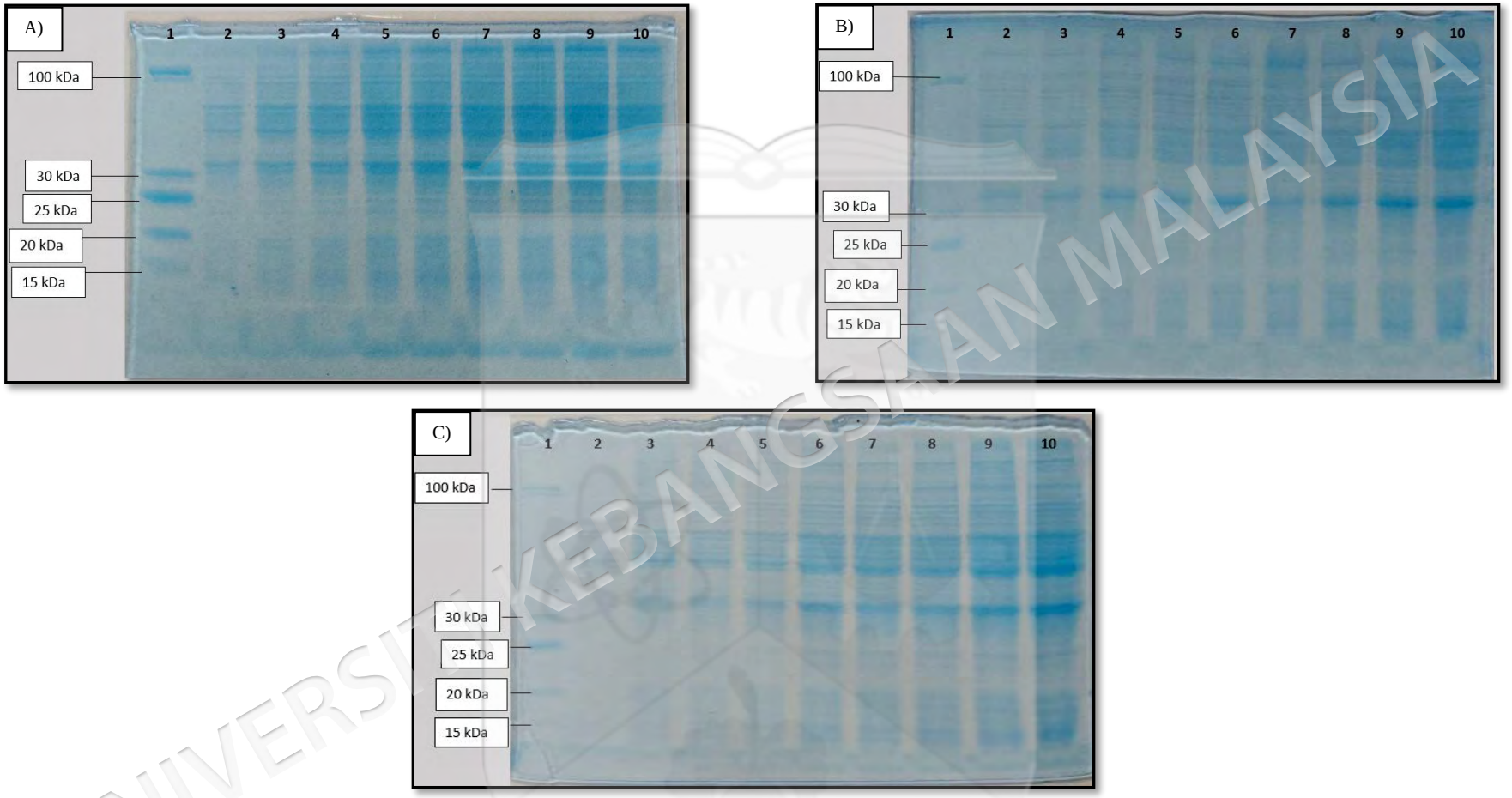

Figure 4.9 SDS-PAGE profile of total soluble protein extracts from PS_UMC083, NI_UMC082, and RS_UMC114 at varying concentrations. (A) PS_UMC083, (B) NI_UMC082, (C) RS_UMC114. Lane 1: 100 kDa protein marker (1st Base, Singapore); Lane 2–10: Protein samples at concentrations of 10 µg, 15 µg, 20 µg, 25 µg, 30 µg, 35 µg, 40 µg, 45 µg, and 50 µg, respectively.

UNIVERSITI KEBANGSAAN MALAYSIA

4.5.3 Overview of proteomic profiles of PS_UMC083, NI_UMC082 and RS_UMC114

a. Proteomic characterisation and overlap analysis of PS_UMC083, NI_UMC082 and RS_UMC114

A total of 1,015 proteins were identified through LC-MS analysis of total soluble proteins extracted from the three *B. pseudomallei* clinical strains. The raw data underwent stringent post-processing to remove contaminants, reverse hits, and low-confidence identifications, ensuring high-quality protein assignments. A Venn diagram was used to visualise the distribution of identified proteins across strains PS_UMC083, NI_UMC082, and RS_UMC114 (Figure 4.10).

The number of proteins identified was 725 for PS_UMC083, 821 for NI_UMC082, and 832 for RS_UMC114. Of these, 671 proteins were shared among all three strains. Pairwise comparisons revealed 25 proteins shared exclusively between PS_UMC083 and NI_UMC082, 21 between PS_UMC083 and RS_UMC114, and 103 between NI_UMC082 and RS_UMC114. In addition, unique proteins were identified in each strain: NI_UMC082 had 22, RS_UMC114 had 37, and PS_UMC083 had eight proteins. These unique proteins are listed in Table 4.3, organised by strain and ranked according to their iBAQ intensity values.

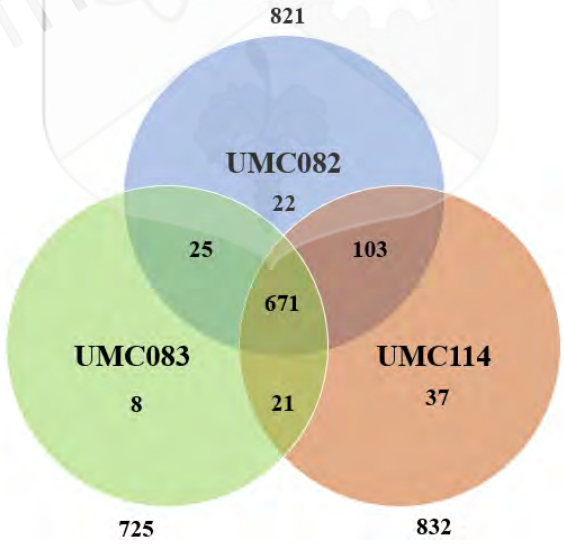

Figure 4.10 Venn diagram of total proteins identified across strains PS_UMC083, NI_UMC082, and RS_UMC114. The diagram illustrates the common proteins identified among all three clinical strains, along with the unique proteins for each strain and those shared between pairs of strains. In the Venn diagram, PS_UMC083 is represented in green, NI_UMC082 in blue, and RS_UMC114 in red.

UNIVERSITI KEBANGSAAN MALAYSIA

Table 4.3 Overview of unique proteins identified across PS_UMC083, NI_UMC082 and RS_UMC114 *B. pseudomallei* clinical strains

Strain	Accession	Protein name	iBAQ intensity	PANTHER protein class
PS_UMC083	Q63U14	Efflux pump membrane transporter	5.74E+08	-
	Q3JKP8	Uncharacterized protein	3.03E+08	-
	Q63V83	Phosphoglucosamine mutase	2.93E+08	mutase
	Q63RG0	glycerophosphodiester phosphodiesterase	2.32E+08	phosphodiesterase
	Q63TI6	Lipoprotein	1.33E+08	-
	Q63JZ7	N-acylhomoserine lactone-dependent regulatory protein	1.18E+08	winged helix/forkhead transcription factor
	Q3JSJ9	Outer membrane efflux protein	9.53E+07	-
	Q63PZ2	Phenylacetic acid degradation protein PaaC	6.75E+07	oxidoreductase
NI_UMC082	Q63TP8	Translation initiation factor IF-2	1.18E+09	translation initiation factor
	A0A0H3HUF1	Uncharacterized protein	7.92E+08	-
	Q63M22	Universal stress protein	7.21E+08	-
	A3NUR2	Ribonuclease R (RNase R)	5.19E+08	-
	A3NYV5	WcbC protein	4.79E+08	-
	Q63JX6	Exported protein	4.73E+08	-
	Q63IW0	Acetate kinase (Acetokinase)	4.34E+08	kinase
	A0AA40JIL9	Efflux transporter, outer membrane factor (OMF) lipo, NodT family protein	4.04E+08	-
	Q63SH0	Membrane protein	3.92E+08	oxidase
	A0A0H3HFW0	DUF4347 domain-containing protein	3.90E+08	-

... to be continued

UNIVERSITI KEBANGSAAN MALAYSIA

...continuation

	A3NZY5	Helicase, C-terminal	3.43E+08	-
	Q63YT5	Uncharacterized protein	3.23E+08	-
	Q63QZ2	RNA-methylase protein	2.59E+08	RNA processing factor
	Q63WG6	ABC transporter ATP-binding protein	2.39E+08	ATP-binding cassette (ABC) transporter
	A3NTA4	Triosephosphate isomerase (TIM) (TPI)	2.26E+08	-
	Q3JNI8	Ribonuclease II (RNB) family protein	1.66E+08	-
	Q63SN5	Chaperone protein HscA homolog	1.62E+08	Hsp70 family chaperone
	Q63HY9	DksA/TraR C4-type zinc finger protein	1.19E+08	DNA-binding transcription factor
	Q63SL2	Nitrate/nitrite transporter	7.19E+07	transporter
	Q63PL0	L-serine dehydratase (EC 4.3.1.17)	6.45E+07	dehydratase
	Q63NL2	Selenide, water dikinase (Selenium donor protein) (Selenophosphate synthase)	4.41E+07	transferase
	Q63L07	Iron transport receptor protein	3.16E+07	-
RS_UMC114	Q63PB1	Fatty aldehyde dehydrogenase	2.15E+10	dehydrogenase
	Q63WT2	Exported protein	7.87E+09	-
	Q63LQ2	Uncharacterized protein	3.60E+09	-
	Q63Q57	3-dehydroquinate synthase (DHQS)	1.39E+09	lyase
	Q63K35	Effector protein BipC	1.18E+09	-
	A0A0H3HGR2	Fatty acid desaturase domain-containing protein	7.92E+08	-
	Q3JUV0	Glutamine-dependent NAD(+) synthetase (NAD(+) synthase [glutamine-hydrolysing])	7.21E+08	-
	A0AAP8HAQ0	deleted	5.19E+08	-

... to be continued

UNIVERSITI KEBANGSAAN MALAYSIA

... continuation

Q63RZ7	phosphoglycolate phosphatase	5.13E+08	phosphatase
A3NYX4	Para-aminobenzoate synthase, component I	4.79E+08	-
Q3JNC5	Enoyl-CoA hydratase/isomerase family protein	4.73E+08	-
Q3JL70	N-acetylmuramoyl-L-alanine amidase	4.34E+08	-
Q63S80	Large ribosomal RNA subunit accumulation protein YceD (23S rRNA accumulation protein YceD)	4.21E+08	-
A0AA40J823	D-isomer-specific 2-hydroxyacid dehydrogenase, NAD-binding domain protein	4.04E+08	-
Q63K04	Kumamolisin	3.92E+08	serine protease
A0A0E1W4C9	Ubiquinol oxidase subunit 2	3.90E+08	-
Q63YC0	Negative regulator of flagellin synthesis (Anti-sigma-28 factor)	3.61E+08	-
A3P299	Multidrug efflux pump BpeE	3.43E+08	-
Q63PE0	2-amino-3-ketobutyrate coenzyme A ligase (AKB ligase) (Glycine acetyltransferase)	3.43E+08	transaminase
Q63Y60	2-nitropropane dioxygenase	3.30E+08	oxygenase
Q63LB7	DNA-binding protein H-NS-like C-terminal domain-containing protein	3.23E+08	-
Q63J38	Dehydrogenase	2.59E+08	dehydrogenase
Q63K69	Type VI secretion system contractile sheath small subunit	2.39E+08	-
Q63S32	tRNA (guanine-N(1)-)-methyltransferase (M1G-methyltransferase) (tRNA [GM37] methyltransferase)	2.35E+08	RNA processing factor
A0AA40MET5	UDP-N-acetylmuramate--L-alanyl-gamma-D-glutamyl-meso-2,6-diaminoheptandioate ligase (Murein peptide ligase) (UDP-N-acetylmuramate: L-alanyl-gamma-D-glutamyl-meso-diaminopimelate ligase)	2.26E+08	-

... to be continued

UNIVERSITI KEBANGSAAN MALAYSIA

...continuation

Q939D3	Bacterial regulatory helix-turn-helix, lysR family protein (Hydrogen peroxide-inducible genes activator) (Oxidative stress regulatory protein OxyR)	2.24E+08	-
Q63VL8	Nudix hydrolase domain-containing protein	2.05E+08	pyrophosphatase
A3P6X2	GTP cyclohydrolase I	1.66E+08	-
Q63K33	Surface presentation of antigen proteins	1.62E+08	-
A3P715	Type III secretion system needle protein	1.19E+08	-
Q63K19	Type III secretion system protein	7.19E+07	-
Q63J07	Isochorismatase-like domain-containing protein	6.45E+07	hydrolase
Q63UU0	Predicted 3'-5' exonuclease PolB-like domain-containing protein	6.28E+07	DNA metabolism protein
Q63IV4	Deoxyribose-phosphate aldolase	4.41E+07	aldolase
Q63VZ5	Cytochrome C-related protein	3.98E+07	oxidase
Q3JRL4	Molybdopterin molybdenumtransferase	3.16E+07	-
Q63QN4	Histone H1-like protein	6.96E+05	-

UNIVERSITI KEBANGSAAN MALAYSIA

b. Top 20 abundant proteins identified across PS_UMC083, NI_UMC082 and RS_UMC114

The top 20 most abundant proteins, based on iBAQ intensity, were identified across all three *B. pseudomallei* strains (Table 4.4). Dominating the list is chaperonin *groEL* 1 (majority protein ID: Q3JPF6), with an iBAQ intensity of 5.51×10^{11}, followed by elongation factor Tu (Q63PZ6) at 2.60×10^{11} and arginine deiminase (Q63U73) at 2.05×10^{11}. These top-ranking proteins span several functional categories, including molecular chaperones (e.g., *groEL* 1, co-chaperonin GroES, DnaK), translation elongation factors (e.g., EF-Tu, EF-G), and enzymes involved in central metabolic pathways (e.g., ornithine carbamoyltransferase, citrate synthase).

Proteins associated with oxidative stress responses, such as alkyl hydroperoxide reductase C (Q63T73) and putative oxidoreductase (Q63RC4), were also identified among the most abundant, with iBAQ intensities of 1.70×10^{11} and 4.60×10^{10}, respectively. Structural and metabolic proteins, including flagellin (Q9S639) and ATP synthase subunit β (A0AA40J9A9), were also detected, with iBAQ intensities of 9.29×10^{10} and 4.68×10^{10}. The identified proteins reveal a broad range of functionalities, highlighting several processes essential for bacterial survival and adaptation, such as protein folding, stress response, translation, and central metabolism.

UNIVERSITI KEBANGSAAN MALAYSIA

Table 4.4 List of top 20 proteins with the highest iBAQ intensity across all three *B. pseudomallei* clinical strains

Accession	Protein name	PANTHER protein class	iBAQ intensity	PANTHER protein class
Q3JPF6	Chaperonin GroEL 1	-	5.51E+11	-
Q63PZ6	Elongation factor Tu	Translation elongation factor	2.60E+11	Translation elongation factor
Q63U73	Arginine deiminase	-	2.05E+11	-
Q63T73	Alkyl hydroperoxide reductase C	Peroxidase	1.70E+11	Peroxidase
Q63RH4	Co-chaperonin GroES	Chaperonin	1.53E+11	Chaperonin
Q63U72	Ornithine carbamoyltransferase	Transferase	1.46E+11	Transferase
Q63Q08	Elongation factor G	Translation elongation factor	1.18E+11	Translation elongation factor
P0DMK4	DNA-binding protein HU-alpha	DNA metabolism protein	1.06E+11	DNA metabolism protein
Q9S639	Flagellin	-	9.29E+10	-
O68191	Putative DnaK chaperone protein	Hsp70 family chaperone	8.81E+10	Hsp70 family chaperone
Q63JJ0	Aconitate hydratase	RNA metabolism protein	5.77E+10	RNA metabolism protein
Q63S06	30S ribosomal protein S1	Ribosomal protein	5.44E+10	Ribosomal protein
A3NW04	Chaperone protein ClpB	-	5.17E+10	-

to be continued...

UNIVERSITI KEBANGSAAN MALAYSIA

... continuation

Q63RZ9	Outer membrane protein a	-	4.87E+10	-
Q63JK1	Citrate synthase	Transferase	4.76E+10	Transferase
A0AA40J9A9	ATP synthase subunit beta	-	4.68E+10	-
Q63QU9	Putative glutamate dehydrogenase	Dehydrogenase	4.61E+10	Dehydrogenase
Q63RC4	Putative oxidoreductase	Peroxidase	4.60E+10	Peroxidase
Q63WW2	succinyl-CoA synthetase beta chain	Ligase	4.59E+10	Ligase
A3NSX5	Chaperone protein HtpG	-	4.58E+10	-

UNIVERSITI KEBANGSAAN MALAYSIA

4.5.4 Comparative proteomic analysis

a. Criteria for protein selection and differential expression analysis

The identified protein dataset was filtered and subjected to missing value imputation prior to statistical analysis. A stringent inclusion criterion was applied, requiring each protein to be present in at least 70% of the nine replicates in at least one group. Missing values in the filtered dataset were then imputed based on their normal distribution across replicates, further refining the data. Following these steps, a final set of 757 proteins was retained. Importantly, this number represents the overall curated dataset combined across PS_UMC083, NI_UMC082 and RS_UMC114, prior to statistical and pairwise analyses. These 757 proteins were preserved as the foundation for subsequent comparative analyses.

From the curated dataset of 757 proteins across PS_UMC083, NI_UMC082, and RS_UMC114, differential regulation was assessed using a one-way ANOVA followed by post hoc testing. Applying a statistical threshold of $p < 0.05$, 602 proteins were identified as significantly expressed. Post hoc testing was then used to determine significant pairwise comparisons, specifically between (1) NI_UMC082 vs PS_UMC083, and (2) RS_UMC114 vs PS_UMC083. For both comparison groups, fold change was calculated to assess the magnitude of differential expression. A fold change threshold of greater than 1.5 was selected as it represents a moderate but biologically relevant difference in protein expression, commonly used in proteomics studies to identify meaningful changes in abundance. This stringent approach ensured that only proteins with substantial differences in expression were considered for further analysis.

b. Differentially regulated proteins between comparison groups NI_UMC082 vs PS_UMC083

A total of 105 proteins were found to be upregulated, while 56 proteins were downregulated in NI_UMC082 compared to PS_UMC083. Among the upregulated proteins (Figure 4.11a), five exhibited more than 5-fold increases in expression. These included a hydrolase (Q63I95, fold change = 14.3), translation initiation factor IF-2 (Q63TP8, fold change = 12.3), and an exported protein (Q63LY1, fold change = 8.8),

UNIVERSITI KEBANGSAAN MALAYSIA

indicating substantial upregulation of proteins potentially involved in metabolic activity and protein synthesis.

Within the downregulated group (Figure 4.11b), six proteins showed more than 5-fold reductions in expression. Notable examples include the Hcp protein (Q63K67, fold change = -25.2), a multidrug efflux system putative membrane fusion protein (Q63U13, fold change = -15.2), and a post-SET domain-containing protein (Q63NI9, fold change = -7.4). These findings suggest a marked suppression of proteins potentially associated with secretion systems, AMR, or regulatory functions in NI_UMC082 relative to PS_UMC083.

UNIVERSITI KEBANGSAAN MALAYSIA

a)

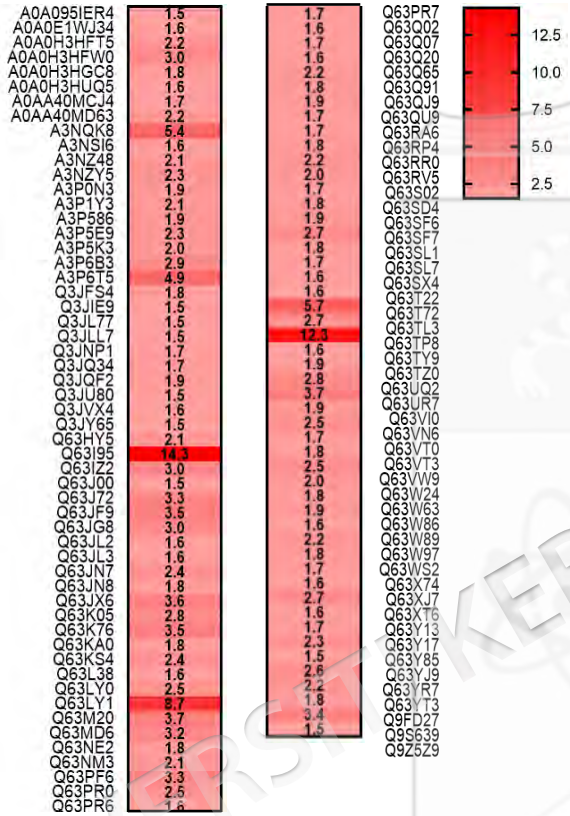

b)

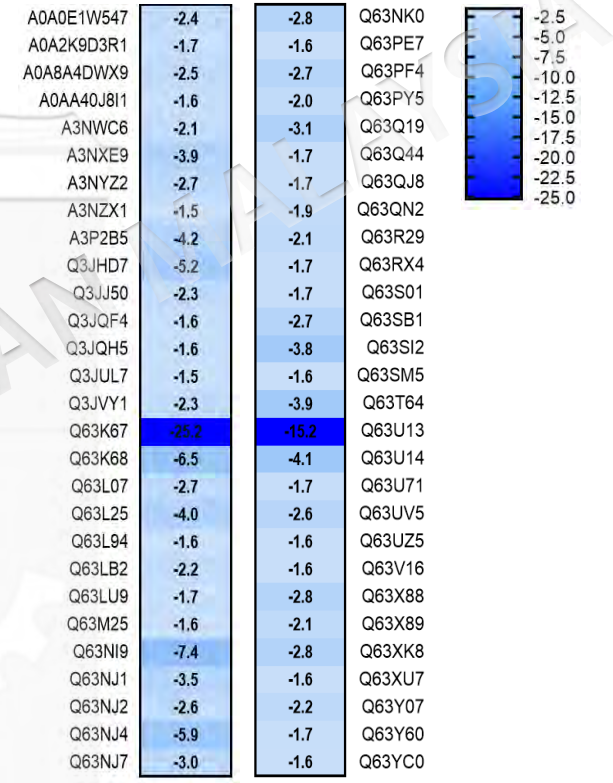

Figure 4.11 Heatmaps of differentially expressed proteins between NI_UMC082 and PS_UMC083. Panel (a) shows 105 proteins (fold change >1.5), with the intensity of red corresponding to the degree of upregulation. Panel (b) displays 56 downregulated proteins (fold change >1.5), with the intensity of blue indicating the extent of downregulation ($p < 0.05$). Among the most significantly upregulated proteins are Q63I95 (hydrolase; fold change = 14.3), Q63TP8 (translation initiation factor IF-2, infB; fold change = 12.3), and Q63LY1 (exported protein; fold change = 8.8). The most significantly downregulated proteins include Q63K87 (Hcp protein; fold change = –25.2), Q63U13 (multidrug efflux system putative membrane fusion protein; fold change = –15.2) and Q63NI9 (post-SET domain-containing protein; fold change = -7.4)

UNIVERSITI KEBANGSAAN MALAYSIA

i. Functional and network characterisation of differentially regulated proteins between NI_UMC082 vs PS_UMC083

Functional annotation and interaction analysis of the upregulated and downregulated proteins in NI_UMC082 compared to PS_UMC083 revealed similar protein group classifications across biological processes, molecular functions, and protein classes (Figure 4.12). Within the biological process category, metabolic processes were the predominant class for both upregulated (Figure 4.12a(i)) and downregulated proteins (Figure 4.12b(i)), accounting for 22.2% and 17.8%, respectively. Cellular processes were also prominent, comprising 21.1% of upregulated proteins and 15.6% of downregulated proteins. Unique categories identified among the upregulated proteins included response to stimuli (3.3%), locomotion (2.2%), and localisation (2.2%), which were absent in the downregulated group.

For molecular functions, catalytic activity and binding activity were the most abundant categories across both upregulated (Figure 4.12a(ii)) and downregulated (Figure 4.12b(ii)) proteins. Catalytic activity was more prominent in the upregulated proteins (28.6%) compared to the downregulated proteins (23.3%), while binding activity followed a similar trend (15.6% versus 9.3%). Other categories included transporter activity and structural molecule activity. Unique molecular functions observed in the upregulated proteins included structural molecule activity (3.9%), molecular transductor activity (2.6%), and molecular function regulator activity (1.3%).

In the PANTHER protein class analysis, metabolic interconversion enzymes represented the largest class in both groups, accounting for 47% of upregulated proteins (Figure 4.12a(iii)) and 42.1% of downregulated proteins (Figure 4.12b(iii)). Translational proteins were also notable, comprising 7.6% and 7.9% of the upregulated and downregulated proteins, respectively. Unique protein classes identified in the upregulated group included DNA metabolism (3.0%), protein-binding activity modulator (1.5%), and viral or transposable element protein (1.5%).

STRING protein-protein interaction network analysis of differentially expressed proteins in NI_UMC082 relative to PS_UMC083 revealed functionally relevant clusters (Figure 4.13). Differentially expressed proteins identified through STRING analysis

UNIVERSITI KEBANGSAAN MALAYSIA

and classified under functional categories relevant to pathogenicity, such as chemotaxis, metabolic processes, and efflux pump membrane transport, were selected for downstream interpretation and reporting. Upregulated chemotaxis-related proteins included the aerotaxis receptor methyl-accepting chemotaxis protein, CheA, CheY1, and an extracellular solute-binding protein (Figure 4.13a). Metabolic proteins such as BPSS2175 were also identified.

Protein infB, essential for translation initiation, was centrally positioned within a STRING cluster, suggesting interactions with multiple regulatory and translational proteins. In contrast, efflux pump transporters amrA and amrB, along with the T6SS effector Hcp, were downregulated in NI_UMC082 (Figure 4.13b). These findings indicate a suppression of AMR and secretion system components in NI_UMC082 compared to PS_UMC083.

UNIVERSITI KEBANGSAAN MALAYSIA

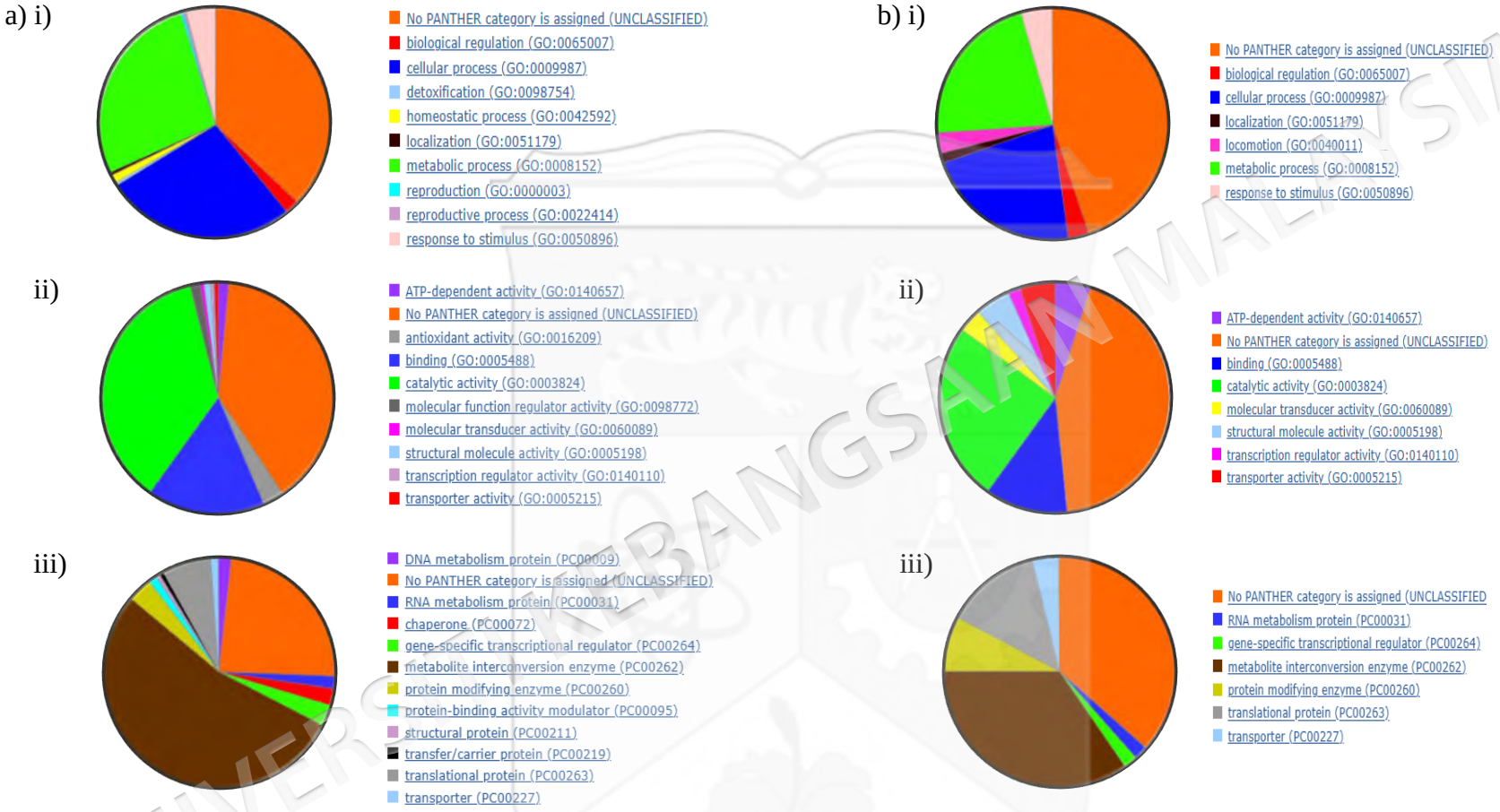

Figure 4.12 Functional classification of the differentially expressed upregulated proteins between NI_UMC082 and PS_UMC083; a) Upregulated proteins and b) Downregulated proteins; with i) biological process, ii) molecular function, iii) PANTHER protein class.

UNIVERSITI KEBANGSAAN MALAYSIA

a) b)

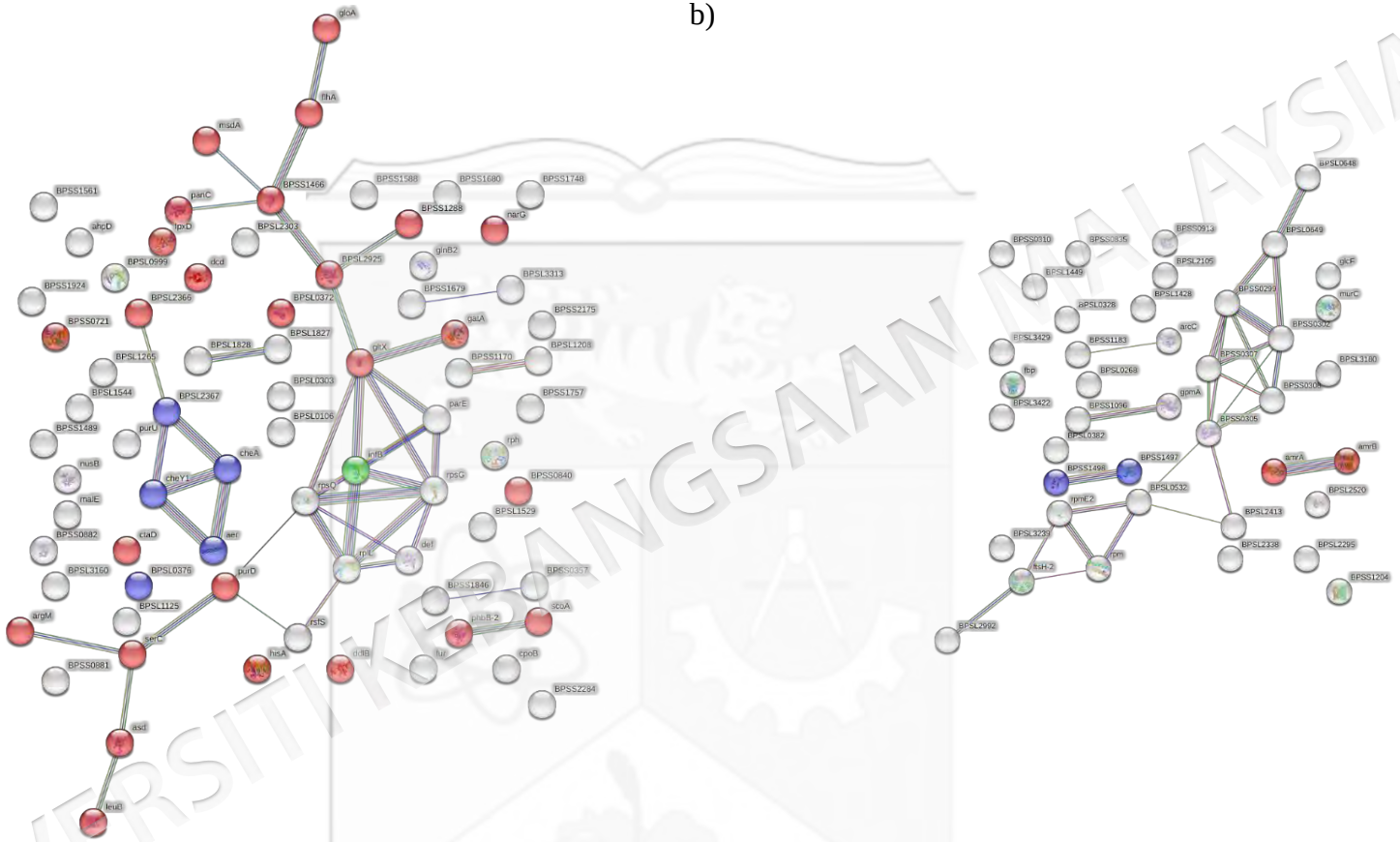

Figure 4.13 STRING prediction of the protein–protein interaction (PPI) networks for the differentially expressed upregulated (a) and downregulated (b) proteins between NI_UMC082 and PS_UMC083. The proteins analysed in this figure represent the entire set of significantly upregulated and downregulated proteins identified in Figure 4.11, based on a fold change >1.5 and $p < 0.05$. a) The blue coloured nodes represent proteins with roles in chemotaxis, red coloured nodes represent proteins involved in metabolic functions, and the green node represents protein infB, a central protein for the initiation of protein synthesis. b) The blue coloured nodes represent proteins involved in the type VI secretion system, and red coloured nodes show proteins involved as efflux pump membrane transporters.

UNIVERSITI KEBANGSAAN MALAYSIA

ii. Proteins of interest with functional roles or disease pathway associations elucidated between NI_UMC082 vs PS_UMC083

The bioinformatics interaction analysis of differentially regulated proteins between PS_UMC083 and NI_UMC082 identified several significantly different ($p < 0.05$) proteins of interest related to functional roles and disease-associated pathways. These proteins are further detailed in Table 4.5, categorised by their expression levels and biological classifications.

Several bacterial chemotaxis proteins were found to be upregulated in NI_UMC082 relative to PS_UMC083, including the aerotaxis receptor, methyl-accepting chemotaxis protein, and chemotaxis protein CheA (fold changes 1.6–2.1). These proteins are components of the chemotaxis signalling pathway. Proteins involved in oxidative stress response and metabolism, such as hydrolase and alkyl hydroperoxide reductase, showed fold changes of 14.3 and 5.7, respectively. Alkyl hydroperoxide reductase is part of the ROS detoxification pathway. Translation initiation factor IF-2, a protein required for ribosomal assembly and protein synthesis, exhibited a fold change of 12.3. Flagellin, a structural protein of the bacterial flagellum, was upregulated with a fold change of 3.4.

Among the downregulated proteins, AmrA and AmrB, components of the multidrug efflux system, showed fold changes of -15.2 and -4.1. In addition, two proteins related to the T6SS, Hcp and BPSS1497, were downregulated with fold changes of -25.2 and -6.5.

These pathways were highlighted as disease-related because they encompass mechanisms directly linked to bacterial pathogenicity, including motility, oxidative stress defence, protein biosynthesis, drug resistance, and secretion systems that influence host-pathogen interactions.

UNIVERSITI KEBANGSAAN MALAYSIA

Table 4.5 Differentially expressed proteins in comparison group NI_UMC082 vs PS_UMC083 with functional roles or disease pathway associations

Expression	Functional category	Protein name	Majority protein ID	Fold change
Upregulated	Bacterial chemotaxis	Aerotaxis receptor	Q63NM3	2.1
		Methyl-accepting chemotaxis protein	Q63SF6	1.9
		Chemotaxis protein CheA	Q63PR7	1.7
		Extracellular solute-binding protein	Q63Y13	1.6
		Chemotaxis two-component response regulator CheY1	Q63PR6	1.6
	Enzymes (catalysis and metabolism)	Hydrolase	Q63I95	14.3
		Alkyl hydroperoxide reductase (ahpD)	Q63T72	5.7
	Translation and protein synthesis	Translation initiation factor IF-2 (infB)	Q63TP8	12.3
	Motility	Flagellin	Q9S639	3.4
Downregulated	Multidrug efflux system	amrA	Q63U13	-15.2
		amrB	Q63U14	-4.1
	Type VI secretion system	HcP	Q63K67	-25.2
		BPSS1497	Q63K68	-6.5

UNIVERSITI KEBANGSAAN MALAYSIA

iii. Differentially expressed biofilm proteins between NI_UMC082 vs PS_UMC083

Biofilm-associated proteins were identified based on functional annotations from the UniProt database and curated literature, which characterised biofilm-related proteins in *B. pseudomallei*. The resulting biofilm-associated proteins were subsequently analysed for differential regulation between PS_UMC083 and NI_UMC082 (Table 4.6).

Upregulated proteins included exported protein (Q63YT3, fold change = 2.2), BON domain-containing protein (Q63IZ2, fold change = 3.0), lipoprotein (Q63Y85, fold change = 2.3), methyl-accepting chemotaxis protein (Q63SF6, fold change = 1.9), enoyl-[acyl-carrier-protein] reductase [NADH] (Q63MD6, fold change = 3.2), and nitrate reductase (quinone) (Q63SL1, fold change = 1.78). In contrast, the multidrug efflux system putative membrane fusion protein (Q63U13, fold change = -15.2) and fatty acid biosynthesis-related CoA ligase (Q63NJ7, fold change = -3.0) were found to be downregulated.

UNIVERSITI KEBANGSAAN MALAYSIA

Table 4.6 Biofilm-associated proteins differentially expressed in comparison group NI_UMC082 vs PS_UMC083, identified based on UniProt annotations and related literature

Expression	Functional category	Protein name	Majority protein ID	Fold change
Upregulated	Two-component signal transduction systems	Exported protein	Q63YT3	2.2
	Lipoproteins	BON domain-containing protein	Q63IZ2	3.0
		Lipoprotein	Q63Y85	2.3
	Miscellaneous	Methyl-accepting chemotaxis protein	Q63SF6	1.9
	Fatty acid biosynthesis	Enoyl-[acyl-carrier-protein] reductase [NADH]	Q63MD6	3.2
	Anaerobic-related, fumarate and nitrate reduction	Nitrate reductase (quinone)	Q63SL1	1.78
Downregulated	Miscellaneous	Multidrug efflux system putative membrane fusion protein	Q63U13	-15.2
	Fatty acid biosynthesis	Fatty acid biosynthesis-related CoA ligase	Q63NJ7	-3.0

UNIVERSITI KEBANGSAAN MALAYSIA

4.5.2 Differentially regulated proteins between comparison group RS_UMC114 vs PS_UMC083

A total of 246 proteins were found to be upregulated, while 76 proteins were downregulated in RS_UMC114 when compared to PS_UMC083. Among the upregulated proteins (Figure 4.14a), nine were identified with more than 5-fold increases in expression. These included translocator protein BipD (Q63K37, fold change = 32.5), surface presentation of antigen protein bsaR (Q63K24, fold change = 8.5), and exported protein (Q63JG8, fold change = 8.3). Notably, BipD (Q63K37) exhibited a substantial fold change of 32.5, indicating considerable upregulation in RS_UMC114. The surface presentation of antigen protein (Q63K24) and exported protein (Q63JG8) was also prominently upregulated, with fold changes of 8.5 and 8.3, respectively.

In the downregulated protein heatmap (Figure 4.14b), ten proteins were found to be more than 5-fold downregulated. These included linear gramicidin synthetase subunit C (A3P5K3, fold change = -16.2), multidrug efflux system putative membrane fusion protein (Q63U13, fold change = -14.9), and large ribosomal subunit protein uL29 (Q63Q19, fold change = -8.5). The linear gramicidin synthetase subunit C (A3P5K3) showed particularly high downregulation, suggesting a marked reduction in expression in RS_UMC114. Additionally, the multidrug efflux system protein (Q63U13) and ribosomal protein uL29 (Q63Q19) were also significantly downregulated, with fold changes of -14.9 and -8.5, respectively.

UNIVERSITI KEBANGSAAN MALAYSIA

a)

b)

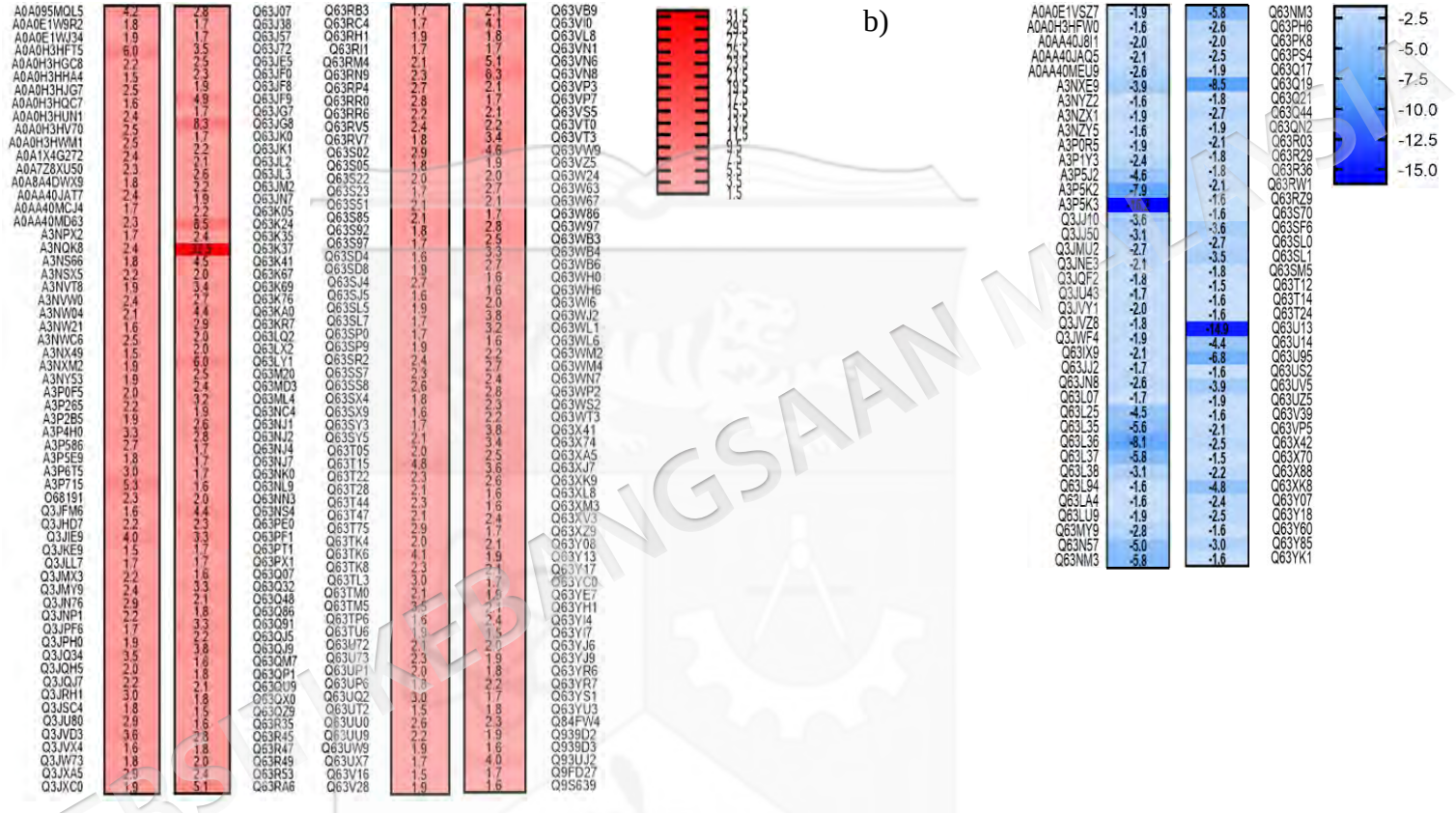

Figure 4.14 Heatmaps of differentially expressed proteins between RS_UMC114 and PS_UMC083. Panel (a) shows 105 upregulated proteins (fold change >1.5), with the intensity of red corresponding to the degree of upregulation. Panel (b) displays 56 downregulated proteins (fold change >1.5), with the intensity of blue indicating the extent of downregulation ($p < 0.05$). Among the most significantly upregulated proteins are Q63K37 (Translocator protein BipD; fold change = 32.5), Q63K24 (Surface presentation of antigens protein bsaR = 8.5), and Q63JG8 (exported protein; fold change = 8.3). The most significantly downregulated proteins include A3P5K3 (Linear gramicidin synthetase subunit C; fold change = –16.2), Q63U13 (multidrug efflux system putative membrane fusion protein; fold change = –14.9) and Q63Q19 (large ribosomal subunit protein uL29; fold change = -8.5).

i. Functional and network characterisation of differentially regulated proteins between RS_UMC114 vs PS_UMC083

Functional annotation and interaction analysis of the upregulated and downregulated proteins in RS_UMC114 compared to PS_UMC083 revealed both shared and distinct patterns across biological processes, molecular functions, and protein classes (Figure 4.15). Smaller subsets of proteins were uniquely identified among the upregulated group, contributing to the overall diversity of functional roles.

In terms of biological processes, both upregulated (Figure 4.15a(i)) and downregulated proteins (Figure 4.15b(i)) were predominantly associated with metabolic and cellular processes. Among the upregulated proteins, metabolic processes accounted for 26.9%, while cellular processes comprised 27.3%. For the downregulated proteins, both categories represented 22.1%. Additional shared categories, although in smaller proportions, included response to stimulus and biological regulation. Unique biological processes identified among the upregulated proteins included homeostatic process (1.2%), reproduction (0.4%), and reproductive process (0.4%).

For molecular functions, catalytic activity and binding activity were the most prominent categories in both upregulated (Figure 4.15a(ii)) and downregulated (Figure 4.15b(ii)) proteins. Catalytic activity accounted for 36.2% of the upregulated proteins and 25.4% of the downregulated proteins. The binding activity represented 16.6% and 11.9%, respectively. Additional molecular functions observed included antioxidant activity and structural molecule activity. Unique categories among the upregulated proteins included antioxidant activity (3.0%) and molecular function regulator activity (1.5%).

PANTHER protein class analysis revealed that metabolic interconversion enzymes formed the largest class in both upregulated (53.5%) and downregulated (36.7%) groups (Figure 4.15a(iii) and 4.15b(iii)). Smaller shared classes included RNA metabolism proteins and protein-modifying enzymes. Unique protein classes identified among the upregulated proteins included chaperone proteins (2.3%), DNA metabolism proteins (1.7%), and structural proteins (0.6%).

UNIVERSITI KEBANGSAAN MALAYSIA

STRING protein-protein interaction network analysis of the upregulated proteins in RS_UMC114 relative to PS_UMC083 (Figure 4.16a) revealed clusters of proteins associated with virulence, stress response, and oxidoreductase activity. A branch of virulence proteins was identified, beginning with translocator protein BipD and extending to effector proteins BipC and BopE. These proteins are well-characterised and belong to the type III secretion system. Numerous oxidoreductases and stress response proteins were also distributed throughout the interaction network.

In contrast, STRING analysis of the downregulated proteins in RS_UMC114 (Figure 4.16b) revealed suppression of proteins involved in AMR and metabolic pathways. This included amrA and amrB, which are associated with β-lactam resistance, as well as arG-2 and aer, which are involved in arginine biosynthesis and bacterial chemotaxis, respectively.

UNIVERSITI KEBANGSAAN MALAYSIA

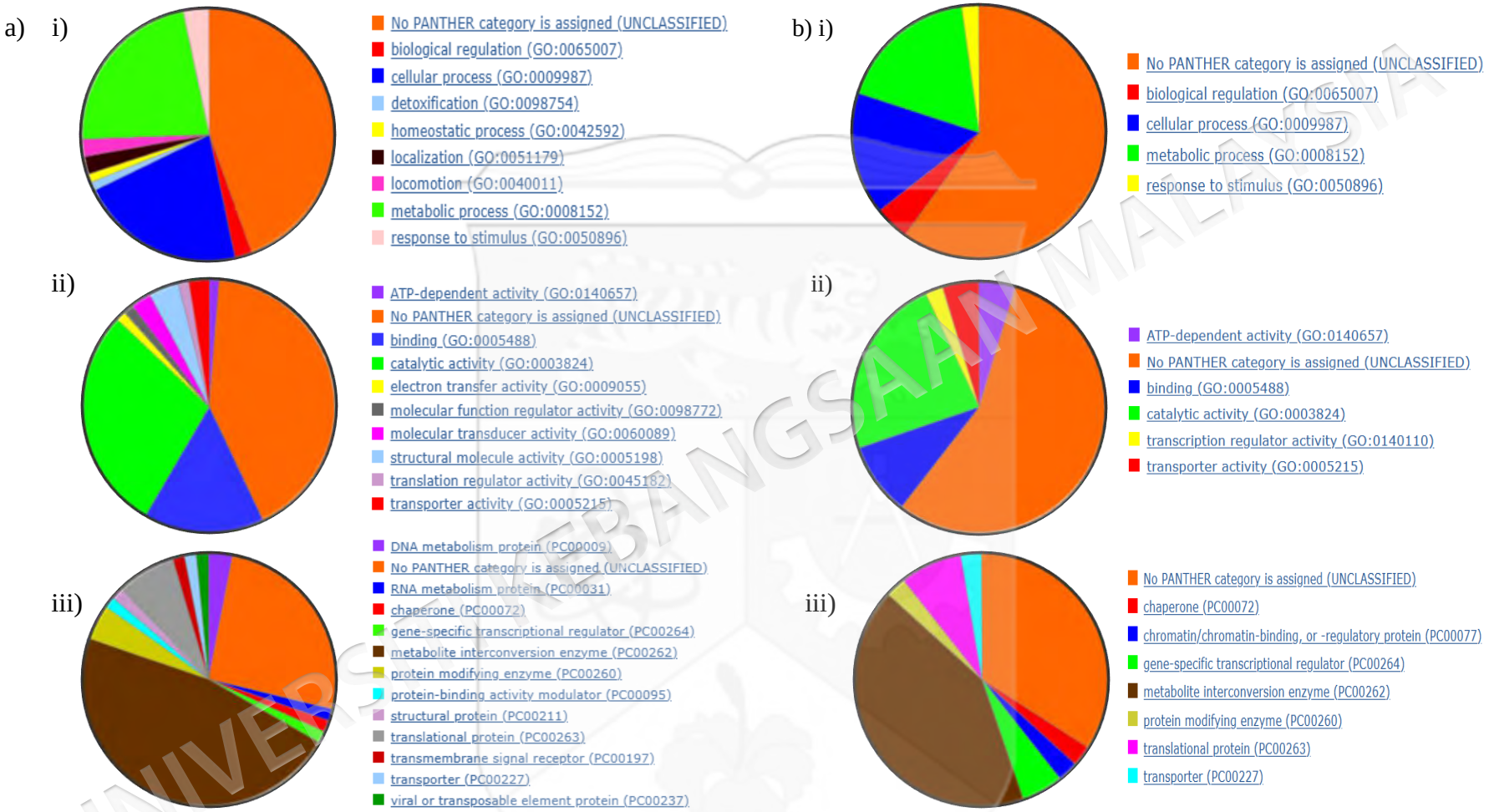

Figure 4.15 Functional classification of the differentially expressed upregulated proteins between RS_UMC114 and PS_UMC083; a) Upregulated proteins and b) Downregulated proteins; with i) biological process, ii) molecular function, iii) PANTHER protein class.

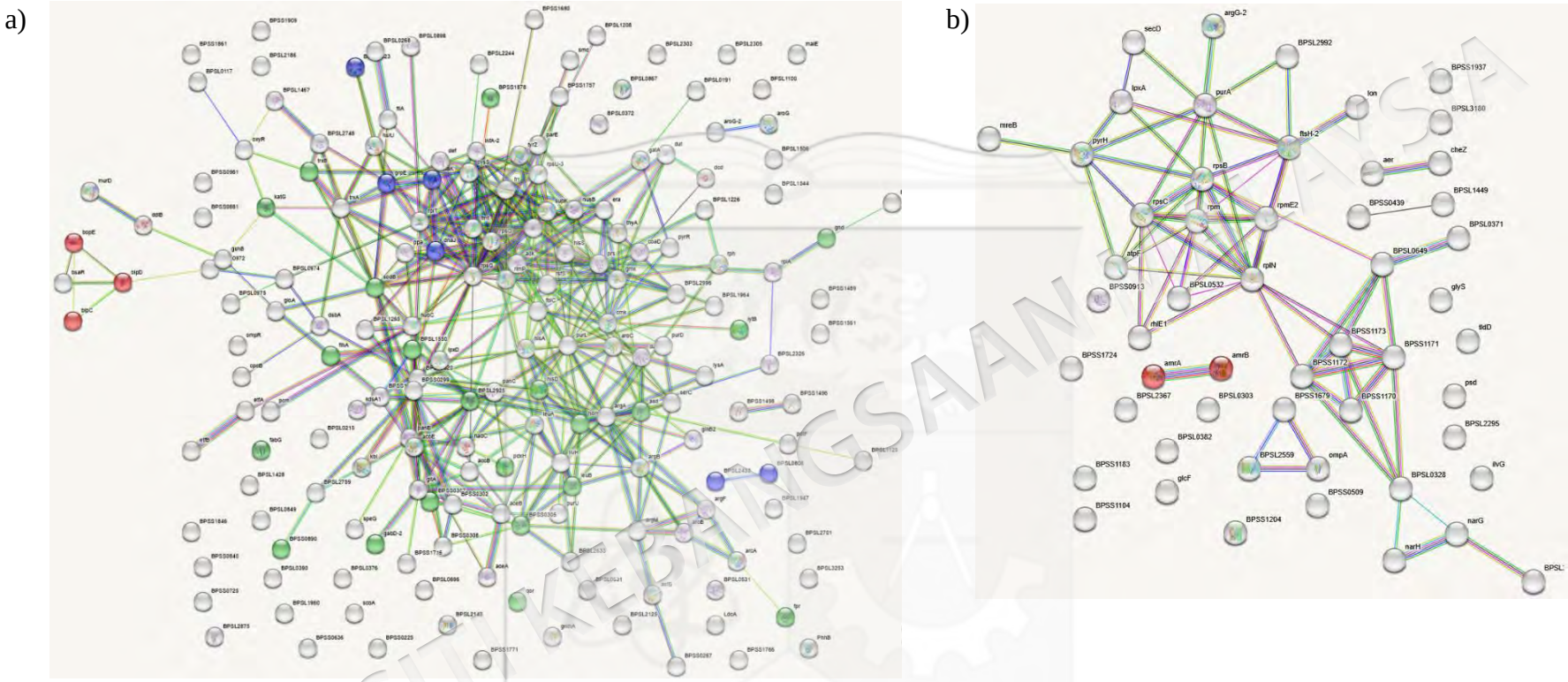

Figure 4.16 STRING prediction of the protein–protein interaction (PPI) networks for the differentially expressed upregulated (a) and downregulated (b) proteins between RS_UMC114 and PS_UMC083. The nodes represent proteins, and the lines connecting them indicate predicted or experimentally confirmed interactions. The different colours of the edges correspond to various types of evidence supporting the interactions, such as experimental data, databases, and co-expression patterns. a) The nodes in red represent virulence proteins, nodes coloured blue are stress response proteins and nodes highlighted in green represent the oxidoreductase proteins. b) Nodes in red represent efflux pump membrane transporters.

UNIVERSITI KEBANGSAAN MALAYSIA

ii. Proteins of interest with functional roles or disease pathway associations elucidated between RS _UMC114 vs PS_UMC083

Bioinformatics interaction analysis of differentially expressed proteins between PS_UMC083 and RS_UMC114 revealed several key proteins relevant to the relapse mechanism of RS_UMC114. These proteins were identified by their majority protein IDs, classified into functional categories, and analysed for fold change. Table 4.7 presents a clear distinction between upregulated and downregulated proteins across various functional groups. Several virulence-associated proteins were upregulated, including BipD (fold change = 32.5), BopE (fold change = 4.5), and BipC (fold change = 2.4). These proteins are components of the T3SS, a pathway directly linked to bacterial pathogenicity through the translocation of effector proteins into host cells. Invasion protein, bsaR (fold change = 8.5), was also found elevated. This protein contributes to surface presentation and host cell entry mechanisms, reinforcing its role in disease progression.

A large group of oxidoreductases showed increased abundance, including superoxide dismutase sodB (fold change = 3.2), aldehyde dehydrogenase (fold change = 2.8), thioredoxin reductase (fold change = 2.2), and catalase-peroxidase (fold change = 1.9). These enzymes are central to oxidative stress defence pathways, protecting bacteria against host-derived reactive oxygen species. Proteins involved in nucleotide biosynthesis were upregulated, such as thymidylate synthase (fold change = 2.1), adenylate kinase (fold change = 1.6), and ribose-phosphate pyrophosphokinase (fold change = 1.6). These proteins support DNA replication and repair, critical for bacterial growth under stress conditions. Stress response proteins, including GrpE (fold change = 2.8), DnaK (fold change = 2.3), DnaJ (fold change = 1.8), and heat shock protein (fold change = 2.1), were also elevated. These are part of the protein folding and chaperone pathways, maintaining proteostasis during host-induced stress.

Among the downregulated proteins, AmrA (fold change = -14.9) and AmrB (fold change = -4.4) from the multidrug efflux system showed reduced expression, indicating modulation of drug resistance pathways. Similarly, argininosuccinate synthase ArgG-2 (fold change = -6.8), part of the arginine biosynthesis pathway, and the aerotaxis receptor Aer (fold change = -5.8) from the chemotaxis pathway were suppressed.

UNIVERSITI KEBANGSAAN MALAYSIA

Table 4.7 Differentially expressed proteins in comparison group RS_UMC114 vs PS_UMC083 with functional roles or disease pathway associations

Expression	Functional category	Protein name	Majority protein ID	Fold change
Upregulated	Virulence	Translocator protein BipD	Q63K37	32.5
		Guanine nucleotide exchange factor BopE	Q63K41	4.5
		Effector protein BipC	Q63K35	2.4
	Invasion	Surface presentation of antigen protein bsaR	Q63K24	8.5
	Oxidoreductase	Superoxide dismutase (sodB)	Q63K24	3.2
		Aldehyde dehydrogenase	Q63WL1	2.8
		Aspartate-semialdehyde dehydrogenase	Q63NJ2	2.6
		Pyridoxine/pyridoxamine 5'-phosphate oxidase	Q63JL3	2.4
		S-(hydroxymethyl)glutathione dehydrogenase	Q63WN7	2.3
		Thioredoxin reductase	Q63WS2	2.2
		3-isopropylmalate dehydrogenase	Q63RR6	2.1
		Quinone oxidoreductase	Q63JL2	2.1
		Glutamate dehydrogenase	Q63VS5	2.1
		3-oxoacyl-[acyl-carrier-protein] reductase	Q63QU9	2.1
		Putative NADH dehydrogenase/NAD(P)H nitroreductase	Q63S85	2.0
		Catalase-peroxidase	Q63LX2	1.9
		ferredoxin--NADP (+) reductase	Q939D2	1.9
		Homoserine dehydrogenase	Q63YE7	1.9
		Betaine aldehyde dehydrogenase	Q63UW9	1.8
		Histidinol dehydrogenase	Q63UP6	1.8

... to be continued

UNIVERSITI KEBANGSAAN MALAYSIA

... continuation

		6-phosphogluconate dehydrogenase, decarboxylating	Q63Q86	1.7
		Dehydrogenase	Q63JG7	1.7
		Ketol-acid reductoisomerase (NADP (+))	Q63J38	1.7
		4-hydroxy-3-methylbut-2-enyl diphosphate reductase 1	Q63NJ4	1.6
		Succinate-semialdehyde dehydrogenase [NADP+]	Q63WH0	1.6
	Nucleotide biosynthesis	Thymidylate synthase	Q63S51	2.1
		Adenylate kinase	Q63WL6	1.6
		Ribose-phosphate pyrophosphokinase	Q63XL8	1.6
	Stress response	Protein grpE	Q63R45	2.8
		Chaperone protein DnaK	O68191	2.3
		Subfamily S1C unassigned peptidase	Q63WT3	2.2
		Heat shock protein	Q63VB9	2.1
		Subfamily S1C unassigned peptidase	Q63S92	1.8
		Chaperone protein DnaJ	Q63R47	1.8
Downregulated	No functional category detected	Linear gramicidin synthetase subunit C	A3P5K3	-16.2
	Multidrug efflux system	amrA	Q63U13	-14.9

to be continued...

UNIVERSITI KEBANGSAAN MALAYSIA

...continuation

	amrB	Q63U14	-4.4
Arginine synthesis	Argininosuccinate synthase (arG-2)	Q63U95	-6.8
Bacterial chemotaxis	Aerotaxis receptor (aer)	Q63NM3	-5.8
Fatty acid, cellular and organic substance biosynthetic process	Non-ribosomal peptide synthase/polyketide synthase (BPSS1171)	Q63L37	-5.8

UNIVERSITI KEBANGSAAN MALAYSIA

iii. Differentially expressed biofilm proteins between comparison group RS_UMC114 vs PS_UMC083

Based on the Uniprot database and curated literature, biofilm-associated proteins were identified for comparative analysis between PS_UMC083 and RS_UMC114. Differential expression analysis of biofilm-related proteins (Table 4.8) revealed several upregulated and downregulated candidates.

Among the upregulated proteins in RS_UMC114, chaperone protein ClpB (A3NW04, fold change = 2.05) was notable, as it was classified under both universal stress proteins and outer membrane or cell surface-associated proteins. Fatty acid biosynthesis-related CoA ligase (Q63NJ7, fold change = 1.68) was also upregulated. Six proteins were found to be downregulated, including nitrate reductase (quinone) (Q63SL1, fold change = -3.47), respiratory nitrate reductase β chain (Q63SL0, fold change = -2.74), lipoprotein (Q63Y85, fold change = -3.02), ABC transport system exported protein (Q63IX9, fold change = -2.14), multidrug efflux system putative membrane fusion protein (Q63U13, fold change = -8.09), and methyl-accepting chemotaxis protein (Q63SF6, fold change = -3.64).

Table 4.8 Biofilm-associated proteins differentially expressed in comparison group RS_UMC114 vs PS_UMC083, identified based on UniProt annotations and related literature

Expression	Functional category	Protein name	Majority protein ID	Fold change
Upregulated	Universal stress protein	Chaperone protein ClpB	A3NW04	2.05
	Outer membrane and cell surface	Chaperone protein ClpB	A3NW04	2.05
	Fatty acid biosynthesis	Fatty acid biosynthesis-related CoA ligase	Q63NJ7	1.68
Downregulated	Anaerobic-related, fumarate and nitrate reduction	Nitrate reductase (quinone)	Q63SL1	-3.47
		Respiratory nitrate reductase beta chain	Q63SL0	-2.74

to be continued...

... continuation

Lipoprotein	Lipoprotein	Q63Y85	-3.02
Lipases and phospholipases	ABC transport system, exported protein	Q63IX9	-2.14
Miscellaneous	Multidrug efflux system putative membrane fusion protein	Q63U13	-8.09
	Methyl-accepting chemotaxis protein	Q63SF6	-3.64

c. Comparative KEGG enrichment across comparison groups RS_UMC114 vs PS_UMC083 and NI_UMC082 vs PS_UMC083

KEGG pathway enrichment analysis was performed to compare transcriptional and proteomic profiles across the four comparison groups: RS_UMC114 vs PS_UMC083 (upregulated), RS_UMC114 vs PS_UMC083 (downregulated), NI_UMC082 vs PS_UMC083 (upregulated) and NI_UMC082 vs PS_UMC083 (downregulated). Enrichment was determined using corrected p-values and gene counts, with significance defined as $p < 0.05$ (Table 4.9).

In the RS_UMC114 vs PS_UMC083 comparison group, 23 pathways were upregulated, including core metabolic functions (e.g., metabolic pathways, biosynthesis of secondary metabolites, biosynthesis of antibiotics, and biosynthesis of amino acids), stress adaptation (e.g., CAMP resistance, carbon metabolism, pyruvate metabolism), and regulatory systems (e.g., two-component system, arginine and proline metabolism). Two pathways were significantly downregulated in this comparison: the ribosome and the two-component system. In the NI_UMC082 vs PS_UMC083 comparison group, three pathways were significantly upregulated: metabolic pathways, bacterial chemotaxis, and β-alanine metabolism.

UNIVERSITI KEBANGSAAN MALAYSIA

Table 4.9 Regulatory pathways enriched across infection stages and regulatory profiles of *B. pseudomallei* clinical strains

KEGG Pathway	RS_UMC114 vs PS_UMC083 upregulated	RS_UMC114 vs PS_UMC083 downregulated	NI_UMC082 vs PS_UMC083 upregulated	NI_UMC082 vs PS_UMC083 downregulated
	Number of genes enriched (corrected p-value)			
Metabolic pathways	76 genes ($p = 4.23 \times 10^{-13}$)	Not enriched	26 genes ($p = 3.14 \times 10^{-4}$)	Not enriched
Biosynthesis of secondary metabolites	38 genes ($p = 6.52 \times 10^{-12}$)	Not enriched	Not enriched	Not enriched
Biosynthesis of antibiotics	29 genes ($p = 2.08 \times 10^{-8}$)	Not enriched	Not enriched	Not enriched
Biosynthesis of amino acids	21 genes ($p = 2.30 \times 10^{-8}$)	Not enriched	Not enriched	Not enriched
2-Oxocarboxylic acid metabolism	8 genes ($p = 2.05 \times 10^{-5}$)	Not enriched	Not enriched	Not enriched
Microbial metabolism in diverse environments	23 genes ($p = 1.38 \times 10^{-4}$)	Not enriched	Not enriched	Not enriched
Arginine and proline metabolism	6 genes ($p = 2.50 \times 10^{-3}$)	Not enriched	Not enriched	Not enriched
CAMP resistance	3 genes ($p = 1.03 \times 10^{-2}$)	Not enriched	Not enriched	Not enriched
Ribosome	Not enriched	5 genes ($p = 2.05 \times 10^{-4}$)	Not enriched	Not enriched
Two-component system	6 genes ($p = 0.403$)	7 genes ($p = 7.20 \times 10^{-4}$)	Not enriched	Not enriched
Bacterial chemotaxis	Not enriched	Not enriched	5 genes ($p = 2.88 \times 10^{-4}$)	Not enriched
Quorum sensing	Present but not significant	Not enriched	Not enriched	Not enriched

to be continued...

UNIVERSITI KEBANGSAAN MALAYSIA

... continuation

Pyrimidine metabolism	7 genes ($p = 2.53 \times 10^{-3}$)	Not enriched	Not enriched	Not enriched
Arginine biosynthesis	6 genes ($p = 3.08 \times 10^{-3}$)	Not enriched	Not enriched	Not enriched
Aminoacyl-tRNA biosynthesis	6 genes ($p = 6.36 \times 10^{-3}$)	Not enriched	Not enriched	Not enriched
Pantothenate and CoA biosynthesis	5 genes ($p = 1.36 \times 10^{-2}$)	Not enriched	Not enriched	Not enriched
Carbon metabolism	11 genes ($p = 1.56 \times 10^{-2}$)	Not enriched	Not enriched	Not enriched
Pyruvate metabolism	7 genes ($p = 1.56 \times 10^{-2}$)	Not enriched	Not enriched	Not enriched
β-Alanine metabolism	4 genes ($p = 1.95 \times 10^{-2}$)	Not enriched	3 genes ($p = 3.74 \times 10^{-2}$)	Not enriched
Lysine biosynthesis	4 genes ($p = 2.18 \times 10^{-2}$)	Not enriched	Not enriched	Not enriched
Valine, leucine and isoleucine biosynthesis	4 genes ($p = 2.81 \times 10^{-2}$)	Not enriched	Not enriched	Not enriched
Purine metabolism	7 genes ($p = 2.81 \times 10^{-2}$)	Not enriched	Not enriched	Not enriched
Chloroalkane and chloroalkene degradation	3 genes ($p = 3.47 \times 10^{-2}$)	Not enriched	Not enriched	Not enriched
Lysine degradation	4 genes ($p = 3.47 \times 10^{-2}$)	Not enriched	Not enriched	Not enriched
Histidine metabolism	4 genes ($p = 3.47 \times 10^{-2}$)	Not enriched	Not enriched	Not enriched

UNIVERSITI KEBANGSAAN MALAYSIA

Several regulatory pathways associated with persistence and biofilm formation across comparison groups were identified as well (Table 4.10). In the RS_UMC114 vs PS_UMC083 comparison, nine pathways were significantly upregulated in the relapse strain. These included metabolic pathways (76 genes, $p = 4.23 \times 10^{-13}$), biosynthesis of secondary metabolites (38 genes, $p = 6.52 \times 10^{-12}$), biosynthesis of antibiotics (29 genes, $p = 2.08 \times 10^{-8}$), biosynthesis of amino acids (21 genes, $p = 2.30 \times 10^{-8}$), 2-Oxocarboxylic acid metabolism (8 genes, $p = 2.05 \times 10^{-5}$), and microbial metabolism in diverse environments (23 genes, $p = 1.38 \times 10^{-4}$). Additional enriched pathways included arginine and proline metabolism (6 genes, $p = 2.50 \times 10^{-3}$), CAMP resistance (3 genes, $p = 1.03 \times 10^{-2}$), and two-component system (7 genes, $p = 7.20 \times 10^{-4}$). The QS pathway was present but did not reach statistical significance.

In the same comparison, two pathways were significantly downregulated: Ribosome (5 genes, $p = 2.05 \times 10^{-4}$) and Two-component system (7 genes, $p = 7.20 \times 10^{-4}$). In the PS_UM083 vs N_UMC082 comparison, two pathways were significantly upregulated: metabolic pathways (26 genes, $p = 3.14 \times 10^{-4}$) and bacterial chemotaxis (5 genes, $p = 2.88 \times 10^{-4}$). No significant enrichment was observed in the NI_UMC082 vs PS_UMC083 downregulated comparison group.

UNIVERSITI KEBANGSAAN MALAYSIA

Table 4.10 Regulatory pathways associated with persistence and biofilm formation enriched across infection stages and regulatory profiles of *B. pseudomallei* clinical strains

KEGG Pathway	RS_UMC114 vs PS_UMC083 upregulated	RS_UMC114 vs PS_UMC083 downregulated	NI_UMC082 vs PS_UMC083 upregulated	NI_UMC082 vs PS_UMC083 downregulated	Biological interpretation
	Number of genes enriched (corrected p-value)				
Metabolic pathways	76 genes ($p = 4.23 \times 10^{-13}$)	Not enriched	26 genes ($p = 3.14 \times 10^{-4}$)	Not enriched	Core metabolic activity; conserved across conditions
Biosynthesis of secondary metabolites	38 genes ($p = 6.52 \times 10^{-12}$)	Not enriched	Not enriched	Not enriched	Stress adaptation and survival under hostile conditions
Biosynthesis of antibiotics	29 genes ($p = 2.08 \times 10^{-8}$)	Not enriched	Not enriched	Not enriched	Defence mechanisms; relapse persistence
Biosynthesis of amino acids	21 genes ($p = 2.30 \times 10^{-8}$)	Not enriched	Not enriched	Not enriched	Nutrient synthesis; metabolic flexibility
2-Oxocarboxylic acid metabolism	8 genes ($p = 2.05 \times 10^{-5}$)	Not enriched	Not enriched	Not enriched	Energy production; relapse-specific metabolic rewiring
Microbial metabolism in diverse environments	23 genes ($p = 1.38 \times 10^{-4}$)	Not enriched	Not enriched	Not enriched	Environmental adaptability
Arginine and proline metabolism	6 genes ($p = 2.50 \times 10^{-3}$)	Not enriched	Not enriched	Not enriched	Nitrogen metabolism; biofilm and persistence
CAMP resistance	3 genes ($p = 1.03 \times 10^{-2}$)	Not enriched	Not enriched	Not enriched	Host immune evasion; relapse-specific
Ribosome	Not enriched	5 genes ($p = 2.05 \times 10^{-4}$)	Not enriched	Not enriched	Downregulated in relapse; reduced translational activity

to be continued...

UNIVERSITI KEBANGSAAN MALAYSIA

... continuation

Two-component system	6 genes ($p = 0.403$)	7 genes ($p = 7.20 \times 10^{-4}$)	Not enriched	Not enriched	Signal transduction; biofilm regulation
Bacterial chemotaxis	Not enriched	Not enriched	5 genes ($p = 2.88 \times 10^{-4}$)	Not enriched	Virulence and host invasion; new infection-specific
Quorum sensing	Present but not significant	Not enriched	Not enriched	Not enriched	Biologically relevant; involved in biofilm regulation

UNIVERSITI KEBANGSAAN MALAYSIA

e. Identification, network visualisation, and pathway enrichment of hub proteins across comparison groups RS_UMC114 vs PS_UMC083 and NI_UMC082 vs PS_UMC083

To identify central regulators within each comparison group, PPI networks were constructed using STRING with a medium confidence threshold (combined score ≥0.4). Hub proteins were defined as nodes with a degree ≥10, indicating high connectivity and potential functional importance. Table 4.11 presents the hub proteins stratified by differential expression status.

A total of 26 upregulated hub proteins were found in the RS_UMC114 vs PS_UMC083 comparison group. Many of these proteins are linked to ribosome structure (rpsO, rpsG, rplT), purine biosynthesis (purL, prs, adk, gmk), amino acid metabolism (argA, argB, hom, leuA, hisA, hisD), and stress response (sodB, trxA, dnaJ). Their node degrees ranged from 10 to 24, showing that they are well-connected in the network and likely play important roles in biosynthesis, translation, and managing stress.

On the other hand, only two downregulated hub proteins were identified, rplN (degree = 12) and rpsB (degree = 10). Both are ribosomal proteins, and their lower expression and connectivity might point to reduced protein production in this condition, possibly as part of a stress or persistence response. No hub proteins were identified in the NI_UMC082 vs PS_UMC083 comparison groups.

To better illustrate the connections between hub proteins, a hub interactome network diagram was generated using STRING (Figure 4.17). This network includes all proteins listed in Table 4.11 with node degree ≥10, based on medium confidence interactions (score ≥0.4). Node labels show gene symbols, and colours indicate regulation status: red for upregulated and blue for downregulated in RS_UMC114 vs PS_UMC083. Both upregulated and downregulated hubs are visibly integrated into the network of the RS_UMC114 vs PS_UMC083 group.

UNIVERSITI KEBANGSAAN MALAYSIA

Table 4.11 High-degree hub proteins from group-specific protein–protein interaction networks

Comparison group	Gene symbol	Uniprot ID	Node degree
RS_UMC114 vs PS_UMC083 upregulated proteins	purL	BPSL1416	24
	rpsO	BPSL1206	24
	adk	BPSL0875	22
	rpsG	BPSL3217	21
	argA	BPSL2325	19
	frr	BPSL2156	18
	prs	BPSL0521	18
	sodB	BPSL0880	17
	BPSS0299	BPSS0299	15
	gltX	BPSL2197	15
	gmk	BPSL2563	15
	hom	BPSL1477	15
	dnaJ	BPSL2826	14
	rplT	BPSL1942	14
	argB	BPSL0200	12
	cmk	BPSL2516	12
	nuoC	BPSL1213	12
	trxA	BPSL1497	12
	acoE	BPSS0375	11
	leuA	BPSL1201	11
	rpsU-3	BPSS1758	11
	BPSS0305	BPSS0305	10
	hisA	BPSL3134	10
	hisD	BPSL3139	10
	infA-2	BPSL3192	10
	rimP	BPSL1920	10
RS_UMC114 vs PS_UMC083 downregulated proteins	rplN	BPSL3203	12
	rpsB	BPSL2159	10

UNIVERSITI KEBANGSAAN MALAYSIA

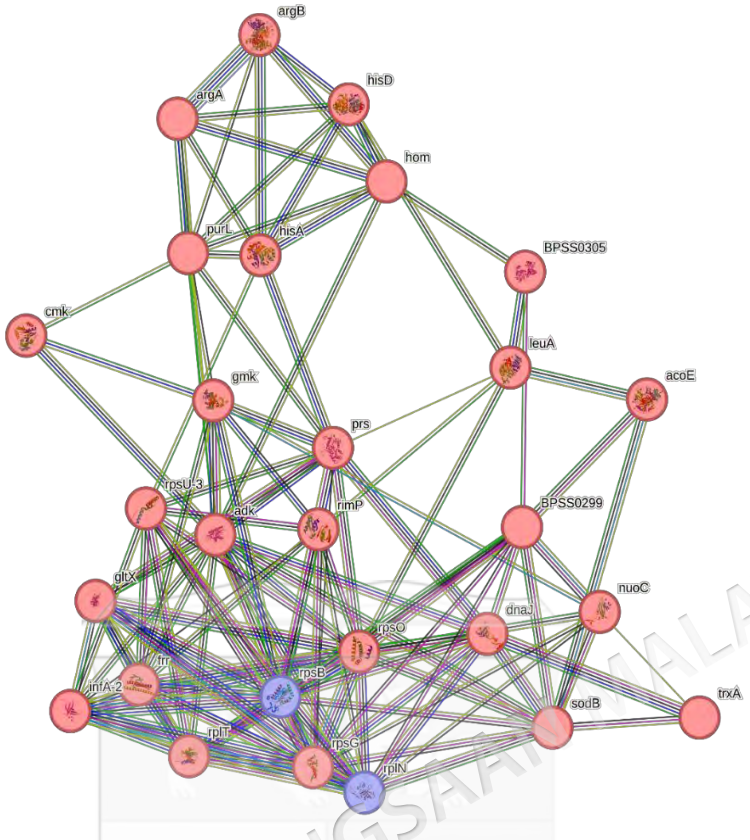

Figure 4.17 PPI network of hub proteins identified across all experimental groups. This figure illustrates the PPI network of hub proteins identified from group-specific STRING analyses. Each node represents a protein with a node degree of 10 or higher, as listed in Table 4.11. The edges indicate predicted interactions retrieved from STRING at medium confidence (combined score ≥0.4). Node colours reflect specific grouping: red nodes correspond to proteins upregulated in RS_UMC114 vs PS_UMC083, while blue nodes represent those that are downregulated in RS_UMC114 vs PS_UMC083. Green and purple nodes denote proteins upregulated and downregulated in NI_UMC082 vs PS_UM083, respectively. Node labels display gene symbols for clarity, and the network layout is directed to emphasise connectivity and clustering patterns.

KEGG pathway enrichment analysis was then performed using STRING's functional annotation tool. The resulting bubble plot summarises significantly enriched pathways among hub proteins, with bubble size indicating gene count and colour reflecting FDR values (Figure 4.18). Notably, pathways such as ribosome, purine metabolism, and biosynthesis of amino acids were consistently enriched across upregulated hubs in comparison group RS_UMC114 vs PS_UMC083.

UNIVERSITI KEBANGSAAN MALAYSIA

In the plot, the x-axis shows the number of hub proteins mapped to each pathway, while the y-axis lists the pathway names. Larger bubbles represent pathways with more hub proteins involved, and darker colours indicate stronger statistical significance. Most of the bubbles are clustered around biosynthetic and metabolic pathways, showing that many of the upregulated hubs are linked to core cellular functions like translation and amino acid production. Interestingly, the ribosome pathway appears as a black bubble (gene count 2), which stands out because it's the only pathway enriched among downregulated hubs. This mixed result was included in the same plot to give a clearer overall view of pathway involvement in RS_UMC114 vs PS_UMC083.

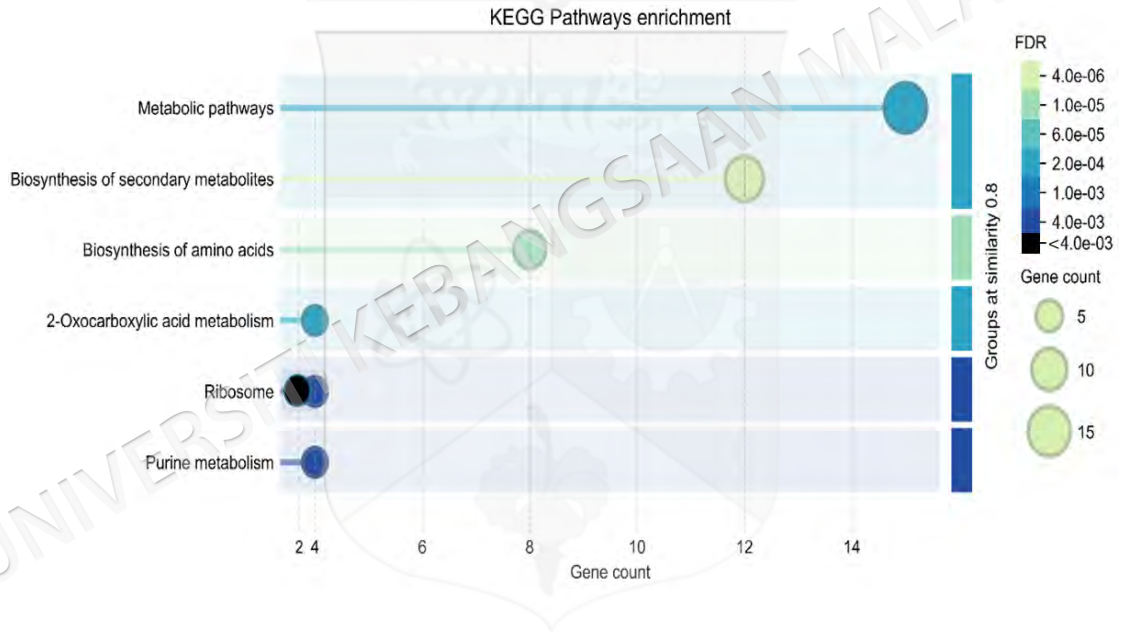

UNIVERSITI KEBANGSAAN MALAYSIA

Figure 4.18 KEGG pathways enriched among hub proteins in comparison group PS_UMC083-RS_UMC114. This bubble plot summarises KEGG pathway enrichment among hub proteins identified in the RS_UMC114 vs PS_UMC083 comparison group. The x-axis represents the number of hub proteins mapped to each pathway (gene count), while the y-axis lists the corresponding KEGG pathway names. Each bubble reflects a pathway, with its size proportional to gene count and its colour indicating the gene ratio. FDR threshold was set to ≤ 0.05. Most pathways were enriched among upregulated hub proteins, except for the ribosome pathway, which was enriched among downregulated hubs as well and is represented by the black bubble (gene count 2). This merged visualisation highlights functional clustering in biosynthesis, metabolism, and translation-related processes.

CHAPTER V

DISCUSSION

5.1 Comparative Analysis of Biofilm Formation Across *B. pseudomallei* Clinical Isolates

Comprehensive analysis of PS_UMC083, NI_UMC082 and RS_UMC114 revealed marked differences in biofilm production and gene expression. Quantitative biofilm assays showed that RS_UMC114 produced significantly higher levels of biofilm compared to PS_UMC083 and NI_UMC082. This elevated biofilm formation is likely a factor contributing to RS_UMC114's persistence and its association with relapse infections (Limmathurotsakul et al., 2014). Chronic infections are frequently linked to biofilm formation because biofilms exhibit increased resilience against antimicrobial agents and host immune responses, which facilitates long-term bacterial survival (Bjarnsholt et al., 2013). In addition, the ability of *B. pseudomallei* biofilms to enhance AMR *in vitro* (Sawasdidoln et al., 2010; Anutrakunchai et al., 2018), further suggests their role in relapsed melioidosis despite ongoing antibiotic therapy.

Meanwhile, PS_UMC083 consistently exhibited the lowest levels of biofilm production. This variation among strains may reflect underlying genetic differences, environmental adaptation, or strain-specific regulatory mechanisms. The enhanced biofilm-forming capacity of RS_UMC114 may be linked to differential expression of biofilm-associated genes, which warrants further investigation into its transcriptional and regulatory landscape.

UNIVERSITI KEBANGSAAN MALAYSIA

5.2 Comparative Expression of Biofilm-Related Genes in *B. pseudomallei* Clinical Isolates

The qPCR analysis revealed significant differences ($p < 0.05$) in the expression levels of biofilm-associated genes across all three clinical strains. Genes *bpsl0603* and *bpsl2026* were upregulated in RS_UMC114 but downregulated in NI_UMC082, relative to the reference strain PS_UMC083. The *bpsl0603* gene encodes an oligosaccharide flippase family protein involved in polysaccharide biosynthesis, a process critical for biofilm formation (Chin et al., 2015). Gene *bpsl2026* encodes a spore coat protein U domain-containing protein, which contributes to surface pilus formation and motility (KEGG, 2025).

In contrast, genes *bpss2016, bpss0312, bpss1214, bpss0124, bpsl1607*, and *bpsl1799* were downregulated in both RS_UMC114 and NI_UMC082. This finding diverges from Chin et al. (2015), where these genes were upregulated in high biofilm producers. The downregulation of most biofilm-related genes in NI_UMC082 and RS_UMC114 suggests a possible suppression of conventional biofilm formation pathways. However, biofilm quantification showed that RS_UMC114 produced higher levels of biofilm than PS_UMC083, presenting a contradiction between gene expression and phenotypic output.

One possible explanation is that alternative genes or regulatory pathways may be activated during infection and relapse. This hypothesis is supported by other studies that have identified non-canonical mechanisms, such as cyclic-di-GMP signalling, as contributors to biofilm formation in *B. pseudomallei* (Nyanasegran et al., 2023). It is plausible that both NI_UMC082 and RS_UMC114 have adapted to their clinical environments by modulating distinct sets of genes involved in biofilm formation. Although the tested genes were downregulated, other genes associated with biofilm development and AMR may be upregulated, which could account for the elevated biofilm production observed in RS_UMC114.

Further investigation is needed to characterise the full spectrum of biofilm-related genes in both the new infection and relapse isolates. This study represents the first to examine biofilm gene expression in a relapse isolate, offering novel insights into

the molecular mechanisms that may underpin biofilm formation during recurrent *B. pseudomallei* infections.

5.3 Differential Expression of Proteins Across PS_UMC083, NI_UMC082 and RS_UMC114

5.3.1 Overview of proteomic characterisation of all three *B. pseudomallei* strains

The differential protein expression between primary and relapse isolates from chronic paediatric melioidosis patients remains poorly characterised. To address this gap, total proteome profiling of PS_UMC083, NI_UMC082 and RS_UMC114 was performed using a label-free quantification approach. This enabled the identification and comparison of proteins differentially expressed in NI_UMC082 and RS_UMC114 relative to the reference strain PS_UMC083.

Proteomic characterisation of all three *B. pseudomallei* clinical strains revealed 671 proteins commonly shared among them. This finding is expected, as many functional proteins universally present in the *B. pseudomallei* species were quantified. Both shared and strain-specific proteins may reflect distinct proteomic adaptations, potentially shaped by antibiotic pressure within the host environment, particularly in the primary and relapse isolates (Velapatino et al., 2012).

Among the 20 most abundant proteins across all three isolates were those involved in nucleic acid metabolism (DNA and RNA processing), oxidative stress response (peroxidases), redox reactions (dehydrogenases), and protein translation (elongation factors and ribosomal proteins). Notably, two peroxidases and one dehydrogenase (oxidoreductase) protein were consistently highly expressed. Oxidoreductases play a central role in managing oxidative stress in *B. pseudomallei*, a known virulence factor in infection (McMahon et al., 2018). Their elevated expression may indicate that the tested clinical strains are well-equipped to withstand oxidative stress, which is critical for intracellular survival under antibiotic exposure. These proteins also contribute to detoxification of reactive carbonyl compounds, regulation of salt stress, and pathogenesis (Chamchoy et al., 2020). Translation elongation factors,

UNIVERSITI KEBANGSAAN MALAYSIA

essential for the elongation phase of protein synthesis, were similarly abundant across all strains, reflecting conserved translational activity.

Further investigation into differential protein expression in NI_UMC082 and RS_UMC114 relative to PS_UMC083 revealed enrichment of proteins involved in metabolic and cellular processes, as categorised under biological processes in functional annotation analyses. PANTHER protein class analysis identified an upregulation (1.5%) of viral or transposable element-related proteins in NI_UMC082. These proteins may contribute to replication or genetic adaptation during co-colonisation with other bacteria (Tokuda & Shintani 2024). Alternatively, their expression may be intrinsic to NI_UMC082's unique sequence type (ST1644), which differs from PS_UMC083 and RS_UMC114 (ST51). Interestingly, RS_UMC114, despite co-colonisation with *B. cepacia*, did not exhibit similar upregulation of these proteins. This suggests that the expression observed in NI_UMC082 is not solely driven by co-infection but may be influenced by strain-specific genomic features. The absence of these proteins in RS_UMC114, which shares the same sequence type as PS_UMC083, further supports this interpretation. Additionally, the complete eradication of NI_UMC082 following antibiotic treatment during the new infection stage implies that these proteins are likely involved in transient adaptive responses rather than mechanisms of persistence.

5.3.2 Differential protein expression between NI_UMC082 vs PS_UMC083

a. Proteins of interest identified between NI_UMC082 vs PS_UMC083

NI_UMC082 exhibited several notable changes in protein expression compared to the reference strain PS_UMC083, offering insights into its adaptive mechanisms and virulence strategies. Moderate upregulation of bacterial chemotaxis proteins was observed, including the aerotaxis receptor (Q63NM3), methyl-accepting chemotaxis protein (Q63SF6), chemotaxis protein CheA (Q63PR7), extracellular solute-binding protein (Q63Y13), and the two-component response regulator CheY1 (Q63PR6), with fold changes ranging between 1.6 and 2.1. Chemotaxis is a critical determinant of *B. pseudomallei* pathogenesis, enabling host cell localisation and invasion (Rao et al., 2024). These findings suggest that NI_UMC082 may possess an enhanced capacity to navigate host environments, thereby promoting infection initiation and persistence.

UNIVERSITI KEBANGSAAN MALAYSIA

Several enzymes involved in catalysis and metabolism were significantly upregulated, including hydrolase (Q63I95) and alkyl hydroperoxide reductase AhpD (Q63T72), with fold changes ranging between 5.7 and 14.3. This pattern indicates elevated metabolic activity alongside enhanced oxidative stress defence, reflecting adaptive responses that may support bacterial survival under hostile host conditions. Such adaptations are essential for bacterial survival in hostile host environments (Phenn et al., 2021). The translation initiation factor IF-2 (infB) was similarly upregulated, suggesting increased protein synthesis to support rapid growth and environmental adaptation (Krishnananthasivam et al., 2017). Additionally, the upregulation of flagellin reinforces the motility profile of NI_UMC082, which may facilitate dissemination within host tissues (Rao et al., 2024).

In contrast, proteins associated with the multidrug efflux system, including amrA (Q63U13, fold change = -15.2) and amrB (Q63U14, fold change = -4.1), were downregulated. This suggests a reduced reliance on efflux-mediated antibiotic resistance, possibly due to alternative adaptive strategies. Moreover, T6SS proteins Hcp (Q63K67, fold change = -25.2) and BPSS1497 (Q63K68, fold change = -6.5) were also downregulated, indicating a potential shift in virulence strategy. Rather than relying on direct host cell invasion via T6SS, NI_UMC082 may employ other immune evasion mechanisms such as capsule formation, LPS modification, or antioxidant enzyme expression (e.g., sodB upregulation). These alternative pathways may enable the bacterium to persist in a less immunogenic state, particularly during early colonisation or co-infection scenarios.

b. Differently regulated biofilm-related proteins relative to PS_UMC083

Several biofilm-related proteins were upregulated between the NI_UMC082 vs PS_UMC083 comparison group, providing insight into the strain's surface attachment and colonisation capabilities. Notably, increased expression of lipoproteins such as the BON domain-containing protein (Q63IZ2, fold change = 3.0) and a general lipoprotein (Q63Y85, fold change = 2.3) suggests an enhanced capacity for surface adherence. Although the specific role of lipoproteins in *B. pseudomallei* biofilm formation remains unclear, studies in *Staphylococcus aureus* have shown that lipoproteins can interact with eDNA within the biofilm matrix to promote structural stability (Kavanaugh et al., 2019).

This upregulation may therefore facilitate bacterial colonisation and biofilm establishment on host tissues.

The elevated expression of enoyl-[acyl-carrier-protein] reductase (Q63MD6, fold change = 3.2) further underscores the importance of fatty acid biosynthesis in maintaining biofilm matrix integrity. While the role of fatty acids in *B. pseudomallei* biofilm formation is not well defined, similar pathways have been shown to promote biofilm development and colony wrinkling in gram-positive bacteria (Arjes et al., 2022). This may partially explain the higher biofilm production observed in NI_UMC082 when compared to PS_UMC083. Additionally, the upregulation of chemotaxis-related proteins, such as the methyl-accepting chemotaxis protein (Q63SF6, fold change = 1.9), highlights the strain's ability to migrate toward favourable microenvironments for biofilm formation. This suggests that *B. pseudomallei* actively seeks out host niches that support survival and biofilm development, enhancing its potential for persistent colonisation.

Adaptation to oxygen-limited environments was also evident through the upregulation of nitrate reductase (quinone) (Q63SL1, fold change = 1.78). This enzyme facilitates anaerobic respiration by reducing nitrate to nitrite, providing an alternative energy source under hypoxic conditions (Mangalea et al., 2017; Mangalea et al., 2020). Nitrate reduction has also been linked to elevated cyclic-di-GMP levels, which promote biofilm formation by regulating EPS biosynthesis (Jiang et al., 2020). These adaptations are critical for maintaining bacterial viability within biofilms and in oxygen-restricted host environments.

Conversely, several proteins were downregulated in NI_UMC082, suggesting a shift in survival strategy. The multidrug efflux system protein AmrA (Q63U13, fold change = -15.2) and the fatty acid biosynthesis-related CoA ligase (Q63NJ7, fold change = -3.0) were both significantly reduced. Downregulation of AmrA may indicate decreased reliance on efflux-mediated antibiotic resistance, potentially reflecting a shift toward biofilm-mediated protection or intracellular persistence. Similarly, reduced expression of CoA ligase, which activates long-chain fatty acids into acyl-CoA, may compromise resistance to abiotic stresses such as desiccation, temperature variation, or nutrient limitation (Wei et al., 2022). This pattern suggests that NI_UMC082 is adapting

to biotic conditions within the host, rather than maintaining traits advantageous in environmental reservoirs.

Given that NI_UMC082 was acquired during the patient's visit to a melioidosis-endemic region, it is plausible that the strain originated from an environmental source such as soil or water, where resistance to abiotic stress would be beneficial. The observed downregulation of these proteins may reflect a shift in expression as the strain transitioned from an external environment to the host. Despite these adaptations, NI_UMC082 was ultimately eradicated by antibiotic treatment and did not cause relapse. This outcome suggests that while the strain was environmentally adapted, it lacked the intracellular survival mechanisms required for persistence and relapse. Its failure to re-establish infection under favourable conditions underscores the importance of host-specific survival traits in chronic melioidosis.

Overall, the expression profile of NI_UMC082 highlights the complex interplay between environmental adaptation, biofilm formation, and host colonisation. The downregulation of key biofilm-related proteins, alongside upregulation of surface attachment and anaerobic survival factors, reflects a transient adaptation strategy that may support initial infection but not long-term persistence.

5.3.3 Differential protein expression between RS_UMC114 vs PS_UMC083

a. Proteins of interest identified between RS_UMC114 vs PS_UMC083

Comparative proteomic analysis between RS_UMC114 relative to PS_UMC083 revealed distinct patterns of protein upregulation and downregulation, offering insights into bacterial persistence. Prolonged antibiotic exposure by the patient underscores the adaptive capacity of *B. pseudomallei* to survive in hostile conditions, which is critical to understanding relapse mechanisms. Notably, co-colonisation with other bacterial species was also observed during the diagnosis of each subsequent strain, complicating the interpretation of the relapse mechanisms. Additionally, horizontal gene transfer from co-infecting species may also have influenced the proteomic landscape of the clinical strains (Moura et al., 2023).

UNIVERSITI KEBANGSAAN MALAYSIA

Several virulence and invasion-associated proteins were significantly upregulated in RS_UMC114, suggesting enhanced persistence and host cell invasion capabilities. Notably, BipD (Q63K37) exhibited the highest increase in expression (fold change 32.5). Other proteins, including BsaR, BopE, and BipC, were also upregulated, with fold changes ranging between 2.4 and 8.5, consistent with their roles in regulating and executing type III secretion system (T3SS) functions essential for host cell manipulation and intracellular survival (Kang et al., 2016; Vander Broek & Stevens, 2017). The substantial upregulation of BipD likely reflects RS_UMC114's enhanced ability to deploy these effectors during relapse. BsaR, although not part of the T3SS, plays a vital role in host cell invasion (Vander et al., 2017), and its elevated expression suggests improved capabilities to invade and survive within host cells, helping the bacterium evade immune responses and persist in the host environment.

The upregulation of virulence proteins BopE and BipC reinforces the RS_UMC114 invasive phenotype. BopE functions as a guanine nucleotide exchange factor, activating Rho GTPases to induce actin cytoskeleton rearrangements and facilitate entry into non-phagocytic cells (Stevens et al., 2002, 2003, 2004). Recent findings also implicate BopE in suppressing host defence pathways to promote intracellular replication (Rao et al., 2024). BipC similarly disrupts host actin dynamics, promoting membrane ruffling and immune evasion (Büttner, 2012; Kang et al., 2016). Although their fold changes were lower than BipD and BsaR, their upregulation supports RS_UMC114's enhanced ability to invade and subvert host cell functions.

Stress-related proteins DnaK (O68191), DnaJ (Q63R47), and GrpE (Q63R45) were also upregulated, with fold changes ranging between 1.8 and 2.8, indicating a robust stress response during relapse. These chaperones assist in protein folding and protect against proteotoxic stress induced by antibiotics and immune pressure (Vanaporn et al., 2008; Khodaparast et al., 2021). DnaJ, as a co-chaperone of DnaK, stabilises unfolded proteins and mitigates damage from hyperosmotic stress and heat shock (Allwood et al., 2011). Their coordinated upregulation suggests that RS_UMC114 employs proteostasis mechanisms to maintain cellular function under relapse conditions.

Oxidative stress management was another prominent feature of RS_UMC114. Twenty-one oxidoreductase proteins were upregulated, including superoxide dismutase

UNIVERSITI KEBANGSAAN MALAYSIA

(sodB), aldehyde dehydrogenase, quinone oxidoreductase, and catalase-peroxidase, with fold changes ranging between 1.9 – 3.2. These enzymes neutralise reactive oxygen species (ROS) generated by host immune responses, enhancing bacterial survival (He et al., 2017). The upregulation of sodB, also observed in a previous relapse study (Velapatino et al., 2012), may contribute to increased resistance against oxidative damage. Oxidoreductases additionally support metabolic flexibility, allowing adaptation to nutrient-limited conditions and persistence within macrophages, where oxidative stress is a primary immune strategy (Wiersinga et al., 2012).

Thymidylate synthase (Q63S51) and ribose-phosphate pyrophosphokinase (Q63XL8) were upregulated, with fold changes ranging between 1.6 and 2.1. This elevation in nucleotide biosynthesis reflects an increased demand for nucleotide precursors, supporting DNA repair and intracellular replication. Importantly, these enzymes are essential for maintaining genomic integrity and have been implicated in regulating virulence through cyclic AMP-mediated signalling pathways (Allwood et al., 2011; Hu et al., 2019; Zhou et al., 2019).

Interestingly, efflux pump components amrA (fold change = -14.9) and amrB (fold change = -4.4), which mediate β-lactam resistance, were downregulated in RS_UMC114. This suggests a strategic shift away from energy-intensive resistance mechanisms toward persistence-focused adaptations. Despite treatment with ceftazidime, amikacin, doxycycline, co-trimoxazole, and azithromycin, RS_UMC114 exhibited reduced expression of these resistance proteins. It is important to note, however, that these molecular data were derived from *in vitro* cultured isolates, which do not fully replicate the host environment or the antibiotic pressures experienced during infection. The absence of antibiotic exposure during culturing likely influenced the regulation of resistance-associated genes, meaning that efflux pump activity may only be induced under direct drug pressure *in vivo*. This context helps explain the apparent discrepancy between the patient's history of repeated β-lactam treatment and the observed downregulation of *amrA* and *amrB*. Taken together, these findings suggest that relapse in this case was not primarily driven by constitutive AMR.

Other downregulated proteins include the linear gramicidin synthetase subunit C (fold change = -16.2), possibly reflecting altered metabolic priorities. Additionally,

UNIVERSITI KEBANGSAAN MALAYSIA

the aerotaxis receptor protein (fold change = -5.8) was downregulated, indicating metabolic adaptation to low-oxygen environments during relapse.

This study is the first to report the upregulation of BipD, BipC, BopE, and BsaR in a clinical relapse isolate of *B. pseudomallei*. While previous studies have characterised their roles in virulence and invasion, their specific upregulation in relapse isolates has not been documented through proteomic analysis. These findings provide novel insights into the adaptive strategies employed by *B. pseudomallei* to persist under immune and antibiotic pressure, highlighting the importance of these proteins in relapse pathogenesis.

b. Differently regulated biofilm-related proteins relative to PS_UMC083

RS_UMC114 demonstrated a significant increase in biofilm production compared to PS_UMC083. Interestingly, only two biofilm-related proteins were found to be upregulated in RS_UMC114: chaperone protein ClpB and fatty acid biosynthesis-related CoA ligase. While both are associated with stress response and biofilm maintenance, they are not considered primary drivers of biofilm formation.

Chaperone protein ClpB is known for its role in cellular stress responses, although it was not categorised under stress-related proteins in the STRING database. Further analysis revealed its function as a stress response protein, which maintains cellular integrity under hostile conditions (Vanaporn et al., 2008). ClpB has been recognised as a key chaperone with disaggregase activity, essential for bacterial survival during heat shock and other stressors. Recent studies have shown that ClpB regulates the secretion of effector molecules associated with the T6SS in *Francisella tularensis* (Brodmann et al., 2017; Alam et al., 2018). In *B. pseudomallei*, ClpB has been characterised as a biofilm-associated protein, suggesting its involvement in maintaining protein integrity under biofilm conditions. It is also considered an outer membrane and cell surface protein (Alam et al., 2021), although its specific functions in *B. pseudomallei* biofilms remain to be fully elucidated.

CoA ligase plays a central role in fatty acid metabolism by activating long-chain fatty acids into acyl-CoA, which are essential for maintaining membrane integrity and

UNIVERSITI KEBANGSAAN MALAYSIA

biofilm matrix structure (Wei et al., 2022). Its modest upregulation (fold change = 1.68) in RS_UMC114 suggests a contribution to biofilm stability. However, as discussed in section 5.3.2a(i), CoA ligase is also implicated in reducing resistance to abiotic stresses. Additional roles in biofilm formation, particularly during relapse, may exist but are yet to be characterised. The relatively small increase in expression indicates that RS_UMC114 may rely on subtle metabolic adjustments rather than classical biofilm pathways to maintain a persistent biofilm under treatment pressure and immune challenge.

Despite its elevated biofilm production, RS_UMC114 exhibited significant downregulation of several biofilm-related proteins. These include nitrate reductase, lipoproteins, lipases, and methyl-accepting chemotaxis proteins, previously discussed in section 5.3.2a(i). This pattern suggests a shift in metabolic focus. Reduced expression of nitrate reductase and chemotaxis proteins may reflect adaptation to a host-specific environment, where biofilm formation is less dependent on external cues such as oxygen gradients and more influenced by internal survival mechanisms.

Similarly, the downregulation of lipoproteins and lipases may indicate a reduced emphasis on early biofilm formation stages, such as surface attachment and lipid hydrolysis. This could represent a strategic shift in RS_UMC114, prioritising biofilm maintenance and resilience over initiation. It is plausible that biofilm production in RS_UMC114 is driven more by stress tolerance and intracellular survival than by conventional biofilm pathways.

One possible explanation for the limited number of upregulated biofilm proteins in RS_UMC114 is the growth conditions used during experimentation. None of the tested biofilm-related genes through qPCR were detected in both RS_UMC114 and NI_UMC082. The primers were derived from Chin et al. (2015), who also cultured *B. pseudomallei* under shaking conditions, which do not favour biofilm growth. Although high biofilm-producing strains in their study showed gene upregulation under a similar growth protocol, only 2 biofilm proteins were upregulated in this study, and none of the qPCR-targeted genes translated into detectable proteins via LC-MS.

This discrepancy suggests that biofilm formation may not be a dominant mechanism for intracellular survival and persistence in *B. pseudomallei*. The bacterium

UNIVERSITI KEBANGSAAN MALAYSIA

may possess enhanced biofilm-forming capabilities under stable conditions, but not necessarily within the host. While studies such as Limmathurotsakul et al. (2014) have reported high biofilm production in relapse strains, there is no definitive evidence that biofilms are actively produced *in vivo* during relapse infections or serve as a primary survival strategy in chronic melioidosis. Hence, further experimentation or direct sampling from relapse cases will be required to clearly establish whether biofilm activity contributes to relapse and to confirm the causal link between biofilm formation and recurrent infection.

5.3.4 Comparative KEGG pathway analysis of *B. pseudomallei* clinical strains

KEGG pathway enrichment analysis was performed to compare transcriptional and proteomic profiles of RS_UMC114 and NI_UMC082 against the reference strain PS_UMC083. The results revealed distinct regulatory patterns that reflect the clinical trajectory of each isolate and provide insight into the molecular adaptations associated with persistence, stress response, and motility.

In the RS_UMC114 vs PS_UMC083 comparison, 23 pathways were significantly upregulated, many of which are linked to biosynthetic and metabolic functions. These include metabolic pathways, biosynthesis of secondary metabolites, biosynthesis of antibiotics, and biosynthesis of amino acids. The enrichment of these pathways suggests that RS_UMC114 may have undergone metabolic rewiring to support survival under antibiotic pressure and host immune stress. This is consistent with previous findings that *B. pseudomallei* encodes a diverse array of biosynthetic gene clusters that contribute to environmental adaptation and virulence (Klaus et al., 2020).

Stress adaptation pathways such as CAMP resistance, carbon metabolism, and pyruvate metabolism were also enriched in RS_UMC114. The upregulation of oxidoreductase and stress response proteins, including SodB and DnaK, supports this observation. These findings align with studies showing that *B. pseudomallei* activates oxidative stress regulators and membrane remodelling systems to survive hostile conditions, including exposure to antimicrobial peptides (Duangurai, 2018).

The ribosome pathway was found to be significantly downregulated in RS_UMC114 when compared to PS_UMC083. This may indicate a shift toward

translational suppression; a strategy associated with bacterial dormancy and persistence. Suppression of ribosomal activity has been previously reported in persistent *Burkholderia* populations, where reduced protein synthesis contributes to antibiotic tolerance and immune evasion (Nierman et al., 2015). The downregulation of ribosomal proteins observed in the proteomic data further supports this interpretation.

In contrast, the NI_UMC082 vs PS_UMC083 comparison group revealed enrichment of bacterial chemotaxis and β-alanine metabolism pathways. This suggests a more motile and responsive phenotype, consistent with early-stage infection. Proteomic analysis showed upregulation of flagellin and methyl-accepting chemotaxis proteins in NI_UMC082, which supports the KEGG findings. Chemotaxis and motility proteins are known to facilitate host cell invasion and are typically upregulated during acute infection phases (Srinon et al., 2019).

Overall, RS_UMC114 appears to adopt a metabolically active but translationally restrained state, enriched in biosynthetic and stress adaptation pathways, while NI_UMC082 exhibits traits associated with motility and early infection.

5.3.5 Identification and functional characterisation of hub proteins in *B. pseudomallei* clinical isolates

A total of 26 upregulated hub proteins and two downregulated hub proteins were identified in the RS_UMC114 vs PS_UMC083 comparison group. However, no hub proteins were detected in the NI_UMC082 vs PS_UMC083 comparison, suggesting a more distributed or transient regulatory architecture in the new infection strain.

The upregulated hub proteins in the RS_UMC114 vs PS_UMC083 group were functionally associated with ribosome structure (rpsO, rpsG, rplT), purine biosynthesis (purL, prs, adk, gmk), amino acid metabolism (argA, argB, hom, leuA, hisA, hisD), and stress response (sodB, trxA, dnaJ). These categories correspond directly with the KEGG-enriched pathways, including metabolic pathways, biosynthesis of amino acids, 2-oxocarboxylic acid metabolism, and CAMP resistance, underscoring the coordinated regulation of core survival processes. The identification of SodB and DnaJ as hub proteins further reinforces the stress adaptation profile of RS_UMC114, consistent with its elevated biofilm production at 72 hours and delayed growth trajectory observed in

the CFU assay. Such phenotypes are hallmarks of persistence-oriented strains, reflecting a strategy in which metabolic activity is maintained at a basal level while stress response pathways are upregulated to withstand host immunity and antibiotic pressure, a pattern also observed in *Burkholderia thailandensis* biofilms, where decreased metabolic activity coincided with increased stress protein expression (Khan et al., 2019). This suggests that RS_UMC114 is not metabolically dormant but rather stress-adapted, enabling long-term survival and relapse potential, in line with recent studies highlighting biofilm regulation and stress signalling in *B. pseudomallei* (Nyanasegran et al., 2023).

The identification of purine biosynthesis and amino acid metabolism proteins as hubs supports the KEGG enrichment of nitrogen and carbon cycling pathways, which are critical for bacterial survival under nutrient-limited or immune-challenged conditions. These biosynthetic hubs likely contribute to the relapse strain's ability to re-establish infection following antibiotic treatment, as previously described in metabolic rewiring models of *B. pseudomallei* (Klaus et al., 2020).

Interestingly, although several ribosomal proteins were upregulated as hubs, the ribosome pathway was downregulated in the KEGG analysis. This contradiction may reflect selective suppression of specific ribosomal subunits rather than global translational shutdown of ribosomes. The downregulated hub proteins rplN and rpsB, both components of the ribosome, may represent targets of post-transcriptional regulation or ribosome remodelling, which are known strategies for persistence in *Burkholderia* species (Nierman et al., 2015). This interpretation is supported by previous studies showing that persistent bacteria reduce protein synthesis to evade immune detection and survive antibiotic exposure.

The absence of hub proteins in the NI_UMC082 vs PS_UMC083 comparison group, however, suggests that the new infection strain does not rely on centralised regulatory nodes. Instead, its enriched KEGG pathway, bacterial chemotaxis and β-alanine metabolism, point to a motile and responsive phenotype. This is consistent with the proteomic upregulation of flagellin and methyl-accepting chemotaxis proteins in NI_UMC082, which are typically associated with acute infection and host cell invasion (Srinon et al., 2019).

UNIVERSITI KEBANGSAAN MALAYSIA

The hub protein analysis reinforces the KEGG pathway findings and highlights the central role of biosynthetic, stress response, and ribosomal regulators in RS_UMC114. These hubs may serve as potential biomarkers or therapeutic targets for distinguishing persistent *B. pseudomallei* infections from acute presentations, thereby guiding more effective diagnostic and therapeutic strategies.

UNIVERSITI KEBANGSAAN MALAYSIA

CHAPTER VI

CONCLUSION AND FUTURE WORKS

6.1 Conclusion

This study presents a comprehensive comparative analysis of *B. pseudomallei* clinical isolates derived from a paediatric melioidosis patient, encompassing primary (PS_UMC083), new infection (NI_UMC082), and relapse (RS_UMC114) strains. Through integrated biofilm quantification, qPCR, proteomic profiling, KEGG pathway enrichment, and hub protein analysis, distinct molecular signatures were identified that correspond to each isolate's clinical trajectory.

RS_UMC114 demonstrated significantly elevated biofilm production compared to PS_UMC083, consistent with previous reports that relapse isolates often exhibit enhanced biofilm formation (Limmathurotsakul et al., 2014). Interestingly, qPCR analysis revealed a consistent downregulation of canonical biofilm-associated genes in RS_UMC114, and proteomic profiling showed that none of the proteins previously reported by Chin et al. (2015) were consistently expressed across all three strains. These findings indicate that biofilm regulation in RS_UMC114 may involve non-canonical or strain-specific pathways, and that the molecular basis of its elevated biofilm phenotype requires further investigation under host-relevant conditions.

Proteomic analysis revealed that RS_UMC114 exhibited marked upregulation of proteins associated with virulence, invasion, oxidoreductase activity, and stress

UNIVERSITI KEBANGSAAN MALAYSIA

response. The stark increased in expression of T3SS components (BipD, BipC, BopE) and the invasion regulator BsaR points to a potential shift in pathogenic strategy, favouring intracellular survival and immune evasion. The coordinated upregulation of oxidoreductases and stress-related chaperones (DnaK, DnaJ, GrpE) further supports the hypothesis that RS_UMC114 has adapted to withstand hostile host conditions, possibly through regulatory mutations that rewire its survival pathways. Importantly, to our knowledge, this is the first study to report proteomic upregulation of T3SS effectors (BipD, BipC, BopE) and the invasion regulator BsaR in a clinical relapse isolate of *B. pseudomallei*, extending relapse-associated proteomic observations beyond stress and anaerobic survival pathways previously described. While relapse studies have highlighted enhanced nitric oxide detoxification and anaerobic metabolism (Velapatino et al., 2014) and documented upregulation of the T6SS (Seng et al., 2023), specific proteomic upregulation of T3SS effectors in relapse isolates has not been previously reported, underscoring the novelty of our findings.

KEGG pathway enrichment and hub protein analysis of RS_UMC114 further revealed that RS_UMC114 is enriched in biosynthetic, stress adaptation, and purine metabolism pathways. The enrichment of biosynthetic and purine metabolism pathways suggests a metabolic rewiring that supports nucleotide turnover and amino acid biosynthesis under nutrient-limited conditions, enabling sustained intracellular survival. The concurrent enrichment of stress adaptation pathways also highlighted as hubs reveals a persistence-oriented phenotype, where oxidative stress defences and protein-folding chaperones assist the bacterium against host immune pressure and antibiotic exposure. KEGG results are consistent with previous relapse studies in which stress response proteins were found upregulated (Velapatino et al., 2014), indicating a

UNIVERSITI KEBANGSAAN MALAYSIA

strategic shift from rapid growth to long-term survival. The coordinated upregulation of oxidoreductases and stress-related chaperones further supports the hypothesis that RS_UMC114 has adapted to withstand hostile host conditions, possibly through regulatory mutations that rewire its survival pathways.

In contrast, NI_UMC082 displayed upregulation of motility and chemotaxis proteins, alongside metabolic enzymes associated with acute infection. Despite moderate biofilm production, NI_UMC082 lacked the stress-adapted proteomic profile observed in RS_UMC114 and was successfully eradicated by antibiotic treatment. This suggests that environmental adaptation alone is insufficient for persistence and that relapse requires specialised host-specific survival mechanisms. KEGG enrichment analysis further supported this interpretation, showing that NI_UMC082 is characterised by pathways linked to chemotaxis and β-alanine metabolism. The prominence of chemotaxis reflects a motile, invasion-oriented phenotype, enabling rapid host colonisation (Chin et al., 2015), while β-alanine metabolism suggests metabolic flexibility during acute infection. Together, these features distinguish NI_UMC082 as an acute infection strain that prioritises motility and metabolic responsiveness over long-term survival strategies.

All molecular data in this study were derived from *in vitro* cultured isolates, which do not fully replicate the host environment or the antibiotic pressures experienced during infection. The absence of antibiotic exposure during culturing likely influenced the regulation of resistance-associated genes, such as *amrA*, which was observed to be downregulated in both NI_UMC082 and RS_UMC114. This discrepancy with the patient's history of repeated β-lactam treatment suggests that AMR mechanisms may not be constitutively expressed, but instead are context-dependent and activated only

UNIVERSITI KEBANGSAAN MALAYSIA

under antibiotic pressure *in vivo*. Consequently, the findings indicate that relapse in this case may be driven more by alternative survival strategies (e.g., biofilm formation or intracellular persistence) rather than by stable upregulation of resistance genes.

Taken together, these findings suggest that virulence proteins, oxidoreductase proteins and stress response proteins may be central to the relapse mechanism of *B. pseudomallei*. The relapse strain may have undergone adaptive changes, potentially at the regulatory level, that enable persistence and intracellular survival without relying heavily on biofilm production. While the *in vitro* nature of this study limits direct extrapolation to the patient's clinical condition, the comparative analysis of strains isolated across different stages of infection provides valuable insight into the molecular adaptations that may underpin chronic relapse in melioidosis. By identifying relapse-associated upregulation of T3SS effectors and stress response proteins, this study highlights potential biomarkers and therapeutic targets that could distinguish persistent *B. pseudomallei*.

UNIVERSITI KEBANGSAAN MALAYSIA

6.2 Study Limitations

A key limitation of this study is the small sample size, as only three clinical isolates were used, one each from the primary, new infection, and relapse phases. While these isolates were carefully selected, they may not fully represent the genetic and phenotypic diversity of *B. pseudomallei* strains involved in chronic melioidosis. Another limitation is the restricted scope of qPCR validation, as only a subset of biofilm-related genes was tested. Many of these genes were found to be downregulated, leaving potential upregulated genes unexplored. Additionally, the lack of funding prevented the inclusion

of a comprehensive transcriptomics analysis to assess biofilm gene regulation across the three strains. This restricted our ability to fully understand the dynamic regulation of biofilm formation throughout infection stages, which could have provided deeper insights into the role of biofilms in relapse infections.

Furthermore, machine learning approaches for biomarker discovery, which could have strengthened the translational impact of this study, could not be pursued. This was not feasible due to the absence of available expertise and the technical challenges of implementing such analyses independently. Attempts to engage industrial services were also unsuccessful, as they were unable to provide the required support.

6.3 Future Works

To strengthen the findings of this study and address its limitations, several future directions are recommended. Firstly, expanding the sample size to include more clinical isolates from each infection phase would improve the generalisability of the results and better represent the diversity of *B. pseudomallei* strains involved in chronic melioidosis. Further investigation into host–pathogen interactions is also warranted. This could include macrophage infection assays to assess intracellular survival and immune evasion strategies, as well as RNA sequencing of host cells post-infection to profile host immune responses and identify pathways affected by different *B. pseudomallei* isolates. These approaches would provide a more holistic view of how the pathogen interacts with and adapts to the host environment.

UNIVERSITI KEBANGSAAN MALAYSIA

In terms of validation, gene knockout or knockdown studies (using CRISPR-Cas) targeting biofilm-related or persistence-associated genes could help confirm their functional roles. Additionally, Western blot analysis should be performed to validate the differential protein expression observed in the LC-MS/MS proteomic data. Although virulence assays such as invasion and adhesion assays and lactate dehydrogenase (LDH) release assays are commonly used to assess pathogenic potential, they were not included in this study as the research objectives focused primarily on biofilm formation and molecular adaptation rather than direct virulence profiling. Nonetheless, these assays could be considered in future studies to complement the current findings.

Moreover, a comprehensive transcriptomic analysis would be highly beneficial to explore the global gene expression landscape across primary, new infection, and relapse isolates. This would allow for the identification of regulatory networks and pathways involved in biofilm formation, persistence, and relapse mechanisms.

In addition, future studies could incorporate machine learning approaches for biomarker discovery, integrating proteomic and transcriptomic datasets to identify predictive signatures of relapse. Such computational methods would enable the detection of complex patterns and hub proteins that may not be apparent through conventional analyses, thereby enhancing the translational potential of this research. Collectively, these future studies would provide critical validation and mechanistic depth to support and extend the findings of this research

UNIVERSITI KEBANGSAAN MALAYSIA

REFERENCES

Ahmad N, Hashim R, Mohd Noor A. 2013. The in vitro antibiotic susceptibility of Malaysian isolates of *Burkholderia pseudomallei*. *International Journal of Microbiology* 2013:121845. doi:10.1155/2013/121845

Alam A, Golovliov I, Javed E, Sjöstedt A. 2018. ClpB mutants of *Francisella tularensis* subspecies holarctica and tularensis are defective for type VI secretion and intracellular replication. *Scientific Reports* 8:11324. doi:10.1038/s41598-018-29745-4

Alam A, Bröms JE, Kumar R, Sjöstedt A. 2021. The role of ClpB in bacterial stress responses and virulence. *Frontiers in Molecular Biosciences* 8:668910. doi:10.3389/fmolb.2021.668910

Alav I, Sutton JM, Rahman KM. 2018. Role of bacterial efflux pumps in biofilm formation. *Journal of Antimicrobial Chemotherapy* 73(8):2003–2020. doi:10.1093/jac/dky042

Allwood EM, Devenish RJ, Prescott M, Adler B, Boyce JD. 2011. Strategies for intracellular survival of *Burkholderia pseudomallei*. *Frontiers in Microbiology* 2:170. doi:10.3389/fmicb.2011.00170

Al Maleki AR, Vellasamy KM, Mariappan V, Venkatraman G, Tay ST, Vadivelu J. 2020. Transcriptome analysis of *Burkholderia pseudomallei* SCV reveals an association with virulence, stress resistance and intracellular persistence. *Genomics* 112(1):501–512. doi:10.1016/j.ygeno.2019.04.002

Anutrakunchai C, Bolscher J, Krom B, Kanthawong S, Chareonsudjai S, Taweechaisupapong S. 2018. Impact of nutritional stress on drug susceptibility and biofilm structures of *Burkholderia pseudomallei* and *Burkholderia thailandensis* grown in static and microfluidic systems. *PLoS One* 13:e0194946. doi:10.1371/journal.pone.0194946

Aranda PS, LaJoie DM, Jorcyk CL. 2012. Bleach gel: A simple agarose gel for analysing RNA quality. *Electrophoresis* 33(2):366–369. doi:10.1002/elps.201100335

Arjes HA, Gui H, Porter R, Atolia E, Peters JM, Gross C, Kearns DB, Huang KC. 2022. Fatty acid synthesis knockdown promotes biofilm wrinkling and inhibits sporulation in *Bacillus subtilis*. *mBio* 13(5):e0138822. doi:10.1128/mbio.01388-22

Ashdown LR. 1979. An improved screening technique for isolation of *Pseudomonas pseudomallei* from clinical specimens. *Pathology* 11(2):293–297. doi:10.3109/00313027909061954

Berne C, Ducret A, Hardy GG, Brun YV. 2015. Adhesins involved in attachment to abiotic surfaces by Gram-negative bacteria. *Microbiology Spectrum* 3(4):MB-0018-2015. doi:10.1128/microbiolspec.MB-0018-2015

Blanco P, Hernando Amado S, Reales Calderon JA, Corona F, Lira F, Alcalde Rico M, Bernardini A, Sanchez MB, Martinez JL. 2016. Bacterial multidrug efflux pumps:

Much more than antibiotic resistance determinants. *Microorganisms* 4(1):14. doi:10.3390/microorganisms4010014

Bradford, M. M. 1976. A rapid and sensitive method for the quantitation of microgram quantities of protein utilizing the principle of protein-dye binding. *Analytical Biochemistry*, 72(1–2), 248–254. https://doi.org/10.1016/0003-2697(76)90527-3

Brodmann M, Dreier RF, Broz P, Basler M. 2017. *Francisella* requires dynamic type VI secretion system and ClpB to deliver effectors for phagosomal escape. *Nature Communications* 8:15853. doi:10.1038/ncomms15853

Bu D, Luo H, Huo P, Wang Z, Zhang S, He Z, Wu Y, Zhao L, Liu J, Guo J, Fang S, Cao W, Yi L, Zhao Y, Kong L. 2021. KOBAS-i: Intelligent prioritization and exploratory visualization of biological functions for gene enrichment analysis. *Nucleic Acids Research* 49(W1):W317–W325. doi:10.1093/nar/gkab447

Burkholder WH. 1950. Sour skin, a bacterial rot of onion bulbs. *Phytopathology* 40(3):115–118.

Butler D. 2012. Viral research faces clampdown. *Nature* 490:456a. doi:10.1038/490456a

Burtnick MN, Brett PJ, DeShazer D. 2014. Proteomic analysis of the *Burkholderia pseudomallei* Type II secretome reveals hydrolytic enzymes, novel proteins, and the deubiquitinase TssM. *Infection and Immunity* 82(8):3215–3226. doi:10.1128/IAI.01739-14

Bjarnsholt T. 2013. The role of bacterial biofilms in chronic infections. *APMIS* Suppl. 136:1–51. doi:10.1111/apm.12099

Bzdyl NM, Moran CL, Bendo J, Sarkar-Tyson M. 2022. Pathogenicity and virulence of *Burkholderia pseudomallei*. *Virulence* 13(1):1945–1965. doi:10.1080/21505594.2022.2139063

Centers for Disease Control and Prevention (CDC). 2023. Bioterrorism agents/diseases. *CDC Emergency Preparedness and Response*. https://emergency.cdc.gov/agent/agentlistcategory.asp

Centers for Disease Control and Prevention (CDC). 2024. Melioidosis. *CDC Yellow Book 2024*. https://wwwnc.cdc.gov/travel/yellowbook/2024/infections-diseases/melioidosis

Chamchoy K, Pumirat P, Reamtong O, Pakotiprapha D, Leartsakulpanich U, Boonyuen U. 2020. Functional analysis of BPSS2242 reveals its detoxification role in Burkholderia pseudomallei under salt stress. *Scientific Reports* 10(1):10453.

Chan YY, Chua KL. 2005. The Burkholderia pseudomallei BpeAB-OprB efflux pump: Expression and impact on quorum sensing and virulence. *Journal of Bacteriology* 187(14):4707–4719. doi:10.1128/JB.187.14.4707-4719.2005

Chantratita N, Wuthiekanun V, Boonbumrung K, Tiyawisutsri R, Vesaratchavest M, Limmathurotsakul D, Chierakul W, Wongratanacheewin S, Pukritiyakamee S, White NJ, Day NP, Peacock SJ. 2007. Biological relevance of colony morphology and

phenotypic switching by Burkholderia pseudomallei. *Journal of Bacteriology* 189(3):807–817.

Chattagul S, Khan MM, Scott AJ, Nita-Lazar A, Ernst RK, Goodlett DR, Sermswan RW. 2021. Transcriptomics analysis uncovers transient ceftazidime tolerance in Burkholderia biofilms. *ACS Infectious Diseases* 7(8):2324–2336.

Chen YS, Chen SC, Kao CM, Wu YL. 2003. Effects of soil pH, temperature, and water content on the growth of *Burkholderia pseudomallei*. *Folia Microbiologica* 48(2):253–256.

Chen Y, Wong J, Sun GW, Liu Y, Tan GY, Gan YH. 2011. Regulation of type VI secretion system during *Burkholderia pseudomallei* infection. *Infection and Immunity* 79(8):3064–3073.

Cheng AC, Currie BJ, Dance DAB. 2005. Melioidosis: Epidemiology, pathophysiology, and management. *Clinical Microbiology Reviews* 18(2):383–416. doi:10.1128/cmr.18.2.383-416.2005

Chetchotisakd P, Chierakul W, Chaowagul W, Anunnatsiri S, Phimda K, Mootsikapun P, Chaisuksant S, Pilaikul J, Thinkhamrop B, Phiphitaporn S, Susaengrat W, Toondee C, Wongrattanacheewin S, Wuthiekanun V, Chantratita N, Thaipadungpanit J, Day NP, Limmathurotsakul D, Peacock SJ. 2014. Trimethoprim sulfamethoxazole versus trimethoprim sulfamethoxazole plus doxycycline as oral eradicative treatment for melioidosis (MERTH): A multicentre, double blind, non-inferiority, randomised controlled trial. *Lancet* 383(9919):807–814.

Chieng S, Carreto L, Nathan S. 2012. *Burkholderia pseudomallei* transcriptional adaptation in macrophages. *BMC Genomics* 13:328. doi:10.1186/1471-2164-13-328

Chin CY, Hara Y, Ghazali AK, Yap SJ, Kong C, Wong YC, Rozali N, Koh SF, Hoh CC, Puthucheary SD, Nathan S. 2015. Global transcriptional analysis of *Burkholderia pseudomallei* high and low biofilm producers reveals insights into biofilm production and virulence. *BMC Genomics* 16:471.

Chowdhury S, Barai L, Afroze SR, Ghosh PK, Afroz F, Rahman H, Ghosh S, Hossain MB, Rahman MZ, Das P, Rahim MA. 2022. The epidemiology of melioidosis and its association with diabetes mellitus: A systematic review and meta-analysis. *Pathogens* 11(2):149. doi:10.3390/pathogens11020149

Ciornei CD, Egesten A, Bodelsson M. 2003. Effects of human cathelicidin antimicrobial peptide LL 37 on lipopolysaccharide induced nitric oxide release from rat aorta in vitro. *Acta Anaesthesiologica Scandinavica* 47(2):213–220. doi:10.1034/j.1399-6576.2003.00045.x

Cox J, Hein MY, Luber CA, Paron I, Nagaraj N, Mann M. 2014. Accurate proteome wide label free quantification by delayed normalization and maximal peptide ratio extraction, termed MaxLFQ. *Molecular & Cellular Proteomics* 13(9):2513–2526. doi:10.1074/mcp.M113.031591

Crowe A, McMahon N, Currie BJ, Baird RW. 2014. Current antimicrobial susceptibility of first episode melioidosis *Burkholderia pseudomallei* isolates from the Northern Territory, Australia. *International Journal of Antimicrobial Agents* 44:160–162.

Cullinane M, Gong L, Li X, Lazar Adler N, Tra T, Wolvetang E, Prescott M, Boyce JD, Devenish RJ, Adler B. 2008. Stimulation of autophagy suppresses the intracellular survival of *Burkholderia pseudomallei* in mammalian cell lines. *Autophagy* 4(6):744–753. doi:10.4161/auto.6246

Currie BJ. 2015. Melioidosis: Evolving concepts in epidemiology, pathogenesis, and treatment. *Seminars in Respiratory and Critical Care Medicine* 36:111–125. doi:10.1055/s-0034-1398389

Dance DAB. 1991. Melioidosis: The tip of the iceberg? *Clinical Microbiology Reviews* 4(1):52–60. doi:10.1128/CMR.4.1.52

Estrada-de los Santos P, Vinuesa P, Martínez-Aguilar L, Hirsch AM, Caballero-Mellado J. 2013. Phylogenetic analysis of *Burkholderia* species by multilocus sequence analysis. *Current Microbiology* 67(1):51–60. doi:10.1007/s00284-013-0330-9

Fazli M, Almblad H, Rybtke ML, Givskov M, Eberl L, Tolker-Nielsen T. 2014. Regulation of biofilm formation in *Pseudomonas* and *Burkholderia* species. *Environmental Microbiology* 16:1961–1981. doi:10.1111/1462-2920.12448

Fong SM, Wong KJ, Fukushima M, Yeo TW. 2015. Thalassemia major is a major risk factor for paediatric melioidosis in Kota Kinabalu, Sabah, Malaysia. *Clinical Infectious Diseases* 60:1802–1807. doi:10.1093/cid/civ189

Foong YC, Tan M, Bradbury RS. 2014. Melioidosis: A review. *Rural and Remote Health* 14(4):2763. doi:10.22605/RRH2763

Gassiep I, Armstrong M, Norton R. 2020. Human melioidosis. *Clinical Microbiology Reviews* 33(2):e00006-19. doi:10.1128/cmr.00006-19

Ghazali AK, Eng SA, Khoo JS, Teoh S, Hoh CC, Nathan S. 2021. Whole genome comparative analysis of Malaysian *Burkholderia pseudomallei* clinical isolates. *Microbial Genomics* 7(2):000527. doi:10.1099/mgen.0.000527

Godoy D, Randle G, Simpson AJ, Aanensen DM, Pitt TL, Kinoshita R, Spratt BG. 2003. Multilocus sequence typing and evolutionary relationships among the causative agents of melioidosis and glanders, *Burkholderia pseudomallei* and *Burkholderia mallei*. *Journal of Clinical Microbiology* 41(5):2068–2079. doi:10.1128/JCM.41.5.2068-2079.2003

Hassan MRA, Pani SP, Peng NP, Voralu K, Vijayalakshmi N, Mehanderkar R, Aziz NA, Michael E. 2010. Incidence, risk factors and clinical epidemiology of melioidosis: A complex socio-ecological emerging infectious disease in the Alor Setar region of Kedah, Malaysia. *BMC Infectious Diseases* 10:302. doi:10.1186/1471-2334-10-302

Hassan MR, Vijayalakshmi N, Pani SP, Peng NP, Mehenderkar R, Voralu K, Michael E. 2014. Antimicrobial susceptibility patterns of *Burkholderia pseudomallei* among melioidosis

cases in Kedah, Malaysia. *Southeast Asian Journal of Tropical Medicine and Public Health* 45:680–688.

Hayden HS, Lim R, Brittnacher MJ, Sims EH, Ramage ER, Fong C, Wu Z, Crist E, Chang J, Zhou Y, Radey M, Rohmer L, Haugen E, Gillett W, Wuthiekanun V, Peacock SJ, Kaul R, Miller SI, Manoil C, Jacobs MA. 2012. Evolution of *Burkholderia pseudomallei* in recurrent melioidosis. *PLoS One* 7(5):e36507. doi:10.1371/journal.pone.0036507

He L, He T, Farrar S, Ji L, Liu T, Ma X. 2017. Antioxidants maintain cellular redox homeostasis by elimination of reactive oxygen species. *Cellular Physiology and Biochemistry* 44(2):532–553. doi:10.1159/000485089

Holden MT, Titball RW, Peacock SJ, Cerdeño-Tárraga AM, Atkins T, Crossman LC, Pitt T, Churcher C, Mungall K, Bentley SD, Sebaihia M, Thomson NR, Bason N, Beacham IR, Brooks K, Brown KA, Brown NF, Challis GL, Cherevach I, Chillingworth T, Cronin A, Crossett B, Davis P, DeShazer D, Feltwell T, Fraser A, Hance Z, Hauser H, Holroyd S, Jagels K, Keith KE, Maddison M, Moule S, Price C, Quail MA, Rabbinowitsch E, Rutherford K, Sanders M, Simmonds M, Songsivilai S, Stevens K, Tumapa S, Vesaratchavest M, Whitehead S, Yeats C, Barrell BG, Oyston PC, Parkhill J. 2004. Genomic plasticity of the causative agent of melioidosis, *Burkholderia pseudomallei*. *Proceedings of the National Academy of Sciences of the United States of America* 101(39):14240–14245. doi:10.1073/pnas.0403302101

How SH, Ng KH, Jamalludin AR, Shah A, Rathor Y. 2005. Melioidosis in Pahang, Malaysia. *Medical Journal of Malaysia* 60(5):606–613.

Hu CM, Tsao N, Wang YT, Chen YJ, Chang ZF. 2019. Thymidylate kinase is critical for DNA repair via ATM-dependent Tip60 complex formation. *FASEB Journal* 33(2):2017–2025. doi:10.1096/fj.201800856r

Idris A, Rachmat RFN, Ali SMM. 1998. Melioidosis: A case of sheep to human transmission. *Journal of Veterinary Malaysia* 10:77–79.

Jiang Y, Geng M, Bai L. 2020. Targeting biofilm therapy: Current research strategies and development hurdles. *Microorganisms* 8:1222. doi:10.3390/microorganisms8081222

Joompa P, Ponnikorn S, Roytrakul S, Tungpradabkul S. 2017. Investigation of host–pathogen interaction between *Burkholderia pseudomallei* and autophagy-related protein LC3 using hydrophobic chromatography-based technique. *Cell & Bioscience* 7:45.

Kang WT, Vellasamy KM, Chua EG, Vadivelu J. 2015. Functional characterizations of effector protein BipC, a type III secretion system protein, in *Burkholderia pseudomallei* pathogenesis. *Journal of Infectious Diseases* 211:827–834. doi:10.1093/infdis/jiu492

Kang WT, Vellasamy K, Vadivelu J. 2016. Eukaryotic pathways targeted by the type III secretion system effector protein, BipC, involved in the intracellular lifecycle of *Burkholderia pseudomallei*. *Scientific Reports* 6:33528. doi:10.1038/srep33528

Kavanaugh JS, Flack CE, Lister J, Ricker EB, Ibberson CB, Jenul C, Moormeier DE, Delmain EA, Bayles KW, Horswill AR. 2019. Identification of extracellular DNA binding proteins in the biofilm matrix. *mBio* 10(3):e01137-19. doi:10.1128/mBio.01137-19

Kyoto Encyclopedia of Genes and Genomes (KEGG). 2025. *Burkholderia pseudomallei* MSHR146 gene BBN_2026 (*bpsl2026*): Spore coat protein U domain-containing protein. Kyoto Encyclopedia of Genes and Genomes. https://www.kegg.jp/dbget-bin/www_bget?bpsu:BBN_2026

Khan MM, Chattagul S, Tran BQ, Freiberg JA, Nita-Lazar A, Shirtliff ME, Sermswan RW, Ernst RK, Goodlett DR. 2019. Temporal proteomic profiling reveals changes that support *Burkholderia* biofilms. *Pathogens and Disease* 77(2):ftz005. doi:10.1093/femspd/ftz005

Khodaparast L, Wu G, Khodaparast L, Schmidt BZ, Rousseau F, Schymkowitz J. 2021. Bacterial protein homeostasis disruption as a therapeutic intervention. *Frontiers in Molecular Biosciences* 8:681855. doi:10.3389/fmolb.2021.681855

Kim SH, Park C, Lee EJ, Bang WS, Kim YJ, Kim JS. 2017. Biofilm formation of Campylobacter strains isolated from raw chickens and its reduction with DNase I treatment. *Food Control* 71:94–100.

Kingsley PV, Leader M, Nagodawithana NS, Tipre M, Sathiakumar N. 2016. Melioidosis in Malaysia: A review of case reports. *PLoS Neglected Tropical Diseases* 10:e0005182. doi:10.1371/journal.pntd.0005182

Kostakioti M, Hadjifrangiskou M, Hultgren SJ. 2013. Bacterial biofilms: Development, dispersal, and therapeutic strategies in the dawn of the postantibiotic era. *Cold Spring Harbor Perspectives in Medicine* 3:a010306. doi:10.1101/cshperspect.a010306

Krishnananthasivam S, Sathkumara HD, Corea E, Natesan M, De Silva AD. 2017. Gene expression profile of human cytokines in response to *Burkholderia pseudomallei* infection. *mSphere* 2(2):e00121-17. doi:10.1128/mSphere.00121-17

Laemmli, U. K. 1970. Cleavage of structural proteins during the assembly of the head of bacteriophage T4. *Nature*, 227(5259), 680–685. https://doi.org/10.1038/227680a0

Lee HS, Gu F, Ching SM, Lam Y, Chua KL. 2010. CdpA is a *Burkholderia pseudomallei* cyclic di-GMP phosphodiesterase involved in autoaggregation, flagellum synthesis, motility, biofilm formation, cell invasion, and cytotoxicity. *Infection and Immunity* 78:1832–1840. doi:10.1128/IAI.00446-09

Lennings J, West TE, Schwarz S. 2019. The *Burkholderia* Type VI Secretion System 5: Composition, regulation and role in virulence. *Frontiers in Microbiology* 9:3339. doi:10.3389/fmicb.2018.03339

Lim ML, Ismail SS, Rahman N, Watanabe M. 2015. Melioidosis: A localized osteomyelitis in a cat. *Journal of Veterinary Malaya* 27:24–26.

Limmathurotsakul D, Golding N, Dance DAB, Messina JP, Pigott DM, Moyes CL, Rolim DB, Bertherat E, Day NP, Peacock SJ, Hay SI. 2016. Predicted global distribution of *Burkholderia pseudomallei* and burden of melioidosis. *Nature Microbiology* 1:15008. doi:10.1038/nmicrobiol.2015.8

Limmathurotsakul D, Peacock SJ. 2011. Melioidosis: A clinical overview. *British Medical Bulletin* 99:125–139. doi:10.1093/bmb/ldr007

Limmathurotsakul D, Paeyao A, Wongratanacheewin S, Saiprom N, Takpho N, Thaipadungpanit J, Chantratita N, Wuthiekanun V, Day NP, Peacock SJ. 2014. Role of *Burkholderia pseudomallei* biofilm formation and lipopolysaccharide in relapse of melioidosis. *Clinical Microbiology and Infection* 20(11):O854–O856.

Limmathurotsakul D, Wuthiekanun V, Chantratita N, Wongsuvan G, Amornchai P, Day NPJ, Peacock SJ. 2010. *Burkholderia pseudomallei* is spatially distributed in soil in Northeast Thailand. *PLoS Neglected Tropical Diseases* 4(6):e694. doi:10.1371/journal.pntd.0000694

Mahenthiralingam E, Urban TA, Goldberg JB. 2005. The multifarious, multireplicon *Burkholderia cepacia* complex. *Nature Reviews Microbiology* 3(2):144–156. doi: https://doi.org/10.1038/nrmicro1085

Mangalea MR, Borlee GI, Borlee BR. 2017. The current status of extracellular polymeric substances produced by *Burkholderia pseudomallei*. *Current Tropical Medicine Reports* 4:117–126.

Mangalea MR, Borlee BR. 2022. The NarX-NarL two-component system regulates biofilm formation, natural product biosynthesis, and host-associated survival in *Burkholderia pseudomallei*. *Scientific Reports* 12:203. doi: https://doi.org/10.1038/s41598-021-03873-9

Mangalea MR, Plumley BA, Borlee BR. 2017. Nitrate sensing and metabolism inhibit biofilm formation in the opportunistic pathogen *Burkholderia pseudomallei* by reducing the intracellular concentration of c-di-GMP. *Frontiers in Microbiology* 8:1353. doi: https://doi.org/10.3389/fmicb.2017.01353

Mariappan V, Vellasamy KM, Onn HH, Vadivelu J. 2011. Profiling of *Burkholderia cepacia* secretome at mid-logarithmic and early stationary phases of growth. *PLoS One* 6:e26518. doi: https://doi.org/10.1371/journal.pone.0026518

Mariappan V, Vellasamy KM, Vadivelu J. 2017. Host adaptation of *Burkholderia pseudomallei* alters metabolism and virulence: A global proteome analysis. *Scientific Reports* 7:9015. doi: https://doi.org/10.1038/s41598-017-09373-0

Mariappan V, Thavagnanam S, Vellasamy KM, Teh CJS, Atiya N, Ponnampalavanar S, Vadivelu J. 2018. Relapse of chronic melioidosis in a pediatric cystic fibrosis patient: First case report from Malaysia. *BMC Infectious Diseases* 18:455. doi: https://doi.org/10.1186/s12879-018-3371-7

McMahon RM, Ireland PM, Sarovich DS, Petit G, Jenkins CH, Sarkar-Tyson M, Currie BJ, Martin JL. 2018. Virulence of the melioidosis pathogen *Burkholderia pseudomallei* requires the oxidoreductase membrane protein DsbB. *Infection and Immunity* 86(5):e00938-17. doi: https://doi.org/10.1128/IAI.00938-17

Miles AA, Misra SS, Irwin JO. 1938. The estimation of the bactericidal power of the blood. *Journal of Hygiene* 38(6):732–749. doi: https://doi.org/10.1017/S002217240001158X

Mohan A, Podin Y, Tai N, Chieng CH, Rigas V, Machunter B, Mayo M, Wong D, Chien SL, Tan LS, et al. 2017. Pediatric melioidosis in Sarawak, Malaysia: Epidemiological, clinical and microbiological characteristics. *PLoS Neglected Tropical Diseases* 11:e0005650. doi: https://doi.org/10.1371/journal.pntd.0005650

Moura de Sousa J, Lourenço M, Gordo I. 2023. Horizontal gene transfer among host-associated microbes. *Cell Host & Microbe* 31(4):513–527. doi: https://doi.org/10.1016/j.chom.2023.02.017

Muthita Vanaporn, P. Vattanaviboon, V. Thongboonkerd & S. Korbsrisate 2008. The rpoE operon regulates heat stress response in *Burkholderia pseudomallei*. *FEMS Microbiology Letters* 284(2): 191–196.

Neubauer, H. (2004). Melioidosis in Animals: A Review on Epizootiology, Diagnosis and Clinical Presentation. *Journal of Veterinary Medicine Series B.*

Naama T, Norazura AH, Chin SW, Mazlan L, Nurul Fatiha AS, Masrin A, Naheed MH, Ramlan M. 2012. Melioidosis in various animal species diagnosed in the Veterinary Research Institute from 2007 to 2011. In: *Proceedings of the International Conference on One Health and 24th VAM Congress*, Putrajaya, Malaysia, 21–23 September 2012, pp.129–130.

Nathan S, Chieng S, Kingsley PV, Mohan A, Podin Y, Ooi MH, Mariappan V, Vellasamy KM, Vadivelu J, Daim S, How SH. 2018. Melioidosis in Malaysia: Incidence, clinical challenges, and advances in understanding pathogenesis. *Tropical Medicine and Infectious Disease* 3(1):25. doi:https://doi.org/10.3390/tropicalmed3010025

Paauw A, Scholz HC, Mars Groenendijk RH, Dekker LJM, Luider TM, van Leeuwen HC. 2023. Expression of virulence and antimicrobial related proteins in *Burkholderia mallei* and *Burkholderia pseudomallei*. *PLoS Neglected Tropical Diseases* 17(1):e0011006. doi:https://doi.org/10.1371/journal.pntd.0011006

Panya M, Thirat S, Wanram S, Panomket P, Nilsakul J. 2016. Prevalence of bla(PenA) and bla(OXA) in *Burkholderia pseudomallei* isolated from patients at Sappasitthiprasong Hospital and their susceptibility to ceftazidime and carbapenems. *Journal of Medical Association of Thailand* 99(Suppl 1):S12–S16.

Pfaffl MW. 2001. A new mathematical model for relative quantification in real time RT-PCR. *Nucleic Acids Research* 29(9):e45. doi:https://doi.org/10.1093/nar/29.9.e45

Phenn J, Pané Farré J, Meukow N, Klein A, Troitzsch A, Tan P, Fuchs S, Wagner GE, Lichtenegger S, Steinmetz I, Kohler C. 2021. RegAB homolog of *Burkholderia pseudomallei* is the master regulator of redox control and involved in virulence. *PLoS Pathogens* 17(5):e1009604. doi:https://doi.org/10.1371/journal.ppat.1009604

Pinweha P, Pumirat P, Cuccui J, Jitprasutwit N, Muangsombut V, Srinon V, Boonyuen U, Thiennimitr P, Vattanaviboon P, Cia F, Willcocks S, Bancroft GJ, Wren BW, Korbsrisate S. 2018. Inactivation of bpsl1039-1040 ATP binding cassette transporter reduces intracellular survival in macrophages, biofilm formation and virulence in the

murine model of *Burkholderia pseudomallei* infection. *PLoS One* 13(5):e0196202. doi: https://doi.org/10.1371/journal.pone.0196202

Pitt TL. 1995. Pseudomonas, Burkholderia and related genera. In: Haussler WJ, Sussman M, editors. *Topley and Wilson's Microbiology and Microbial Infections*, vol.2. Arnold, London, United Kingdom, pp.1109–1138.

Pitt JJ. 2009. Principles and applications of liquid chromatography mass spectrometry in clinical biochemistry. *The Clinical Biochemist Reviews* 30(1):19–34.

Plumb RS, Johnson KA, Rainville P, Smith BW, Wilson ID, Castro Perez JM, Nicholson JK. 2006. UPLC/MS(E); a new approach for generating molecular fragment information for biomarker structure elucidation. *Rapid Communications in Mass Spectrometry* 20(13):1989–1994. doi:https://doi.org/10.1002/rcm.2550

Plumley BA, Martin KH, Borlee GI, Marlenee NL, Burtnick MN, Brett PJ, AuCoin DP, Bowen RA, Schweizer HP, Borlee BR. 2017. Thermoregulation of biofilm formation in *Burkholderia pseudomallei* is disrupted by mutation of a putative diguanylate cyclase. *Journal of Bacteriology* 199(5):e00780-16. doi:https://doi.org/10.1128/JB.00780-16

Puthucheary SD. 2009. Melioidosis in Malaysia. *Medical Journal of Malaysia* 64:266–274.

Queipo Ortuño MI, De Dios Colmenero J, Macias M, Bravo MJ, Morata P. 2008. Preparation of bacterial DNA template by boiling and effect of immunoglobulin G as an inhibitor in real time PCR for serum samples from patients with brucellosis. *Clinical and Vaccine Immunology* 15(2):293–296. doi:https://doi.org/10.1128/CVI.00361-07

Rao C, Zhang Z, Qiao J, et al. 2024. *Burkholderia pseudomallei* BopE suppresses the Rab32 dependent defense pathway to promote its intracellular replication and virulence. *mSphere* 9(11):e00453-24. doi:https://doi.org/10.1128/msphere.00453-24

Reckseidler SL, DeShazer D, Sokol PA, Woods DE. 2001. Detection of bacterial virulence genes by subtractive hybridization: Identification of capsular polysaccharide of *Burkholderia pseudomallei* as a major virulence determinant. *Infection and Immunity* 69(1):34–44. doi:https://doi.org/10.1128/IAI.69.1.34-44.2001

Sam IC, Puthucheary SD. 2006. Melioidosis in children from Kuala Lumpur, Malaysia. *Annals of Tropical Paediatrics* 26:219–224. doi:https://doi.org/10.1179/146532806X120300

Sanderson C, Currie BJ. 2014. Melioidosis: A pediatric disease. *Pediatric Infectious Disease Journal* 33:770–771. doi:https://doi.org/10.1097/INF.0000000000000326

Sawasdidoln C, Taweechaisupapong S, Sermswan RW, Tattawasart U, Tungpradabkul S, Wongrattanacheewin S. 2010. Growing *Burkholderia pseudomallei* in biofilm stimulating conditions significantly induces antimicrobial resistance. *PLoS One* 5(2):e9196. doi:https://doi.org/10.1371/journal.pone.0009196

Seng R, Phunpang R, Saiprom N, Dulsuk A, Chewapreecha C, Thaipadungpanit J, Batty EM, Chantratita W, West TE, Chantratita N. 2023. Phenotypic and genetic alterations of *Burkholderia pseudomallei* in patients during relapse and persistent infections.

Frontiers in Microbiology 14:1103297. doi: https://doi.org/10.3389/fmicb.2023.1103297

Stanton AT, Fletcher W, Kanagarayer K. 1924. Two cases of melioidosis. *Journal of Hygiene (London)* 23:268–276.

Stanton AT, Fletcher W. 1932. *Melioidosis*. Volume 21. London, UK: John Bale and Danielson Ltd.

Stanton AT, Fletcher W. 1925. Melioidosis: A disease of rodents communicable to man. *The Lancet* 205(5288):10–13.

Stanton AT, Fletcher W. 1921. Melioidosis, a new disease of the tropics. *Far Eastern Association of Tropical Medicine: Transactions of the Fourth Congress*, Batavia, Dutch East Indies: Javasche Boekhandel en Drukkerij.

Stevens MP, Friebel A, Taylor LA, Wood MW, Brown PJ, Hardt WD, Galyov EE. 2003. A *Burkholderia pseudomallei* type III secreted protein, BopE, facilitates bacterial invasion of epithelial cells and exhibits guanine nucleotide exchange factor activity. *Journal of Bacteriology* 185(16):4992–4996. doi: https://doi.org/10.1128/JB.185.16.4992-4996.2003

Stevens MP, Haque A, Atkins T, Hill J, Wood MW, Easton A, Nelson M, Underwood Fowler C, Titball RW, Bancroft GJ, Galyov EE. 2004. Attenuated virulence and protective efficacy of a *Burkholderia pseudomallei* bsa type III secretion mutant in murine models of melioidosis. *Microbiology (Reading)* 150(Pt 8):2669–2676. doi: https://doi.org/10.1099/mic.0.27147-0

Stevens MP, Wood MW, Taylor LA, Monaghan P, Hawes P, Jones PW, Wallis TS, Galyov EE. 2002. An Inv/Mxi Spa-like type III protein secretion system in *Burkholderia pseudomallei* modulates intracellular behaviour of the pathogen. *Molecular Microbiology* 46(3):649–659. doi: https://doi.org/10.1046/j.1365-2958.2002.03192.x

Stewart PS, Franklin MJ. 2008. Physiological heterogeneity in biofilms. *Nature Reviews Microbiology* 6:199–210. doi: https://doi.org/10.1038/nrmicro1838

Strauss JM, Jason S, Mariappan M. 1967. *Pseudomonas pseudomallei* in soil and surface water of Sabah, Malaysia. *Medical Journal of Malaysia* 22:31–32.

Strauss J, Ellison D, Gan E, Jason S, Marcarelli JL, Rapmund G. 1969a. Melioidosis in Malaysia. IV. Intensive ecological study of Carey Island, Selangor, for *Pseudomonas pseudomallei*. *Medical Journal of Malaysia* 24:94–100.

Strauss JM, Alexander AD, Rapmund G, Gan E, Dorsey AE. 1969b. Melioidosis in Malaysia: III. Antibodies to *Pseudomonas pseudomallei* in the human population. *American Journal of Tropical Medicine and Hygiene* 18:703–707. doi: https://doi.org/10.4269/ajtmh.1969.18.703

Strauss JM, Groves MG, Mariappan M, Ellison DW. 1969c. Melioidosis in Malaysia. II. Distribution of *Pseudomonas pseudomallei* in soil and surface water. *American Journal*

of Tropical Medicine and Hygiene 18:698–702. doi: https://doi.org/10.4269/ajtmh.1969.18.698

Suppiah J, Thimma JS, Cheah SH, Vadivelu J. 2010. Development and evaluation of polymerase chain reaction assay to detect *Burkholderia* genus and to differentiate the species in clinical specimens. *FEMS Microbiology Letters* 306(1):9–14. doi: https://doi.org/10.1111/j.1574-6968.2010.01925.x

Szklarczyk D, Nastou KC, Koutrouli M, Kirsch R, Mehryary F, Hachilif R, Hu D, Peluso ME, Huang Q, Fang T, Doncheva NT, Pyysalo S, Bork P, Jensen LJ, von Mering C. 2025. The STRING database in 2025: Protein networks with directionality of regulation. *Nucleic Acids Research* 53(D1):D730–D737. doi: https://doi.org/10.1093/nar/gkae1113

Tang RY, Lim SH, Lam JE, Nurasykin S, Eileen T, Chan YW. 2019. A 5-year retrospective study of melioidosis cases treated in a district specialist hospital. *Medical Journal of Malaysia* 74(6):472–476.

Thin RNT, Brown M, Stewart JB, Garrett CJ. 1970. Melioidosis: A report of ten cases. *QJM: An International Journal of Medicine* 39:115–127. doi: https://doi.org/10.1093/qjmed/39.1.115

Tokuda M, Shintani M. 2024. Microbial evolution through horizontal gene transfer by mobile genetic elements. *Microbial Biotechnology* 17(2):e14408. doi: https://doi.org/10.1111/1751-7915.14408

Tolker-Nielsen T. 2015. Biofilm development. *Microbiology Spectrum* 3:51–66. doi: https://doi.org/10.1128/microbiolspec.MB-0001-2014

Truong TT, Seyedsayamdost M, Greenberg EP, Chandler JR. 2015. A *Burkholderia thailandensis* acyl homoserine lactone-independent orphan LuxR homolog that activates production of the cytotoxin malleilactone. *Journal of Bacteriology* 197:3456–3462. doi: https://doi.org/10.1128/JB.00234-15

Tyanova S, Cox J. 2018. Perseus: A bioinformatics platform for integrative analysis of proteomics data in cancer research. *Methods in Molecular Biology* 1711:133–148. doi: https://doi.org/10.1007/978-1-4939-7493-1_7

Tyanova S, Temu T, Cox J. 2016. The MaxQuant computational platform for mass spectrometry-based shotgun proteomics. *Nature Protocols* 11(12):2301–2319. doi: https://doi.org/10.1038/nprot.2016.136

Utari PD, Setroikromo R, Melgert BN, Quax WJ. 2018. PvdQ quorum quenching acylase attenuates *Pseudomonas aeruginosa* virulence in a mouse model of pulmonary infection. *Frontiers in Cellular and Infection Microbiology* 8:119. doi: https://doi.org/10.3389/fcimb.2018.00119

Van Eeckhaut A, Lanckmans K, Sarre S, Smolders I, Michotte Y. 2009. Validation of bioanalytical LC-MS/MS assays: Evaluation of matrix effects. *Journal of Chromatography B* 877(23):2198–2207. doi: https://doi.org/10.1016/j.jchromb.2009.02.041

Vander Broek CW, Chalmers KJ, Stevens MP, Stevens JM. 2015. Quantitative proteomic analysis of *Burkholderia pseudomallei* Bsa Type III secretion system effectors using hypersecreting mutants. *Molecular & Cellular Proteomics* 14(4):905–916. doi: https://doi.org/10.1074/mcp.M114.045971

Vander Broek CW, Stevens JM. 2017. Type III secretion in the melioidosis pathogen *Burkholderia pseudomallei*. *Frontiers in Cellular and Infection Microbiology* 7:255. doi: https://doi.org/10.3389/fcimb.2017.00255

Vellayan S. 1994. Melioidosis in zoo animals in Malaysia. In: Puthucheary SD, Malik YA, editors. *Melioidosis: Prevailing Problems and Future Directions*. Kuala Lumpur: SP Muda Printing.

Wei H, Movahedi A, Zhang Y, Aghaei Dargiri S, Liu G, Zhu S, Yu C, Chen Y, Zhong F, Zhang J. 2022. Long chain acyl-CoA synthetases promote poplar resistance to abiotic stress by regulating long chain fatty acid biosynthesis. *International Journal of Molecular Sciences* 23(15):8401. doi: https://doi.org/10.3390/ijms23158401

Welkos S, Blanco I, Okaro U, Chua J, DeShazer D. 2020. A DUF4148 family protein produced inside RAW264.7 cells is a critical *Burkholderia pseudomallei* virulence factor. *Virulence* 11(1):1041–1058. doi: https://doi.org/10.1080/21505594.2020.1785819

Whitmore A, Krishnaswami CS. 1912. A hitherto undescribed infective disease in Rangoon. *Indian Medical Gazette* 47(7):262–267.

Wiersinga WJ, Virk HS, Torres AG, Currie BJ, Peacock SJ, Dance DAB, Limmathurotsakul D. 2018. Melioidosis. *Nature Reviews Disease Primers* 4:17107. doi: https://doi.org/10.1038/nrdp.2017.107

Wiersinga WJ, Currie BJ, Peacock SJ. 2012. Melioidosis. *New England Journal of Medicine* 367(11):1035–1044. doi: https://doi.org/10.1056/NEJMra1204699

Wuthiekanun V, Amornchai P, Saiprom N, Chantratita N, Chierakul W, Koh GC, Chaowagul W, Day NP, Limmathurotsakul D, Peacock SJ. 2011. Survey of antimicrobial resistance in clinical *Burkholderia pseudomallei* isolates over two decades in Northeast Thailand. *Antimicrobial Agents and Chemotherapy* 55:5388–5391. doi: https://doi.org/10.1128/AAC.05517-11

Zainal Abidin H, Muhd Besari A, Nadarajan C, Wan Shukeri WF, Mazlan MZ, Chong SE, Salmuna Ayub ZN. 2017. Acute bacteremic pneumonia due to melioidosis developing in the intensive care setting. *IDCases* 8:63–65. doi: https://doi.org/10.1016/j.idcr.2017.04.010

Zhou W, Tsai A, Dattmore DA, Stives DP, Chitrakar I, D'Alessandro AM, Patil S, Hicks KA, French JB. 2019. Crystal structure of *Escherichia coli* PRPP synthetase. *BMC Structural Biology* 19(1):1. doi: https://doi.org/10.1186/s12900-019-0105-4

APPENDIX A

Media, Buffers and Reagent Preparations

i. Growth medium and stock solution preparation

The nutrient agar (NA), Luria-Bertani (LB) media, glycerol stock and Ashdown agar mixture were stirred till dissolved. They were then sterilised by autoclaving at 121 ˚C for 15 min. Approximately 20 mL of NA and Ashdown agar were poured into agar plates in a sterile biosafety cabinet and left to solidify. One plate of agar was incubated overnight at 37 ˚C to check for contamination. The rest of the agar was then cooled at 4 ˚C overnight. The LB media and glycerol stock were left to cool at room temperature and then stored at 4 ˚C.

ii. Growth medium, stock solution, tris-acetate-ethylenediaminetetraacetic acid buffer and RNA extraction solution recipe

Table 1 Growth medium, buffers and reagent preparation

Preparations	Ingredients	Amount
Nutrient agar	NA	37 g
	dH_2O	1 L
Luria-Bertani	LB media	43 g
	dH_2O	1 L
60% Glycerol stock	100% Glycerol stock (Merck, Germany)	60 mL
	dH_2O	40 mL
Ashdown agar	0.1% Crystal violet (Oxoid, United Kingdom)	5 mL
	1% Neutral red (Oxoid, United Kingdom)	5 mL
	Tryptone soya powder (Oxoid, United Kingdom)	10 g
	Agar powder (HiMedia, India)	15 g

UNIVERSITI KEBANGSAAN MALAYSIA

	Glycerol (Merck, Germany)	40 mL
	Gentamicin (Oxoid, United Kingdom)	4 mg
	dH_2O	950 mL
50 x Tris-acetate-EDTA buffer	Tris base (Sigma-Aldrich, USA)	242 g
	MiliQ water	700 mL
	0.5 M, pH 8.0, EDTA (Sigma-Aldrich, USA)	100 mL
	Glacial acetic acid (Merck, Germany)	57.1 mL
1X TAE buffer	50X TAE buffer	20 mL
	MiliQ water	980 mL
1 x Tris-EDTA (TE) buffer	1 x TE buffer	10 mL
(15 mg/ mL lysozyme)	Lysozyme (Sigma-Aldrich, USA)	150 mg

UNIVERSITI KEBANGSAAN MALAYSIA

APPENDIX B

Proteomics Preparation

i. Bradford assay standard curve preparation (REF)

Bovine serum albumin (BSA) was used as the standard to plot a protein standard curve. Approximately 0.2 g of BSA was dissolved in 10 mL of sterilised dH_2O to obtain a concentration of 20 mg/mL (solution A). Following that, 2 mL of solution A was diluted with 8 mL of sterilised dH_2O for a concentration of 4 mg/mL (solution B). Then, 1 mL of solution B was diluted with 19 mL of sterilised dH_2O to bring the final concentration to 0.2 mg/mL (solution C). Six microcentrifuge tubes were prepared as follows in triplicates (Table 3.1). Next, 1 mL of Bradford reagent (Appendix B) was added to each tube, following the dye-binding principle originally described by Bradford (1976). The tubes were left for 10 min in a dark room and the absorbance of 1 mL of each tube was read at OD_{595nm} using a spectrophotometer. A standard curve of absorbance OD_{595nm} vs BSA amount (µg) was plotted and the R^2 was noted. The curve equation was then generated.

Table 2 Preparation of protein amounts for Bradford assay

Solution C volume (µL)	Sterilized dH_2O (µL)	Protein amount (µg)
0 µL	100 µL	0 µg
20 µL	80 µL	4 µg
40 µL	60 uL	8 µg
60 µL	40 µL	12 µg
80 µL	20 µL	16 µg
100 µL	0 µL	20 µg

ii. Sodium dodecyl sulphate-polyacrylamide gel electrophoresis (SDS-PAGE) protein sample preparation (REF)

Protein samples were diluted with dH_2O to final amounts of 10–50 µg. Subsequently, 2× Laemmli solution was added at a 1:1 ratio in 200 µL microcentrifuge tubes. The mixtures were heated to 95 °C for 5 min in a thermocycler, cooled to room temperature, and then placed on ice. This preparation followed the standard SDS-PAGE protocol

UNIVERSITI KEBANGSAAN MALAYSIA

described by Laemmli (1970), enabling protein denaturation and uniform migration during electrophoresis.

iii. Proteomics reagent preparation

Table 3 Proteomics reagents, gels and buffers preparation

Preparations	Ingredients	Amount
Bradford reagent	Coomassie Brilliant Blue (Sigma-Aldrich, USA)	100 mg
	95% Ethanol (Merck, Germany)	50 mL
	85% Phosphoric acid (Merck, Germany)	100 mL
	dH_2O	850 mL
12% Resolving gel	dH_2O	2 mL
	1.5 M Tris HCL (pH 8.8) (Sigma-Aldrich, USA)	1.5 mL
	10% SDS (Sigma-Aldrich, USA)	60 µL
	30% acrylamide (Bio-Rad, USA)	2.4 mL
	10% APS (Bio-Rad, USA)	60 µL
	TEMED (Bio-Rad, USA)	5 µL
5% Stacking gel	dH_2O	1.4 mL
	1.5 M Tris HCL (pH 8.8)	625 µL
	10% SDS	25 µL
	30% acrylamide	425 µL
	10% APS	25 µL
	TEMED	2.5 µL
1 x EB buffer	10 x EB buffer (Sigma-Aldrich, USA)	50 mL
	dH_2O	450 mL

UNIVERSITI KEBANGSAAN MALAYSIA

APPENDIX C

Supplementary Data

i. Biofilm quantification data

Table 4 Biofilm quantification data of all three *B. pseudomallei* clinical strains at 24, 48 and 72 hour time points

Time (Hours)	Avg UMC083 (SD)	Avg UMC082 (SD)	Avg UMC114 (SD)
24	1.150 (±0.006)	1.275 (±0.015)	1.264 (±0.009)
48	1.415 (±0.077)	2.075 (±0.201)	3.482 (±0.372)
72	4.210 (±0.353)	7.133 (±0.195)	10.51 (±0.641)

ii. RNA extraction purity and concentration data

Table 5 Extracted RNA purity and concentration data of all three *B. pseudomallei* clinical strains

Strain ID no.	Nucleic acid (ng/uL)	A260/A280	A260/A230
UMC083A	438.0	2.04	2.22
UMC083B	559.3	2.09	1.78
UMC083C	385.4	2.07	2.13
UMC083D	262.3	2.09	2.08
UMC083E	237.5	2.11	1.37
UMC082A	556.5	2.12	2.00
UMC082B	287.2	2.04	2.07
UMC082C	152.5	2.07	2.19
UMC082D	18.0	2.17	0.21
UMC082E	36.0	2.19	1.27
UMC114A	84.4	2.09	2.08
UMC114B	228.8	2.11	0.75
UMC114C	336.7	2.07	1.99
UMC114D	270.4	2.09	2.08
UMC114E	300.5	2.08	2.19

UNIVERSITI KEBANGSAAN MALAYSIA

iii. QPCR standard curve

bpsl0603

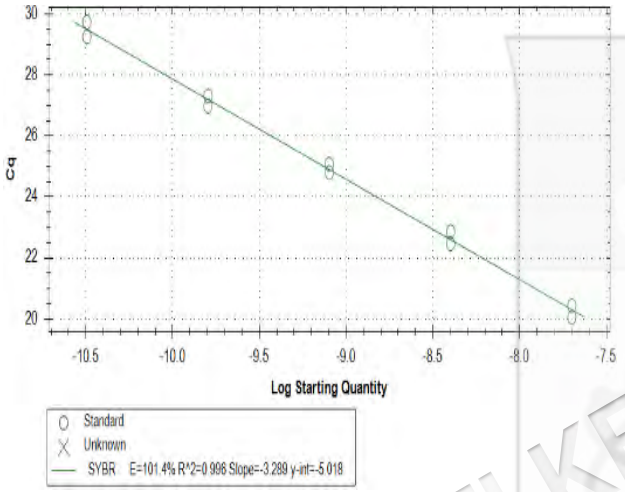

bpsl2026

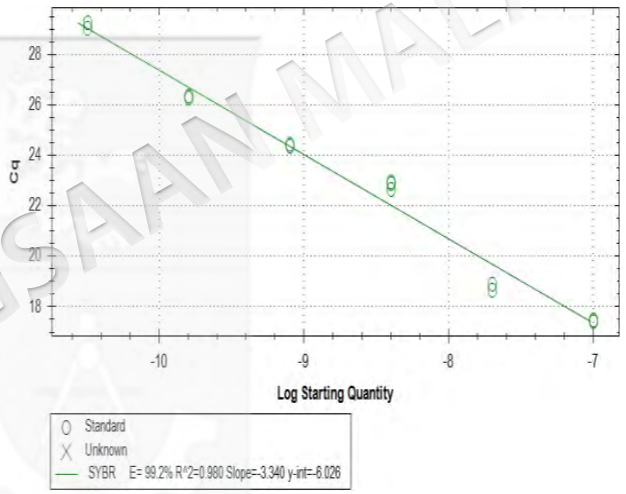

UNIVERSITI KEBANGSAAN MALAYSIA

bpsl1607

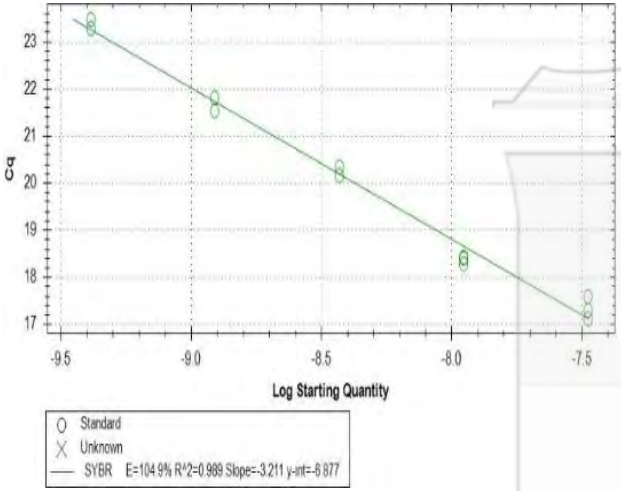

bpsl1799

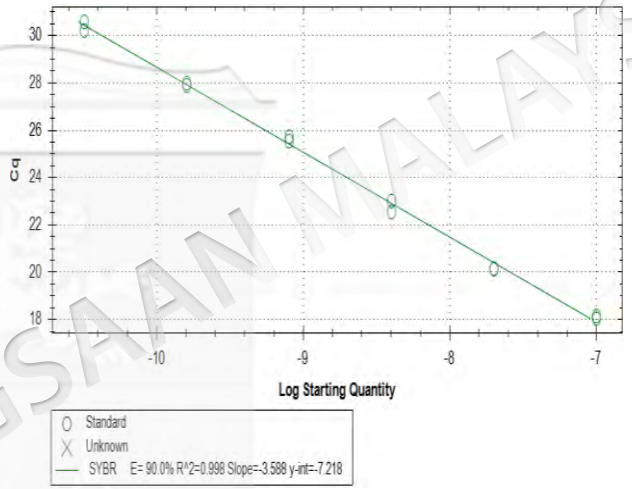

bpss2016

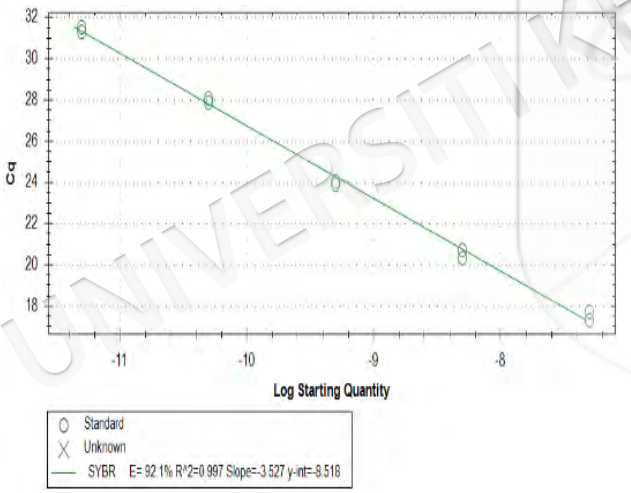

bpss0312

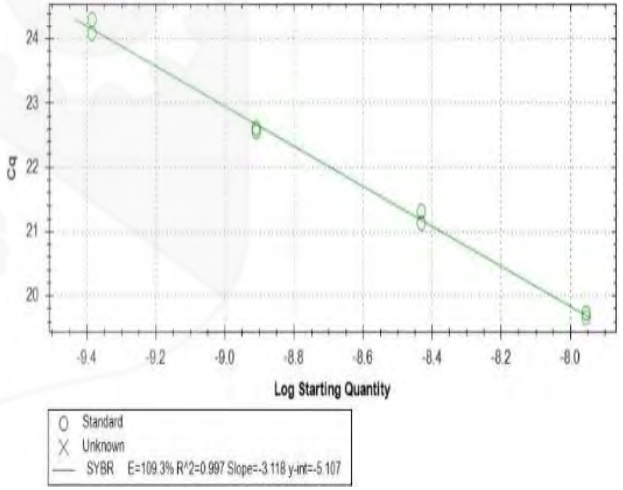

UNIVERSITI KEBANGSAAN MALAYSIA

bpss1214

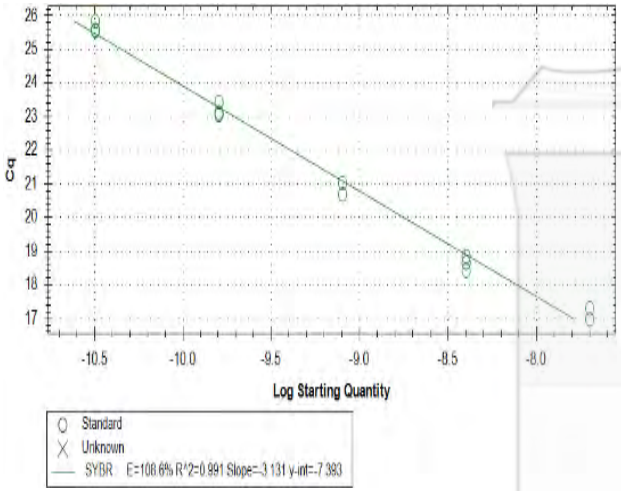

bpss0124

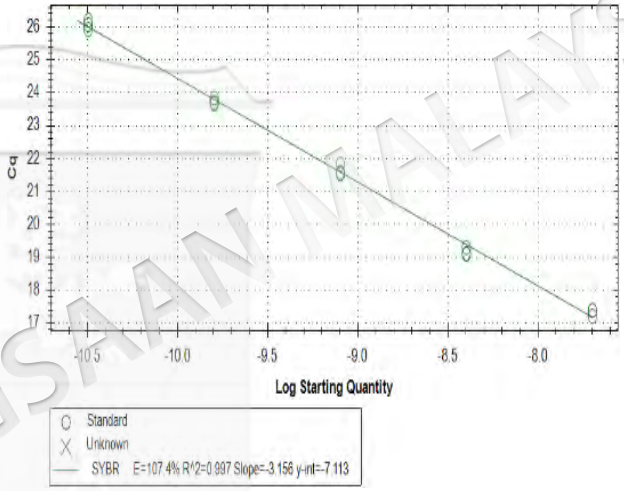

16s rRNA

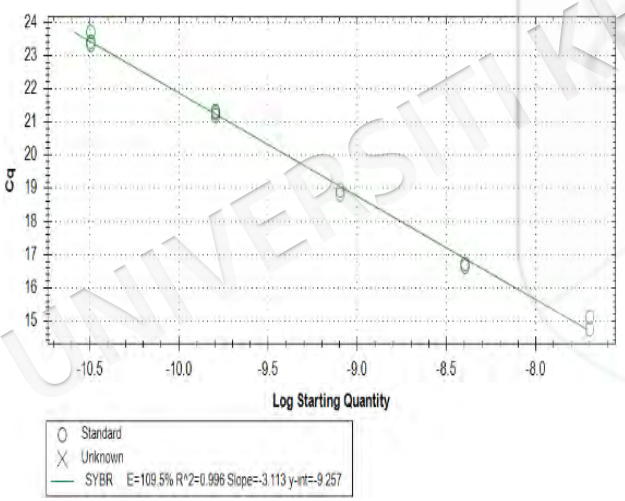

DnaK

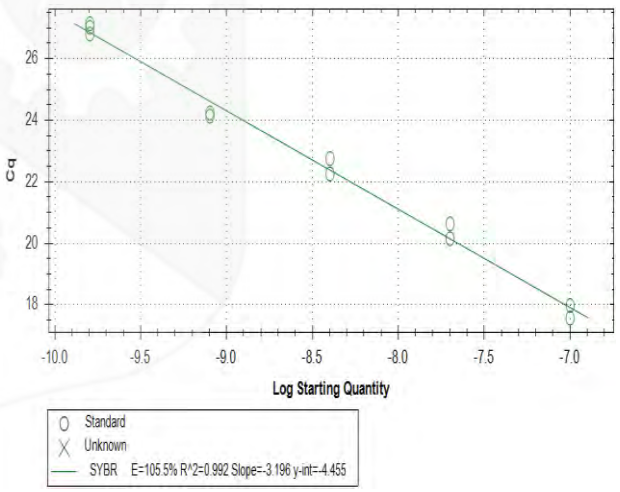

UNIVERSITI KEBANGSAAN MALAYSIA

iv. Bradford assay standard curve

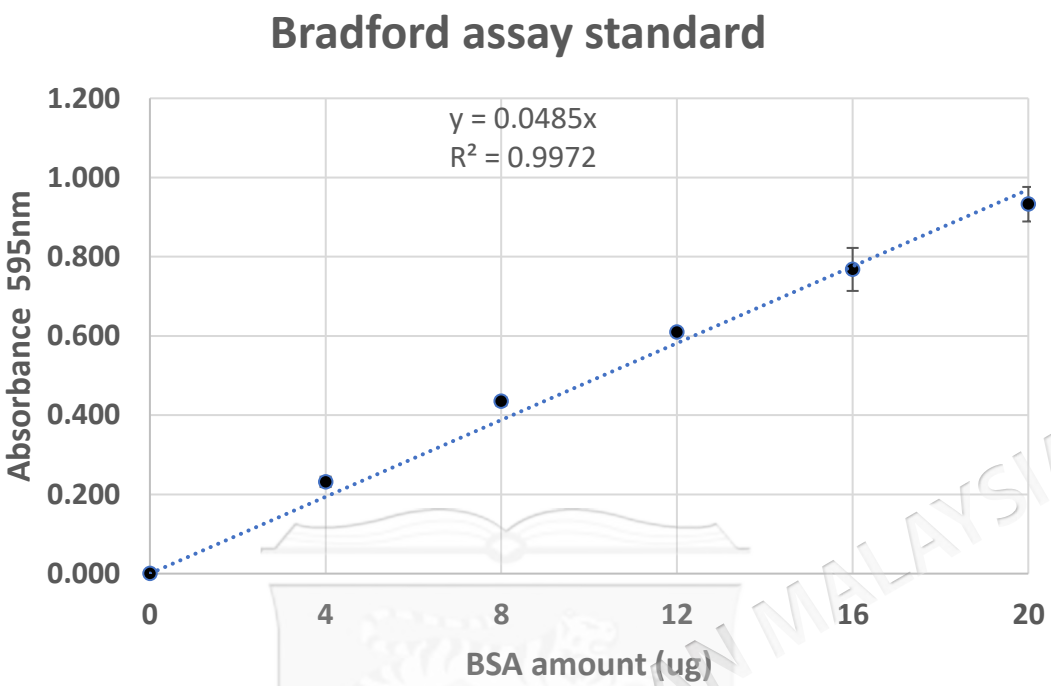

Figure 1: Bradford assay standard curve where the m value = 0.0485 and R^2 = 0.9972

Table 1 Bradford assay standard curve results

Amount (ug)	R1	R2	R3	Average (SD)
0	0.000	0.000	0.000	0.000 (±0.000)
4	0.219	0.245	0.231	0.232 (±0.013)
8	0.439	0.442	0.423	0.435 (±0.010)
12	0.615	0.608	0.607	0.610 (±0.004)
16	0.725	0.75	0.829	0.768 (±0.054)
20	0.978	0.891	0.929	0.933 (±0.044)

UNIVERSITI KEBANGSAAN MALAYSIA

Conferences Attended

Conference name	Role	Title	Year
FSK Postgraduate Colloquium 2023	Oral presenter	Elucidation of *Burkholderia pseudomallei* in chronic relapse melioidosis: understanding adaptation and pathogenic persistence using genomics and proteomics approaches	2023
28th Biological Sciences Graduate Congress	Oral presenter	The elucidation of *Burkholderia pseudomallei* whole genome sequencing: primary, relapse and new infection strains	2024

Manuscripts in preparation

	Title	Projected publication	Category
	Combatting *Burkholderia pseudomallei* biofilms: enhanced strategies through antibiotic combinations and anti-biofilm agents	2026	Review paper
	Proteomic landscape of clinical *Burkholderia pseudomallei* strains highlights virulence and resistance mechanisms	2026	Research paper

UNIVERSITI KEBANGSAAN MALAYSIA